UNIVERSITÀ
DEGLI STUDI
DI PADOVA

UNIVERSITA DI PADOVA

DIPARTIMENTO DI INGEGNERIA INDUSTRIALE

LAUREA MAGISTRALE IN INGEGNERIA CHIMICA E DEI PROCESSI INDUSTRIAL

Assessment of the contribution of the Advance Oxidation Processes(AOPs) to the degradation of per- and poly-fluoroalkyl substances(PFAS) in aqueous media

Relatrice: *Prof. Martina Roso*

Correlatore*: Ing. Abhishek Anand*

Laureando: *Mahdi Miravandi*

2025-2026

Abstract

Many studies have shown that UV radiation promotes advanced oxidation processes(AOPs) that degrade perfluoroalkyl substances(PFAS) and that UV radiation is required for accelerating and enhancing the degradation process of our contaminant. The primary objective of this Thesis was to assess the contribution of each of these processes individually for fluorinated compound removal from water, focusing on perfluorooctanoic acid (PFOA). This review systematically evaluates various potential pathways developed to degrade PFAS through Persulfate activation, Heterogeneous Photocatalysis, and Photo-Fenton reactions as well as employing Metal-Organic frameworks (MOFs) for degrading pollutant species.

The membranes used in the experimental tests are made of polyimide, a polymer well known for its excellent chemical and physical properties, it provides good performance even at high temperatures and high resistance to irradiation with UV without negative impact providing as support for the catalyst which is Tetrabutyl Titanate (TBT).

During the Electrospinning, there are various parameters need to be controlled to prepare a proper membrane, one of the most important one could be the support solution viscosity, it has to stay within its production-efficient range for making fibers.

The membranes have been characterized by several analyses: Fourier-transformed infrared spectroscopy(FT-IR), to confirm that the imidation process occurs, thermo-gravimetric analysis (TGA), to determine the amount of TiO2 in the membranes, and environmental scanning electron microscope (ESEM), to analyze the nanostructure of the membrane in order to determine the diameter of the fibers if they are in the proper size for capturing PFOA molecules.

According to the experiments, it is necessary to prepare two types of membranes, one with catalyst, one without, to establish role of catalyst in the degradation. HPLC analyses also were performed to determine the specific contribution involved in the removal of PFOA. By using these HPLC data, we can then derive the deflourination corresponding to each advanced oxidation process.

Table of Contents

Introduction

PFAS (poly- and perfluoroalkyl substances) are synthetic chemicals with unique properties that have made them essential in various industries, including firefighting, manufacturing of polymers, non-stick cookware, and water-resistant textiles. In the first Chapter, mostly focused on the structure of this substance which consist of a fluorine-saturated carbon chain and a functional group which is either a carboxylic acid (PFCAs) or a sulfonic acid (PFSAs). Among environmental pollutants, PFAS are known because of their persistence, toxicity, and potential to cause severe health problems. Exposure to these chemicals may cause dangerous diseases such as asthma, developmental allergies in children, liver damage, kidney dysfunction, and thyroid issues. In April 2024, the U.S. Environmental Protection Agency (EPA) finalized the first-ever national, legally enforceable drinking water standards for six PFAS compounds, including PFOA and PFOS. The new Maximum Contaminant Levels (MCLs) are set at 4.0 parts per trillion (ppt) for both PFOA and PFOS [1].

Because of their high chemical stability, PFAS resist traditional degradation processes, such as photolysis, hydrolysis, and biological decomposition. Consequently, scientists develop innovative methods for breaking them down. One of these methods is based on the use of Advanced Oxidation Processes (AOPs) that in the second Chapter I tried to provide all the useful information related to AOPs which rely on highly reactive radicals to degrade fluorinated molecules and actually the deflourination process takes place. Techniques using hydroxyl radicals, persulfate radicals, and photocatalysis have proven effective, often requiring UV light as an energy source. However, partial degradation often produces smaller PFAS molecules that retain harmful properties. Despite extensive research, there are still many questions remain about the precise mechanisms and pathways involved in PFAS breakdown, and conflicting explanations often arise from experimental studies.

The purpose of this study is to address these gaps by reviewing each mechanism behind PFAS degradation in advanced oxidation systems separately by using a specialized photoreactor and a polymeric membrane produced by electrospinning which in Chapter 4 and Chapter 5 all the membrane preparation steps have been mentioned, then the MilliQ-water containing PFOA and regents circulate for 1hr without UV lamp and 6hr under the UV lamp and taking sample each

hour to bring them for HPLC analysis, there the concentration of PFAS in each sample can be derived using the peaks area in each chromatogram. All the results regarding to different AOPs have been collected in Chapter 6.

This research is divided into six key chapters, each addressing a critical component of the study:

- Chapter 1: Introduces fluorinated compounds and how to distinguish them from non-fluorinated compounds, exploring their fundamental characteristics, industrial uses, and the risks they pose to ecosystems and human health.
- Chapter 2: Introducing advanced chemical degradation techniques that form the basis of the experimental work presented, their mechanism in PFOA degradation and their experimental insights
- Chapter 3: Details the materials, instruments, and analytical methods used for preparing membranes and testing water contamination.
- Chapter 4: Discusses the principles of electrospinning, focusing on the mechanics and variables that shape its outcomes.
- Chapter 5: Explains the fabrication of nano-fibers membranes and the diagnostic techniques employed to study their properties and characterization
- Chapter 6: Providing the information regarding to experimental setup and the results achieved from HPLC analysis for each individual AOP.

All experimental activities were carried out in the laboratories of the Polymer Engineering Group at the Department of Industrial Engineering, University of Padua.

Chapter 1

Definition, industrial uses, and the risks of PFAS

This chapter is concerned with the key features of the properties of fluorinated chemicals and their broad range of industrial applications, as well as their potential risks to the environment and human health, particularly PFOA. On PFAS regulation Over the years, informing world health organizations to limit the sister chemical's spread—and the chapter ends on a short discussion of this.

1.1 Definition of perfluoroalkyl substances

Fluorinated compounds in which a fluorine atom is bonded to a carbon atom are still a major category of chemical compounds widely used in industry and for scientific studies. A subgroup within the group exists called the per- and polyfluoroalkyl substances or PFAS. These have recently caused more concern due to their extensive use as well as persistence in the environment. PFAS are synthetic fluorine-containing organic chemical substances made up of a series of fluorine atoms attached to an alkyl group in order to convey typical chemical stability and resistance properties.

The Organisation for Economic Cooperation and Development defined PFAS in 2002 as having hydrophobic fully fluorinated alkyl chain (C4 to C16) and hydrophilic functional group. It was generalized to a group of products in 2021 more generally as a fluorinated organic chemical having a fully fluorinated methyl group (–CF_3 group) or fully fluorinated methylene group (–CF_2– group), wherein there are no attached hydrogen, chlorine, bromine, or iodine atoms. Expansion was done to make identification and classification easier for experts and government agencies [2]. By 2024 a more expansive approach was needed in the face of developing scientific knowledge and the need for regulation. Worldwide efforts by the U.S. Environmental Protection Agency (EPA), the European Chemicals Agency (ECHA), to name a few agencies involved, now focus on clustering

PFAS by similarity in persistence, mobility, and toxicity in the place of monitoring each and every chemical separately [3]. Up through 2025 the example databases in the U.S. EPA's CompTox Chemicals Dashboard include more than 14,000 unique structurally characterized PFAS though several million forms of PFAS are estimated theoretically including industrial derivatives as well as products of degradation. The continued rise in PFAS identification reflects the increasing need to effectively address the molecules in light of PFAS's far reaching dissemination in the environment as well as PFAS's expected impact on human health [4].

1.2 The structure and properties of PFAS

Per- and polyfluoroalkyl substances (PFAS) have certain physical and chemical properties that make them both industrially valuable and environmentally concerning. At the molecular level, what defines these compounds is their super strong carbon-fluorine bonds, having bond dissociation energies (BDE) in between 425 and 485 kJ/mol. The strength of this remarkable bond is due to the high electronegativity of the fluorine atom (4.0 according to Pauling scale) and significant orbital overlap between carbon and fluorine atomic orbitals.

Typical molecular structure of PFAS is shown in Figure 1.1. They are comprised of carbon chains of varying lengths where the hydrogen atoms have been replaced with fluorine atoms(tail) They can be linear or branched and often end with different functional groups (head) like carboxylic acids (-COOH) or sulfonic acids (-SO_3H). It is the unique arrangement of fluorine atoms around the carbon chain that imparts the helical three-dimensional structure, giving them their unique properties [5].

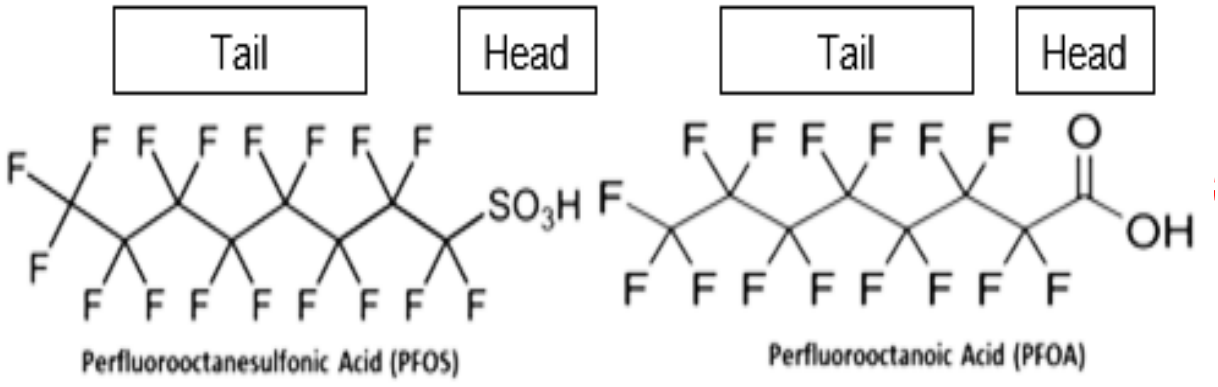

Figure 1.1. *Chemical structure of PFOS and PFOA*

1.2.1 Chemical and Thermal properties

PFAS are known for their extreme thermal and chemical stability. A theoretical measurement of stability to heat is vital for calculating environmental persistence for a given chemical substance and is termed thermal stability. PFASs (e.g. PFOA and PFOS) are previously known to be chemically- and thermally-stable molecules, and their breakdown and oxidation is reluctant.

This stability is primarily attributed to the strong C-F bond of their fluoroalkyl tail. As for the high temperatures required to decompose PFASs, scientific studies are still ongoing: exact figures differ, but temperatures over 1,000°C may be necessary to destroy PFASs in the soil. They are also highly resistant to chemical degradation, exhibiting stability in the presence of strong acids, bases, and oxidizing agents. While this stability is beneficial for industrial applications, contributes to their resistance in the environment. Due to the chemical stability of PFAS, it presents a serious obstacle to its conventional treatment methods [6][9].

The outstanding chemical stability of fluorinated compounds can be broadly explained by the strong carbon-fluorine (C-F) bond, the arrangement of fluorine atoms around the carbon, often referred to as the shielding effect, and the high electronegativity of fluorine. Usually, electron-rich chemical species, or nucleophiles, will be drawn towards the partial positive charge of carbon atoms. In principle, these nucleophiles could attach to the carbon, potentially displacing a fluorine atom, destabilizing the molecule. Nevertheless, the high atomic radius of fluorine when compared to hydrogen creates a steric shield surrounding the carbon atom with a much larger atomic radius, which blocks neighboring nucleophiles and prevents them from approaching the carbon. The spatial hindrance in addition to the strength of C−F bond leads to the molecule's resistance to chemical degradation [7].

Traditional abatement approaches, such as hydrolysis, cannot degrade PFAS as fluorine atoms cannot be removed from perfluorinated chains. Many PFAS compounds are resistant to oxidative degradation processes, which are based on the loss of electrons. Like PFAS are resistant to reductive degradation mechanisms that involve the acceptance of electrons. While fluorine has a high electron affinity, but the inability to accommodate more electrons into empty orbitals must also contribute to the chemical resilience of these substances [8].

1.2.2 Physical properties

Due to the low polarizability of the fluorine atoms, the weak intramolecular and intermolecular forces between the molecules of the PFASs leads to their relatively higher volatility, as well as lower boiling points than similar hydrocarbon compounds of the same molecular mass. PFAS are especially characterized by their surface properties, which may significantly decrease surface tension in aqueous and non-aqueous systems [5].

PFAS-treated surfaces have very low surface tension values between 15-20 mN/m, making them both water and oil repellant. PFAS makes a distinct fluorinated layer that is coexistent with the aqueous and organic layers when dissolved in water with an organic solvent as shown in Figure 1.2. Fluorinated compounds are unique in their amphiphilic nature — simultaneously hydrophobic and lyophobic — which is important for their use in numerous applications [10].

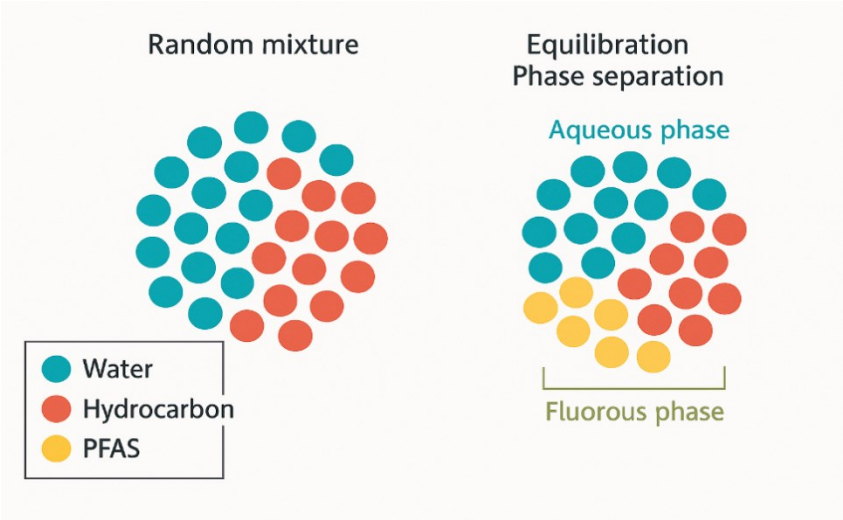

Figure 1.2. *Distinct fluorinated phase as dissolved in water with organic solvent*

PFAS display complex solubility profiles that are highly dependent on their molecular structure. Although the fluorinated tail is both hydrophobic and lyophobic, the polar functional groups like carboxylates or sulfonates can make the compounds water-soluble. As the chain length increases they become less soluble, which are surface active agents, therefore which form micelles at low concentrations.

1.3 Industrial uses and applications

Per- and polyfluoroalkyl substances(PFAS have been manufactured since the 1950s and used in a wide range of commercial products. These compounds are irreplaceable in numerous applications due to the unique properties conferred by fluorine atoms, such as high electronegativity and strength of the carbon-fluorine bond, including:

These compounds have been embraced by culinary technologies for the production of next-generation cooking surfaces with unprecedented release characteristics. Extractive industries employ them for improving operational efficacy. Their function in textile engineering is also central in the development of high-performance textiles, offering both aqueous and oleaginous resistance properties from everyday clothes to engineered technical fabrics [11].

The aviation and defense industries include these compounds in central mechanical components, and automotive engineering uses them to improve fuel systems. These are useful for cable and wire manufacturing due to their flame-retardant properties [12].

These compounds develop materials which are resistant to combustion and environmental degradation, finding critical applications in construction and building technology [13]. The electronics industry exploits their unique combination of insulating and moisture-repelling properties. The Dual Phase Change Material (DPCM) technology enhances the weather resistance of Solar Power Systems, which is highly efficient and sustainable, as renewable energy is a major driving force in the power grid sector. Figure 1.3 shows an overview of industrial use of per- and polyfluoroalkyl (PFAS) substances [14].

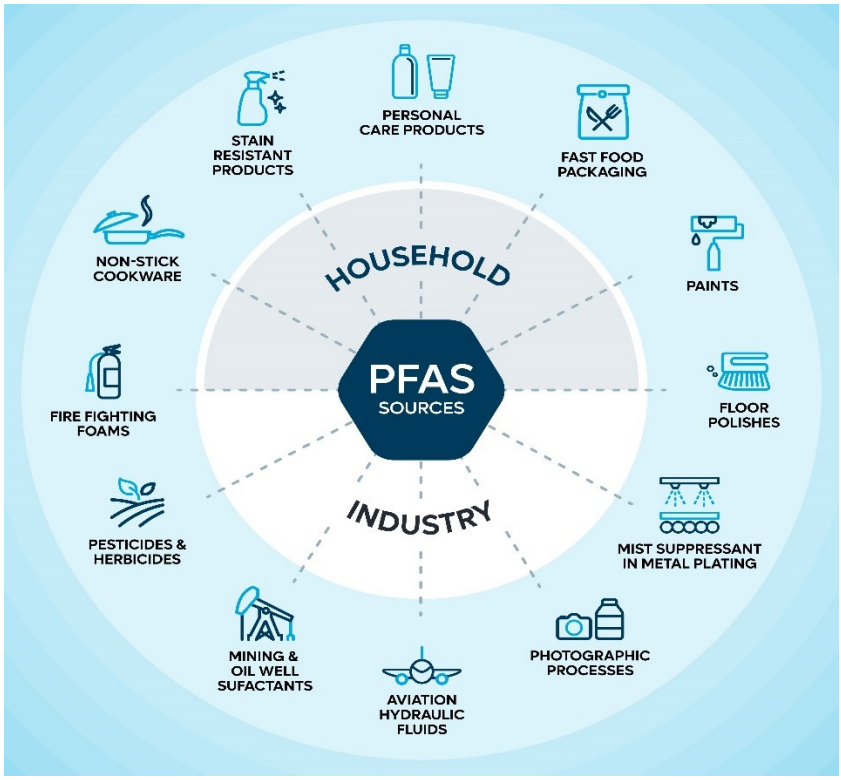

Figure 1.3. *Industrial applications of PFAS*

1.4 Human health and ecological concerns of PFAS

Per- and polyfluoroalkyl substances (PFAS) are known to affect human and ecological health following exposure by multiple pathways. Recent studies have pointed towards these compounds' potential carcinogenicity, mechanisms of which include inducement of oxidative stress and DNA repair interference. One of the most disturbing consequences of PFAS exposure is its immunotoxocity; PFAS exposure impairs antibody production and alters immune cell function, leading to increased susceptibility towards a multitude of infections [15].

Studies in reproductive health have shown that PFAS exposure can have substantial effects on ovarian function which impact hormone generation and fertility. The compounds have been associated with developmental problems, including low birth weight and developmental delays, as demonstrated in large epidemiological studies. Specific concern is their ability to cross the placental barrier and potentially affect fetal development.

PFAS exhibit complex bioaccumulation patterns and transfer through food webs in ecological systems. These studies have included examination of freshwater ecosystems, where these compounds can be transmitted from mother to offspring (fish and reptiles like turtles in particular seem to have been affected by PFAS affecting egg biochemistry). Due to factors like plant uptake, food products seem to be especially vulnerable to PFAS contamination, and agricultural systems are particularly at risk [9][16].

PFAS compounds are highly persistent in the environment, posing challenges to conventional treatment systems. Because these substances can be resistant to conventional water treatment processes, they can be chemically stable in extreme environmental conditions. This adaptation to travel across environmental compartments such as air, water and soil in which enables their abundance in ecosystems.

This will be a concern for health and ecological risks recognized increasingly around the world and regulatory interest in these areas is increasing. As a result, it is the international consensus of the PFAS compounds to be included in the Stockholm Convention, which classifies them as persistent organic pollutants that require monitoring and control. New studies are revealing more potential problems with these compounds, especially with their long-term impact on both human and environmental health [17].

1.5 Prevention and regulatory evolution of PFAS

Global pressure to prevent health and environmental effects of PFAS avoidance and polyfluoroalkyl substances (PFAS) has mounted. Prevention and regulation efforts now focus on preventing PFAS exposure at source, prioritizing drinking water protection. Following is a snapshot of the latest PFAS prevention and regulatory developments in significant regions of the world.The fluorinated chemicals were being produced in massive amounts during the 1940s, and chemical production and selling them to companies like DuPont was within the control of 3M. DuPont had been known for some time by the early 1950s to utilize the chemicals in its Teflon® product. As valuable to business as PFAS was, internal testing within 3M throughout the 1960s had already demonstrated their toxic biological properties, including mouse, rabbit, and dog test liver enlargement. Those findings weren't known outside the company for decades [18] [19].

The first regulatory shift came in 2001, when litigation forced the United States Environmental Protection Agency to officially recognize the toxic nature of perfluorooctanoic acid, or PFOA. Before the toxin was recognized, no PFAS chemicals were under serious regulatory control.

Greater incidence of pollution accidents and tougher scientific research led to PFOS being included as a Persistent Organic Pollutant (POP) in Annex B of the Stockholm Convention in 2009. A proposal for the EU REACH (Registration, Evaluation, Authorisation, and Restriction of Chemicals) system was also made to consider taking into account PFAS Persistent, Bioaccumulative, and Toxic (PBT) chemicals [20].

The EU is now home to some of the world's toughest legislation, with drinking water capped at no more than 0.1 µg/L for individual PFAS or 0.5 µg/L for all PFAS summed, as contained in the new Drinking Water Directive (2020/2184/EU) that went into effect in 2023.

Canada has gone ahead with similar guidelines. Health Canada's most recent advisory (2023) is to be at a level of 30 parts per trillion (ppt) for a combination of PFAS chemicals in potable water, more stringent than World Health Organization interim guidance. The Canadian approach is not merely government regulation but to education and promotion of clean water treatment technology, like high-pressure membranes and activated carbon filtration, to utilize to help eliminate PFAS from the water supply.

The US EPA finalized in April 2024 rules setting maximum contaminant levels (MCLs) for six of the most critical PFAS chemicals in drinking water:

- 4 slides for PFOA and PFOS
- 10 ppt for each GenX, PFBS, PFNA, and PFHxS

It is the first-ever US national drinking water standard for PFAS and will drive broad upgrades to drinking water treatment systems [21].

Worldwide, the WHO continues to establish drinking water quality standards. Their new guideline in 2022 proposes a provisional guideline level for PFOA and PFOS together in drinking water of 100 ng/L (100 ppt), but they acknowledge that lower levels are preferable due to the mounting evidence of injury at even very low concentrations. Authors like Southerland and Birnbaum quote precautionary policy action as of top priority, following more recent PFAS alternatives, referred to as "short-chain PFAS" in general parlance, already showing persistence and potential dangers.

Meanwhile, EU-level PFAS ban proposals have been delayed in the EU until 2024 to prohibit more than 10,000 PFAS chemicals under the REACH by 2025, a historic "group approach" regulation rather than dealing with each chemical separately [22].

Chapter 2

Advance Oxidation Process (AOPs)

In this chapter, Advanced Oxidation Processes (AOPs) are proposed for the abatement of persistent pollutants, specifically targeting fluorinated compounds such as PFOA in water systems. Given the chemical resilience of PFOA, the study employs a variety of degradation methods, including Photo-Fenton reactions, Photocatalysis, persulfate radical oxidation and using Metal-organic frameworks (MOFs) to investigate their effectiveness on breaking down the PFOA molecules, separately. Each technique was selected and utilized to address the challenges posed by the compound's strong resistance to conventional treatment methods.

2.1 Theoretical backgrounds of using AOPs

Perfluorooctanoic acid (PFOA) is a polymerizable organic chemical substance, which is gifted with extremely rigid chemical stability due to the inert nature of its carbon-fluorine (C–F) bonds. Such stability makes very difficult to remit water remediation treatment. Conventional treatment methods such as adsorption, coagulation, and nanofiltration are not applicable for PFAS removal in the majority of instances and always produce secondary pollution. This limitation has been surpassed by stronger focus on Advanced Oxidation Processes (AOPs) that employ extremely reactive free radicals—e.g., hydroxyl and sulfate radicals—to oxidize long-lived pollutants.

AOPs employ hydroxyl radicals and other in-situ generated oxidizing species to oxidize contaminants and were first envisioned in the late 1980s. AOPs have the advantage of being able to work at ambient temperatures effectively. To the degradation of PFOA, radicals are attacking the carboxylic part of the molecule, activating a series of events that ultimately result in mineralization of the compound to carbon dioxide (CO_2) and fluoride ions (F^-). Because radicals possess short residence times and are of high redox potential, they are ideally equipped to shatter the solid molecular structure of PFAS compounds [23].

Current studies have investigated thermal and photo-induced decompositions for perfluorinated carboxylic acid mechanisms to confirm that hot heat and UV irradiation by light can synergistically

cause cleavage of C-F bonds and trigger the destruction of PFAS. On this foundation, UV lamps are routinely part of experimental designs when optimizing oxidative reactions.

Structural dependence of UV/electrochemical PFAS defluorination efficiency has also been studied. Findings show that breakdown rates are highly reliant on molecular structure and that simpler structures have greater breakdown rates [24].

Complementary processes have been designed in parallel to AOPs, such as application of novel magnetic fluorinated carbon nanotube-based adsorbents for pre-concentration of PFAS from water before degradation. Parallel treatment processes have also been designed; for example, synergy between aerated electrocoagulation and peroxi-coagulation modified has been demonstrated to enhance mineralization of PFOA, through in situ release of coagulants that interact with oxidative radicals to optimize treatment performance [25].

Another potential application is the use of electrospun bimetallic metal-organic framework (MOF) lignin-based nanofibers as solar-light-driven catalysts to activate peroxymonosulfate. It integrates solar power with solar-light-driven catalytic AOPs for effective and sustainable PFAS degradation.

While such advances are to be encouraged, caution is needed. Hydroxyl radical-mediated AOPs may yield shorter and potentially more mobile PFAS species if the mineralization reactions are not complete. System parameters should therefore be tuned with maximum caution to achieve complete mineralization and avoid unanticipated environmental effects [26]

2.2 Heterogeneous Photocatalysis

Heterogeneous photocatalysis has become an important AOPs technique, mainly for the removal of organic contaminants in water and wastewater. Conventional photocatalytic oxidation (PCO) systems employ a solid semiconductor material (such as titanium dioxide (TiO_2)) that becomes activated under light irradiation to generate reactive oxygen species (ROS) which degrade contaminants. In this section, heterogeneous photocatalytic processes are examined, covering their reactive mechanisms, critical parameters, and applications, particularly in the context of water treatment and disinfection.

2.2.1 Fundamental Principles of Heterogeneous Photocatalysis

Heterogeneous photocatalysis is based on the light-absorption and electron-hole pairs (e^-/h^+) generation capability of semiconductors. Upon light irradiation of energy equal to or larger than the bandgap of the semiconductor (3.2 eV for anatase TiO_2), electrons in the valence band of TiO_2 are excited to the conduction band, leading to the formation of holes in the valence band. Charge carriers photogenerated participate in redox reactions at catalyst surface.

Oxygen molecules are reduced to superoxide radicals ($O_2^{-}\cdot$) by conduction band electrons as seen in reaction 2.1 while holes oxidize water or hydroxide ions to generate hydroxyl radicals ($OH\cdot$). Both radicals are very reactive and non-selective and attack organic pollutants breaking them down to smaller enzymes(usually) biodegradable molecules or fully mineralizing them to CO_2 and H_2O, creating positive charges or holes in the valence band and negatively charged electrons in the conduction band. The excitons are important in the redox reactions that take place on the surface of the semiconductors [28]. The redox reactions are illustrated in figure 2.1.

$$e^- + O_2 \rightarrow O_2^{\cdot -} \quad (2.1)$$

$$h^+ + H_2O \rightarrow OH\cdot + H^+ \quad (2.2)$$

$$h^+ + OH^- \rightarrow OH\cdot \quad (2.3)$$

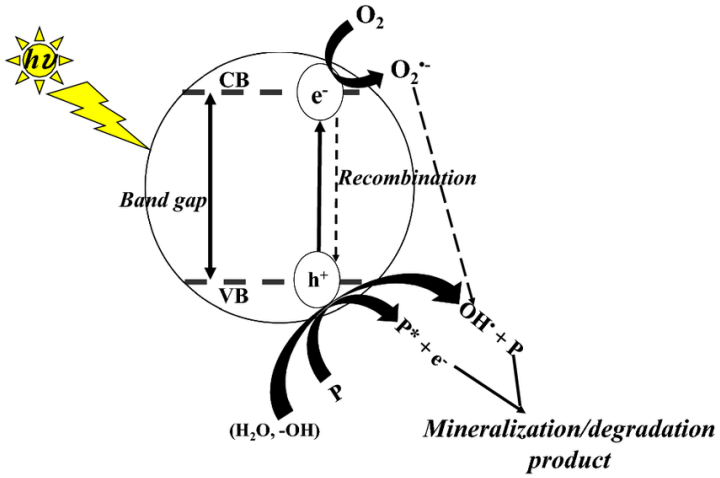

Figure 2.1. *Representation of redox reactions*

Heterogeneous photocatalysis is governed by multiple factors including the bandgap energy of the catalyst, the recombination rate of the electron-hole pairs, and the availability of reactive species. TiO_2 has a bandgap of 3.2 eV, so it is only active under ultraviolet light. But since UV is only a small fraction of the sun's light, TiO_2 has been doped with impurities, such as vanadium, nitrogen or carbon, in order to extend its activity into the visible region.

2.2.2 Mechanism of TiO_2 Photocatalytic Degradation

The use of titanium dioxide (TiO_2) for the photocatalytic degradation of organic pollutants is widely known, taking advantage of the semiconductor characteristic of this material to use reactive species for the oxidation and mineralization of pollutants. This mechanism occurs when TiO_2 is irradiated by light energy equal to or greater than its bandgap energy (~3.2 eV for the anatase phase). When photons are absorbed, electrons (e^-) in the valence band (VB) are excited to the conduction band (CB), generating electron-hole pair. This initial step can be expressed as:

$$TiO_2 + h\nu \rightarrow e^-_{CB} + h^+_{VB} \tag{2.4}$$

This population of charge carriers is fundamental to the photocatalytic mechanism. However, one of the largest hurdles is the recombination of electron-hole pairs, which waste energy as heat or light without performing a chemical reaction. There are several strategies to minimize

recombination and promote the charge carrier participating in the surface reactions, enhancing photocatalytic efficiency.

Photogenerated holes in the valence band have potent oxidative properties, allowing them to react with adsorbed water molecules or surface hydroxyl groups (OH^-) to form hydroxyl radicals ($OH^{\cdot}$), one of the most powerful oxidizing agents in photocatalysis. These reactions might be described as:

$$Ti^{IV}{-}OH^- + h^+_{VB} \rightarrow Ti^{IV}{-}OH^{\cdot} \quad (2.5)$$

$$Ti^{IV}{-}H_2O + h^+_{VB} \rightarrow Ti^{IV}{-}OH^{\cdot} + H^+ \quad (2.6)$$

At the same time, the electronegative electrons in conduction band are highly reductive and could react with O_2, adsorbed on the TiO_2 surface, leading to superoxide radicals formation ($O_2^{\cdot -}$). This step serves a dual purpose — it not only mitigates electron-hole recombination, but also aids in the formation of a new set of reactive oxygen species (ROS):

$$O_2 + e^-_{CB} \rightarrow O_2^{\cdot -} \quad (2.7)$$

Superoxide radicals may proceed to react with protons to form hydrogen peroxide (H_2O_2), which then decomposes to generate more hydroxyl radicals:

$$O_2^{\cdot -} + 2H^+ + e^-_{CB} \rightarrow H_2O_2 \quad (2.8)$$

$$H_2O_2 + e^-_{CB} \rightarrow OH^{\cdot} + OH^- \quad (2.9)$$

In the various reactive oxygen species, hydroxyl radicals ($OH^{\cdot}$) are the major species involved in the degradation of organic contaminants that are adsorbed on TiO_2 surface. The degradation process typically begins with the adsorption of the organic compound (S) on the TiO_2 surface. Subsequently, oxidation would be achieved either by means of direct hole transfer or radical attack via the hydroxyl radicals [29]. The overall reactions can be summarized as follows:

$$Ti^{IV}-S+h_{VB}^{+}\rightarrow Ti^{IV}+Oxidized\ Intermediates\rightarrow CO_2+H_2O \quad (2.10)$$

$$Ti^{IV}-S+\ OH\cdot\rightarrow Ti^{IV}+Oxidized\ Intermediates\rightarrow CO_2+H_2O \quad (2.11)$$

The total mineralization process of organic pollutants leads to the generation of carbon dioxide (CO_2), water (H_2O) and inorganic ions such as F^- ions in the case of perfluorinated compounds. As a particular example of this mechanism, we report on the photocatalytic degradation of perfluorooctanoic acid (PFOA), a persistent organic pollutant. The degradation process includes multiple steps, starting with the photogenerated holes that destabilize PFOA and lead to the formation of perfluorocarboxylic radicals. In the next step, the radicals undergo decarboxylation to afford perfluoroalkyl radicals which are then attacked by hydroxyl radicals leading to unstable alcohols. The alcohols are then eliminated as HF and hydrolyzed to shorter-chain PFCAs. This progresses until the pollutant has been entirely mineralized to CO_2 and F^- ions. The main reactions in this pathway are:

$$C_7F_{15}COO^-+\ h_{VB}^{+}\rightarrow\ C_7F_{15}COO\cdot \quad (2.12)$$

$$C_7F_{15}COO\cdot\ \rightarrow C_7\ F_{15}^{\cdot}+\ CO_2 \quad (2.13)$$

$$C_7\ F_{15}^{\cdot}+\ OH\cdot\rightarrow C_7F_{15}OH \quad (2.14)$$

$$C_7F_{15}OH\rightarrow C_6F_{13}COF+HF \quad (2.15)$$

$$C_6F_{13}COF+H_2O\ \rightarrow C_6F_{13}COOH+HF \quad (2.16)$$

The photocatalytic degradation process primarily comprises five steps: (1) diffusion of the reactants to the TiO_2 surface, (2) adsorption of the reactants on the surface of TiO_2, (3) surface reactions between reactive oxygen species and adsorbed pollutants, (4) desorption of products from the surface of TiO_2, and (5) diffusion of products away from the surface. Each of these steps plays a critical role in determining the overall efficiency of the photocatalytic process [30].

2.3 Photo-Fenton process

The Photo-Fenton process represents an advanced class of the classical Fenton reaction, which leads to the production of hydroxyl radicals ($OH^{\cdot}$) under the action of ultraviolet (UV) light. Compared with this, it has recently become a promising route for degrading recalcitrant organic

pollutants in particular per- and poly-fluoroalkyl substances (PFAS). In this section, the mechanisms, critical parameters, and the practical applications of the Photo-Fenton process has been studied with a special emphasis on the application of this process for PFAS remediation.

2.3.1 Discovery and Fundamental Chemistry

Since the initial discovery of the Fenton reaction in 1876 by John H. H. Fenton, this particular catalytic decomposition of hydrogen peroxide (H_2O_2) using transition metals, such as ferrous ions (Fe^{2+}), has become commonly used as a component of many environmental processes. This reaction generates hydroxyl radicals ($OH^{\cdot}$) which are powerful oxidants (redox potential = 2.7 V), initially used in organic synthesis and analytical chemistry, the Fenton reaction has been widely studied since 1930 for environmental applications, especially for the treatment of organic pollutants.

At the center of the traditional Fenton reaction (reaction 2.17) is the reaction between ferrous ions and hydrogen peroxide to generate hydroxyl radicals, ferric ions (Fe^{3+}), and hydroxide ions. As indicated in the reaction (2.18), the Photo-Fenton process achieves reduction of ferric ions back to ferrous ions through the action of UV light thereby enabling a continuous cycle of radical generation. Photochemical improvement augments Photo-Fenton process from the previous one with a notable rise in hydroxyl radicals production, paving a way for faster pollutant degradation.

Basic Fenton Reaction: $Fe^{2+} + H_2O_2 \rightarrow Fe^{3+} + OH^- + OH^{\cdot}$ (2.17)

Photo-Fenton Reaction: $Fe^{2+} + H_2O_2 + h\upsilon \rightarrow Fe^{3+} + H^+ + OH^{\cdot}$ (2.18)

2.3.2 Mechanisms of PFAS Degradation

In the Photo-Fenton method, the increasing generation of hydroxyl radicals facilitates the degradation of PFAS by attacking the pollutant molecules through different oxidation mechanisms. Hydroxyl radicals affect PFAS predominantly via hydrogen atom abstraction, by adding to unsaturated carbon-carbon bonds, or by single-electron oxidations. "Because the strongest bonds in PFAS molecules are carbon-fluorine bonds, a lot of the initial degradation is at

the carboxylic head group, and the molecule will systematically fall apart. UV light plays an important role in the involved chemistry, which promotes the continuously regeneration of Fe^{2+} from Fe^{3+}, ensuring significant production of radicals and retaining the oxidation reaction efficiency [31].

2.3.3 Key Parameters Influencing Performance

There are several interrelated process parameters influencing the efficiency of the Photo-Fenton process. The pH of the solution is one of the most important factors. A reaction pH of 2 -- 4 is ideal; when pH is too high, Fe^{3+} precipitates out of solution as ferric hydroxide ($Fe(OH)_3$), hence becoming unavailable to react. On the other hand, very low pH values hampered the reduction of Fe^{3+} to Fe^{2+} while possibly creating too many H^+ ions, which are harmful for hydroxyl radical production. At pH levels optimal for these reaction conditions, hydrolysis of Fe^{3+} forms $Fe(OH)^{2+}$, a species with a wide absorption range in the UV spectrum which also promotes this reaction.

Another key variable is the concentration of hydrogen peroxide, which needs to be finely tuned. However, excess H_2O_2 can cause free radicals to recombine, which lowers the radical species concentrations and limits their interaction with the contaminants to be degraded. Another key factor is temperature, with 20–30°C being the optimal range, since high temperatures may lead to hydrogen peroxide volatilization, decreasing process efficiency.

Wavelength and intensity of the UV light source largely affect the reaction and the wavelength at the range of 180–400 nm is most active to perform the reactions. Thus, it can lead to the production of more hydroxyl radicals and the recycle of Fe^{2+} ions, which in turn promote the overall degradation reaction [31].

2.3.4 Advantages and disadvantages of Photo-Fenton

Compared to the traditional Fenton process, the Photo-Fenton process has some advantages that enable it to be a competent option for the degradation of the recalcitrant pollutants, namely PFAS. Ultraviolet (UV) light enhances the generation of hydroxyl radicals and regenerates Fe^{2+} ions from Fe^{3+} ions to decrease the consumption of reagents. This facilitates a faster degradation of the pollutants and a lower consumption of hydrogen peroxide and iron precursors.

Furthermore, the Photo-Fenton process works well at ambient temperatures, being thus energy saving. It can break down a wide range of organic pollutants, including many that are resistant to other methods, highlighting its versatility and efficiency [32].

The Photo-Fenton process has many advantages, but faces challenges that need to be resolved for its further application. A major one is the precipitation of iron as ferric hydroxide at high pH that decreases its catalytic availability. Another issue is the dosing of hydrogen peroxide, since an excess of this reactive species can cause radical recombination that eventually reduces the reaction efficiency. Moreover, the AOP methods do not provide selective removal of PFAS (e.g., generating harmful products) because of the stable carbon–fluorine bonds in PFAS molecules and hence, generation of additional mineralization (further methods) may be needed for complete degradation.

2.3.5 Experimental Insights

Several experimental studies have been conducted to optimize the Photo-Fenton process to treat PFAS by varying concentration of reagents and operational parameters. For instance, it has been found that the most effective degradation results under optimal conditions could be achieved by using 25 mg/L of Fe^{2+} and 100 mg/L of H_2O_2.The additional results from these experiments must consider the improvement of the efficiency of the removal rate by applying Photo-Fenton with advanced oxidation processes or in a combination of Photo-Fenton with other oxidation processes, including the use of this method with biological methods or others [31].

The Photo-Fenton process is one of the most promising advanced oxidation processes to date for degrading PFAS and other recalcitrant contaminants. This method offers a scalable and sustainable solution for environmental remediation by harnessing the synergistic effects of UV light, iron catalysts, and hydrogen peroxide. The current status of this research outlines the potential obstacles for application, predominantly related to iron precipitation and hydrogen peroxide administration, although the development of this methodology is a continuous one and the opportunities for its incorporation in water treatment technologies are broad [32].

2.4 Mechanism of Persulfate-Based Degradation of PFOA

Persulfate ($S_2O_8^{2-}$) activation for the degradation of perfluorooctanoic acid (PFOA) is a type of advanced oxidation process (AOP), in which highly reactive sulfate radicals ($SO_4^{\cdot-}$) are produced to oxidize and mineralize recalcitrant organic compounds. Persulfate, a strong proton and oxidant with high redox potential, needs to be activated to generate sulfate radicals, the main reactive species, accounting for PFOA degradation. Persulfate can be activated by a number of different methods including thermal, UV, and chemical activation and transition metal catalysis. The general activation mechanism consists of the cleavage of the peroxide bond in persulfate, resulting in two sulfate radicals represented in the following equations:

$$S_2O_8^{2-} + \textit{Activation Energy} \rightarrow 2\ SO_4^{\cdot-} \tag{2.19}$$

Thermal activation, for instance, involves heating persulfate to break the peroxide bond, producing sulfate radicals. Similarly, UV activation utilizes light energy to cleave the persulfate bond, while transition metal ions, such as Fe^{2+}, activate persulfate through a redox reaction, generating sulfate radicals alongside metal oxidation. These activation methods are critical for initiating the degradation process, as sulfate radicals are highly reactive and capable of oxidizing a wide range of organic pollutants, including PFOA.

The degradation pathway of PFOA begins with the attack of sulfate radicals on the perfluorooctanoic acid molecule. Sulfate radicals abstract electrons from PFOA, leading to the formation of perfluorocarboxylic radicals ($C_7F_{15}COO^{\cdot}$). These radicals undergo decarboxylation, producing perfluoroalkyl radicals ($C_7F_{15}^{\cdot}$). The degradation process can be described through a series of oxidative reactions [33]. Initially, sulfate radicals attack the carboxyl group of PFOA, forming perfluorocarboxylic radicals, as shown in the following reaction:

Thermal activation, for example, entails heating the persulfate to cleave the peroxide bond, generating sulfate radicals. UV activation works by cleaving the persulfate bond using light energy, and transition metal ions (e.g., Fe2+) activate persulfate using a redox reaction that results in sulfate radical and metal oxidation. These activation methods are essential for the beginning of the process of degradation, as sulfate radicals are extremely reactive and can oxidize a broad spectrum of organic contaminants, including PFOA.

PFOA degradation pathway commences with the attack of sulfate radicals on perfluorooctanoic acid molecule. When sulfate radicals abstract electrons from PFOA , perfluorocarboxylic radicals ($C_7F_{15}COO^{\cdot}$) are produced. These radicals are decarboxylated, yielding perfluoroalkyl radicals ($C_7F_{15}^{\cdot}$). The degradation process is a complex process and can be illustrated through a series of oxidative reactions. The first step involves the attack of sulfate radicals on carboxyl groups of PFOA to form perfluorocarboxylic radicals (the reaction is shown below).

$$C_7F_{15}COO^- + SO_4^{\cdot-} \rightarrow C_7F_{15}COO^{\cdot} + SO_4^{2-} \quad (2.20)$$

These perfluorocarboxylic radicals ($C_7F_{15}COO^{\cdot}$) then decarboxylate, releasing carbon dioxide (CO_2) and generating perfluoroalkyl radicals ($C_7F_{15}^{\cdot}$), as represented by the equation:

$$C_7F_{15}COO^{\cdot} \rightarrow C_7F_{15}^{\cdot} + CO_2 \quad (2.21)$$

Perfluoroalkyl radicals ($C_7F_{15}^{\cdot}$) subsequently react with sulfate radicals as well as other reactive moieties, producing corresponding perfluoroalkyl alcohols ($C_7F_{15}OH$) including potentially unstable intermediates. The main intermediates are further degraded through a serial of other reactions such as, HF elimination and hydrolysis to yield shorter-chain perfluorocarboxylic acids (PFCAs). Further, perfluoroalkyl radical reacts with sulfate radicals ($SO_4^{\cdot-}$) to form perfluoroalkyl sulfate intermediates, followed by hydrolysis to give perfluoroalkyl alcohols in the reactions:

$$C_7F_{15}^{\cdot} + SO_4^{\cdot-} \rightarrow C_7F_{15}COSO_3^- \quad (2.22)$$

$$C_7F_{15}COSO_3^- + H_2O \rightarrow C_7F_{15}OH + HSO_4^- \quad (2.23)$$

The perfluoroalkyl alcohols ($C_7F_{15}OH$) then undergo HF elimination, producing perfluoroacyl fluorides ($C_6F_{13}COF$), as represented by the equation:

$$C_7F_{15}OH \rightarrow C_6F_{13}COF + HF \quad (2.24)$$

These perfluoroacyl fluorides are subsequently hydrolyzed to form shorter-chain perfluorocarboxylic acids ($C_6F_{13}COOH$), as shown in the following reaction:

$$C_6F_{13}COF + H_2O \rightarrow C_6F_{13}COOH + HF \quad (2.25)$$

The degradation process continues stepwise that each cycle results in shorter-chain PFCAs. This continues until complete mineralization of PFOA to the end products, carbon dioxide (CO_2), water (H_2O), and fluoride ions (F^-).

The degradation of PFOA by persulfate is a complex process that depends on many factors. The solution pH is a critical factor, given the reactivity of sulfate radicals is highly dependent on the pH of the solution and often achieves optimal activity in acidic or neutral conditions. Temperature is another key aspect in this process, because an increase in the temperature favors persulfate activation and also promotes radical production. Another important factor is the concentration of persulfate, where more persulfate guarantees enough radical production to completely degrade contaminants completely. Moreover, the competition between coexisting substances in the water matrix (organic and inorganic matter) for reactive species formation can compromise the degradation efficiency.

Persulfate-based AOPs have some advantages over classical hydroxyl radical-based systems Compared to hydroxyl radicals (E^0 = 1.8–2.7 V), sulfate radicals possess a much higher oxidative potential (E^0 = 2.5–3.1 V), which play a significant role in degrading highly stable compounds such as PFOA. In addition, it should be noted that compared to hydrogen peroxide widely used in hydroxyl radical-based AOPs, persulfate is more stable in water. Nevertheless, there are several limitations that must be overcome, such as toxic byproduct formation and the quest for activation strategies, to accelerate this process towards scalable applicability [34].

Tetrazoles, thiols, methyls, acetals, and other functionalized amides are all good groups that can be functionalized for treating resistant organic pollutants, including PFOA. It holds a great potential for wastewater treatment and environmental restoration due to its efficiency in degrading recalcitrant pollutants. Nevertheless, the potential environmental concerns related to persulfate and its byproducts should be adequately examined to confirm its sustainable deployment. In particular, UV-Oxidation or Catalysis of Transition Metals based activation of persulfate have been well-established AOPs to achieve high degradation efficiencies against pollutants like PFOA. Previous researches have confirmed that macrolide antibiotics could be effectively degraded using persulfate activated by gamma radiolysis, indicating that this technology may be also applied for remediating complex matrices of water [35].

2.5 Mechanism of PFOA Degradation using MOF(UIO-67/TiO_2)

Metal-organic frameworks (MOFs) consist of metal clusters connected by organic ligands to provide high surface area and modifiable functionality. One of them, UIO-67 (Universitetet I Oslo-67), is a zirconium-based MOF with excellent chemical and thermal stabilities. After being coupled with TiO2 nanorods which serve as excellent photocatalysts, the composite (UIO-67/TiO2) exhibits synergetic effect to improve the degradation of PFOA.

Removing PFOA by UIO-67/TiO_2 includes several crosslinking processes: PFOA adsorption, photocatalytic reaction activation, and radical formation and cleavage of fluorine chains [27].

2.5.1 Adsorption of PFOA on UIO-67/TiO_2

Owing to its high surface area and porous structure frameworks, PFOA can be adsorbed easily with electrostatic forces between the negatively charged carboxylate groups of PFOA and the positively charged Zr^{4+} in the UIO-67. In addition, hydrophobic interaction existed between the fluorinated carbon chain of PFOA and the aromatic rings of BPDC linker. Adsorption is further promoted by the hydroxyl-rich surface of the TiO_2 nanorods, which can establish hydrogen bonds with PFOA [32].

2.5.2 Photocatalytic Activation Under UV/Visible Light

When TiO_2 is exposed to UV or visible light, the electron-hole pairs (e^-/h^+) are formed. The electrons (e–) in the conduction band (CB) reduce oxygen molecules to form superoxide radicals ($O_2^{\cdot-}$), and the holes (h+) in the valence band (VB) oxidize the water or hydroxyl groups to generate hydroxyl radicals ($OH^{\cdot}$). The UIO-67 framework facillitates the charge separation by serving as the electron sink, which suppresses the electron-hole recombination and prolongs the lifetime of ROS.

2.5.3 Radical-Mediated Degradation of PFOA

The generated radicals, like hydroxyl and superoxide radicals, initiate the breakdown of PFOA through a series of reactions. First, the carboxyl group (–COO^-) on PFOA is cleaved in a process called decarboxylation, which creates a perfluoroheptyl radical($C_7F_{15}^{\cdot}$). After that, more radical attacks happen, which slowly shorten the carbon chain by breaking C–C bonds, creating shorter

perfluorinated compounds such as $C_6F_{13}^-$ and $C_5F_{11}^-$. In the end, the tough C–F bonds break thanks to electron transfers from zirconium sites or captured holes, which releases fluoride ions (F^-) and completing the defluorination process.

2.5.4 Role of UIO-67 in Enhancing Degradation

The zirconium nodes in UIO-67 act as Lewis acid sites, which helps break down the C–F bonds. The porous design of UIO-67 traps PFOA molecules, making them more concentrated and boosting their interaction with reactive elements. The charge transfers between TiO_2 and UIO-67 also improve the photocatalytic efficiency, so the composite performs better than each part on its own [36].

2.5.5 Degradation Pathway and Byproducts

The degradation of PFOA follows a stepwise pathway. Initially, PFOA ($C_7F_{15}COOH$) is converted into perfluoroheptanoate ($C_7F_{15}COO^-$). Decarboxylation then occurs, producing a perfluoroheptyl radical ($C_7\ F_{15}^{\cdot}$) and releasing CO_2. Further degradation leads to the formation of shorter-chain perfluorinated intermediates such as $C_6F_{13}^-$ and $C_5F_{11}^-$. Ultimately, complete mineralization occurs, yielding CO_2, fluoride ions (F^-), and water (H_2O).

$$C_7F_{15}COO^- + OH\cdot \rightarrow C_7\ F_{15}^{\cdot} + CO_2 + OH^- \quad (2.26)$$

$$C_7\ F_{15}^{\cdot} + OH\cdot \rightarrow C_6\ F_{13}^- + CF_2^{\cdot} + HF \quad (2.27)$$

$$C_6\ F_{13}^- + OH\cdot \rightarrow C_5\ F_{11}^- + CF_2^{\cdot} + HF \quad (2.28)$$

$$C_n\ F_{2n+1}^- + Zr_4^+ \rightarrow C_n\ F_{2n-1}^- + 2F^- + Zr_4^+ \quad (2.29)$$

$$C_7F_{15}COOH \rightarrow 7\ CO_2 + 15F^- + H_2O \quad (2.30)$$

2.5.6 Factors Affecting Degradation Efficiency

The effectiveness of PFOA degradation by UIO-67/TiO_2 is influenced by a number of parameters. The pH of the solution is important because neutral or alkaline conditions promote the formation of radicals, whereas acidic conditions increase the adsorption of PFOA. Charge carrier generation is strongly impacted by light intensity, with higher exposure to UV or visible light resulting in higher photocatalytic activity. To enhance degrading efficiency, the catalyst loading needs to be tuned, especially the ratio of UIO-67 to TiO_2. Furthermore, coexisting ions can compete with PFOA for adsorption sites, which could prevent breakdown [37].

Chapter 3

Materials and Instruments

In this chapter, we provide details of materials and methods utilized in the synthesis of nanostructured membranes and chemical agents involved in the PFOA degradation experiments. It also describes the equipments needed for material characterization.

3.1 Materials

Polyvinylpyrrolidone (PVP), polyimide (PI) and polysulfone are all polymeric materials used in this research for the design of membranes for PFOA capture and degradation. These membranes are further synthesized from the following chemicals. This research focuses on membranes which need to possess dual functionalities: First, the developed membranes should have excellent mechanical strength to stand up to the continuous flow of water and second, they have high catalytic efficiency to facilitate optimal photocatalysis for the process discussed in Chapter 2. Thus, a new strategy for preparing membranes possessing both photocatalytic activity and structural integrity is implemented based on simultaneous deposition on a cylindrical collector. This approach depends on concurrent electrospinning of two different solutions, one of which provides mechanical support, while the other supplies catalytic function. Both solutions consist of solid compounds dissolved in a solvent by stirring at room temperature before electrospinning.
The membranes that only contain the structural part has to be prepared to observe the influence of photocatalysis on degradation since we will be investigating the effect of different advanced oxidation processes (AOPs) on PFOA degradation.

3.1.1 Chemical properties of structural solution

The polyimide (PI) matrix plays a key role in the membrane, offering mechanical strength, thermal stability, and chemical resistance. Polyimide is synthesized as a precursor, an

intermediate compound called polyamic acid (PAA), then heat treated to achieve the final PI structure. The key reagents for this process are described in below.

I. 4,4'-Oxydianiline (ODA)

4,4'-Oxydianiline (ODA) is an aromatic diamine and is one of the main reactants used in polyamic acid synthesis. It is an ether-derived aniline, which is a colorless and grainy solid. ODA forms the polyamic acid intermediate by reacting with the dianhydride as a crosslinking agent. Its ether linkage gives flexibility to the polymer chain leading to elastic and flexible final polyimide membrane. Safety-wise, it is considered toxic and carcinogenic, meaning the chemist should be concerned when working with it, so one should use it in a fume hood and wear some personal protective equipment (PPE).

Table 3.1 *Properties of 4,4'-Oxydianiline*

	Chemical formula	$C_{12}H_{12}N_2O$
	Molecular weight [g/mol]	200.24
	Density [kg/m3]	~1150-1200
	Melting point [°C]	186-189
	CAS Number	101-80-4
	Pictograms	

II. Pyromellitic Dianhydride (PMDA)

Pyromellitic dianhydride (PMDA) is a white crystalline solid and the second essential reactant in polyamic acid synthesis. It is the dianhydride form of a carboxylic acid and is widely used in the production of high-performancepolymers.

The polyamic acid intermediate is formed by the reaction of PMDA with ODA. The rigid aromatic structure enhances the thermal stability and mechanical strength of the resulting polyimide membrane. Like ODA, PMDA is toxic and carcinogenic, necessitating strict safety protocols during handling and storage.

Table 3.2 *Properties of Pyromellitic Dianhydride*

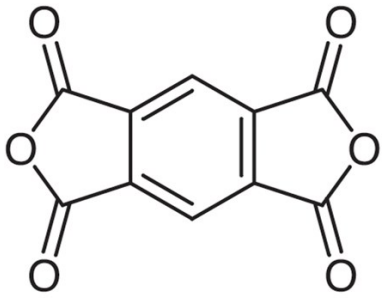	Chemical formula	C10H2O6
	Molecular weight [g/mol]	218.12
	Density [kg/m3]	~1689
	Melting point [°C]	286–289
	CAS Number	89-37-2
	Pictograms	

III. Dimethylformamide (DMF)

Dimethylformamide (DMF) is the solvent used to dissolve ODA and PMDA, facilitating their reaction to form polyamic acid. This is an entirely colorless liquid with a subtle amine associated smell that has become very popular in chemical synthesis due to excellent solvation properties. Since DMF is a uniform medium for reacting ODA with PMDA, the polyamic acid intermediate is formed efficiently. Its high water solubility also enables ease of removal in washing steps. DMF is harmful and has reproductive toxicity. Appropriate PPE should be worn along with performing work in a well-ventilated area to limit exposure.

Table 3.3 *Properties of Dimethylformamide*

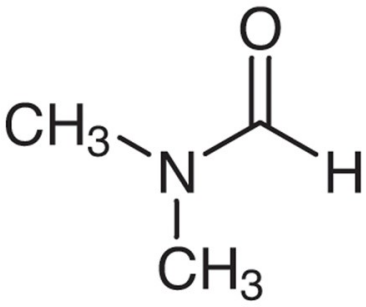	Chemical formula	C_3H_7NO
	Molecular weight [g/mol]	73.09 g/mol
	Density [kg/m3]	944
	Boiling point [°C]	153
	CAS Number	68-12-2
	Pictograms	

3.1.2 Chemical properties of catalytic solution

The catalytic solution has a modified membrane that contains active catalytic sites on a micro-scale which can be utilized for degradation of the pollutant. In the end, the solution of the catalyst precursor was then mixed with polymeric support. This catalytic solution acts to integrate active catalytic sites into the membrane for implementation in pollutant degradation. The catalyst precursor and the polymeric support are prepared separately and combined.

I. *Polyvinylpyrrolidone (PVP)*

The catalyst support material is polyvinylpyrrolidone (PVP), a water-soluble polymer. It is a white electrostatic powder that has good film-forming ability and good electrospinning compatibility. The PVP provides a support for the catalyst precursor, allowing it to be uniformly dispersed throughout the membrane in the same way catalytic sites are throughout a membrane. Its mechanical properties also have a bearing on the final product's structural integrity. PVP is considered to be safe for handling, although precaution is recommended to prevent inhalation of the fine powders.

Table 3.4 *Properties of Polyvinylpyrrolidone*

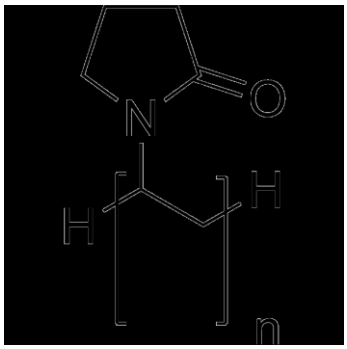	Chemical formula	[C6H9NO]n
	Molecular weight [g/mol]	~1,000,000 g/mol
	Density [kg/m3]	~1200
	Melting point [°C]	~150–180 °C
	CAS Number	9003-39-8
	Pictograms	-

II. Ethanol

Ethanol is the solvent used to dissolve PVP, forming the support solution. It is a volatile and flammable liquid which has good solvation properties. Ethanol allows PVP to completely dissolve, resulting in a homogenous solution that can be simply added to the catalyst precursor solution. It's also evaporates quickly, making the electrospinning process easier. As it is highly flammable, needs to be stored and handled away from open flames and heat sources.

Table 3.5 *Properties of Ethanol*

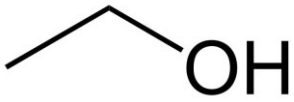	Chemical formula	C2H6O
	Molecular weight [g/mol]	46.07 g/mol
	Density [kg/m3]	789
	Boiling point [°C]	78.2
	CAS Number	64-17-5
	Pictograms	

III. Tetrabutyl Titanate (TBT)

Tetrabutyl titanate (TBT) is the catalyst precursor used to generate titanium dioxide (TiO_2), the active catalyst for pollutant degradation. It is a pale yellow liquid with no smell and soluble in organic solvents. TBT decomposes and hydrolyzes to produce TiO_2 nanoparticles that are intermixed in the PVP matrix. These nanoparticles are sites for the reactivity of organic pollutants degradation. Due to this, TBT is sensitive to moisture, and needs to be stored in a dry environment. It is also poisonous and must be handled carefully.

Table 3.6 *Properties of Tetrabutyl Titanate*

[redacted]	Chemical formula	C16H36O4Ti
	Molecular weight [g/mol]	340.36
	Density [kg/m3]	998
	Boiling point [°C]	312
	CAS Number	5593-70-4
	Pictograms	

IV. Acetic acid

Acetic acid is the solvent used to dissolve TBT, forming the catalyst precursor solution. It is a polar protic solvent with a pungent odor and is widely used in chemical synthesis. Acetic acid ensures complete dissolution of TBT, forming a homogeneous solution that can be mixed with the PVP/ethanol solution. Acetic acid is corrosive and should be handled with gloves and eye protection.

Table 3.7 *Properties of Acetic Acid*

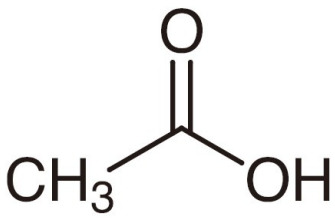	Chemical formula	C2H4O2
	Molecular weight [g/mol]	60.05
	Density [kg/m3]	1049
	Boiling point [°C]	118.1
	CAS Number	64-19-7
	Pictograms	

The PVP/ethanol and TBT/acetic acid solutions are prepared separately, then mixed thoroughly before use. The properties of all materials provided in the tables, were sourced from PUBCHEM.

3.1.2 Chemical properties of experimental Reagents

The following reagents were utilized in the experiments, each selected for its specific role and the advanced oxidation used in the degradation process:

I. Perfluorooctanoic Acid (PFOA)

Perfluorooctanoic acid (PFOA) is a synthetic fluorinated organic compound that has been widely used in industrial applications due to its unique chemical stability and surfactant properties as mentioned in chapter 1. However, its persistence in the environment and potential health risks have made it a target for degradation in this study. PFOA appears as a semi-transparent white powder at room temperature. It has a high molecular weight and density, contributing to its stability in aqueous environments. It has been extensively used in the production of non-stick coatings,

waterproof fabrics, and firefighting foams. Its strong carbon-fluorine bonds make it resistant to natural degradation, leading to its accumulation in water bodies and living organisms.

PFOA serves as the primary contaminant in the aqueous solution, and the goal of the study is to degrade it using different advanced oxidation processes (AOPs).

Table 3.8 *Properties of Perfluorooctanoic Acid (PFOA)*

	Chemical formula	$C_8HF_{15}O_2$
	Molecular weight [g/mol]	414.07
	Density [kg/m3]	1700
	Boiling point [°C]	189-192
	CAS Number	335-67-1
	Pictograms	

II. Ferrous Sulfate ($FeSO_4 \cdot 7H_2O$)

Ferrous sulfate, also known as iron(II) sulfate, is a blue-green crystalline compound that plays a critical role in generating free radicals for oxidation reactions.

Ferrous sulfate is typically produced by reacting metallic iron with dilute sulfuric acid. It is widely used in water treatment, agriculture (as a soil amendment), and as a precursor for other iron-based compounds. In the presence of hydrogen peroxide, ferrous sulfate catalyzes the Fenton reaction, producing hydroxyl radicals ($OH^{\cdot}$) that degrade organic pollutants like PFOA.

Table 3.9 *Properties of Ferrous Sulfate ($FeSO_4 \cdot 7H_2O$)*

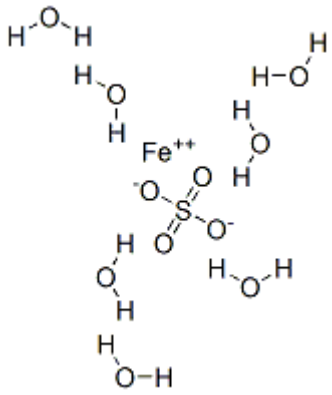	Chemical formula	$FeSO_4 \cdot 7H_2O$
	Molecular weight [g/mol]	278.02
	Density [kg/m3]	1895
	Melting point [°C]	60-64
	CAS Number	7782-63-0
	Pictograms	

III. Potassium Persulfate ($K_2S_2O_8$)

Potassium persulfate is a strong oxidizing agent used to generate sulfate radicals ($SO_4^{\cdot -}$) in the reaction system. It can be synthesized through the electrolysis of potassium bisulfate or by reacting potassium disulfate with ammonium peroxidisulfate. It is commonly used as an initiator in polymerization reactions and as an oxidant in chemical synthesis. The compound ensures the presence of sulfate radicals in the reactive system, which contribute to the degradation of PFOA through advanced oxidation processes.

Table 3.10 *Properties of Potassium Persulfate ($K_2S_2O_8$)*

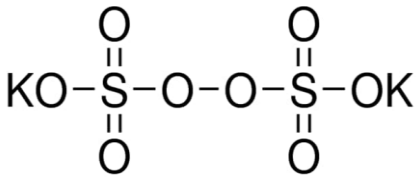	Chemical formula	$K_2S_2O_8$
	Molecular weight [g/mol]	270.33
	Density [kg/m3]	2477
	Melting point [°C]	~100
	CAS Number	7727-21-1
	Pictograms	

IV. Hydrogen Peroxide (H_2O_2)

Hydrogen peroxide is a simple yet powerful oxidizing agent that plays a pivotal role in Fenton and Fenton-like reactions. Due to its high reactivity and instability, hydrogen peroxide is typically used in diluted aqueous solutions. It is widely employed in disinfection, bleaching, and chemical synthesis. Hydrogen peroxide reacts with ferrous ions to produce hydroxyl radicals, which are highly effective in breaking down organic pollutants like PFOA.

Table 3.11 *Properties of Hydrogen Peroxide (H_2O_2)*

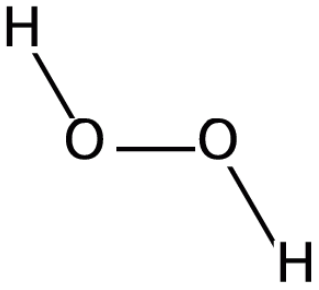	Chemical formula	H_2O_2
	Molecular weight [g/mol]	34.01
	Density [kg/m3]	~1450
	Boiling point [°C]	~150.2
	CAS Number	7722-84-1
	Pictograms	

I. Sulfuric Acid (H_2SO_4)

Sulfuric acid is a strong mineral acid used to maintain an acidic environment in the reaction system. It is one of the most widely used industrial chemicals, with applications in fertilizer production, chemical synthesis, and wastewater treatment. It is highly corrosive and requires careful handling. The acid is added in small quantities to ensure the optimal pH for Fenton reactions, which are most effective under acidic conditions. Therefore, it is only used in the experiments that only Photo-Fenton or combined advanced oxidation processes carried out.

Table 3.12 *Properties of Sulfuric Acid (H_2SO_4)*

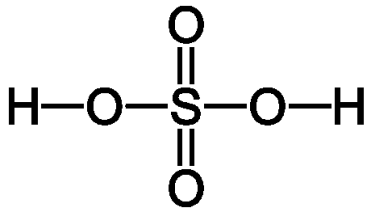	Chemical formula	H_2SO_4
	Molecular weight [g/mol]	98.079
	Density [kg/m3]	~1840
	Boiling point [°C]	~337
	CAS Number	7664-93-9
	Pictograms	

The properties of all materials provided in this section, were sourced from PUBCHEM.

3.2 Instruments

The following instruments were employed for the preparation, characterization, and analysis of the nanostructured membranes and also experimental setup:

I. Viscometer

A cone-and-plate viscometer (ATAC NuLine) was used to measure the viscosity of the polymeric solutions(PAA). The instrument operates by placing the sample on a flat plate and lowering the cone onto it as shown in figure 3.1. By turning the viscometer on, the cone start rotating and the viscosity monitor on the screen we need to change the speed of the cone in a way to be in optimal range.

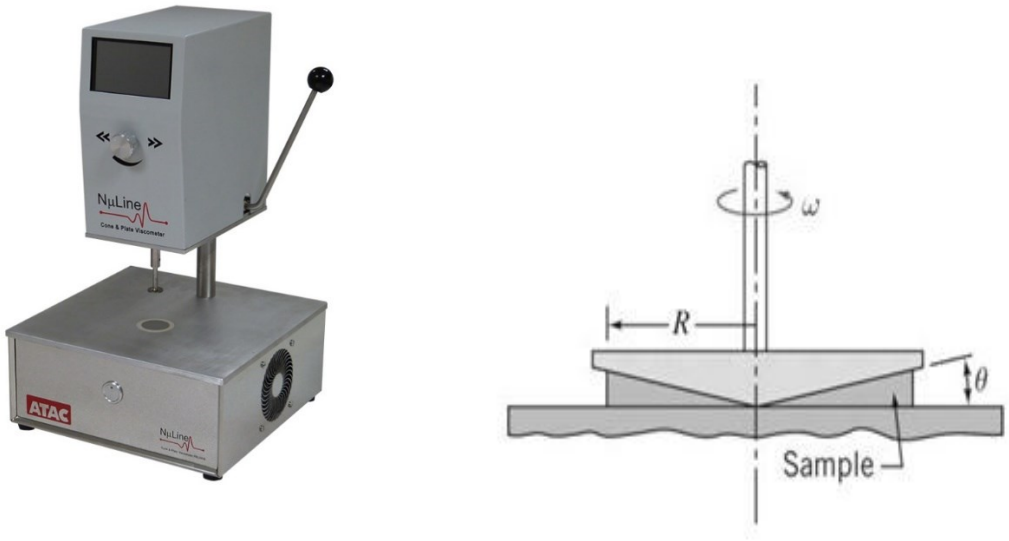

Figure 3.1. *Scheme of a cone-and-plate viscometer and the configuration of placed sample*

The viscosity is calculated based on the shear stress and shear rate, derived from the torque and rotational speed of the cone. High viscosity is essential for the successful electrospinning of polymeric solutions, as it ensures the formation of continuous fibers. In this instrument the viscosity is monitored for different rotational speed using the equations below actually viscosity shows how shear stress and shear rate change relatively according to equation 3.3.

$$\text{Shear Stress } (\tau): \quad \tau = \frac{3T}{2\pi R^3} \tag{3.1}$$

$$\text{Shear Rate } (\dot{\gamma}): \quad \dot{\gamma} = \frac{\omega}{\sin\theta} \tag{3.2}$$

$$\text{Viscosity } (\mu): \quad \mu = \frac{\tau}{\dot{\gamma}} \tag{3.3}$$

Here, T represents the torque [N·m], R [m] the cone radius, ω [rad/sec] the cone speed and θ the angle between the cone and the plate that has been shown in Figure 3.1[38].

II. Electrospinning Setup

The electrospinning is used to fabricate nanostructured membranes. In Figure 3.2, we can see The setup used for the simultaneous electrospinning of the PAA solution and the catalyst solution which includes the following instruments:

- A polycarbonate chamber to control temperature and humidity.
- A thermo-hygrometer to monitor environmental conditions.
- High-voltage generators to create the electric field necessary for fiber formation.
- Volumetric pumps and syringes to regulate the flow of polymeric solutions.
- A cylindrical collector wrapped in aluminum foil to deposit the fibers.

Figure 3.2. *Setup for a simultaneous electrospinning*

The solutions are loaded into syringes and pumped through needles, which act as the positive electrode. A high voltage between 10-20 KV is applied, creating an electric field that draws the solution into fine fibers, these fibers are then deposited on the collector, forming a nanostructured membrane. The flowrate and voltage must be adjusted in a way to create a stable jet also as the catalyst solution has viscosity lower than the PAA solution viscosity therefore, the voltage and the distance between the needle and collector must be lower comparing to the PAA solution [39].

III. Fourier-Transform Infrared Spectroscopy (FTIR)

Fourier-transform infrared spectroscopy (FTIR) is a powerful technique used to analyze the molecular structure of solid, liquid, or gas samples by measuring their absorption or emission of infrared (IR) radiation. This method is based on the principle that molecules absorb IR light at specific frequencies corresponding to the vibrational energy levels of their atomic bonds. When

the energy of the IR radiation matches the vibrational energy of a bond, absorption occurs. Each bond type absorbs distinct wavelengths, creating a unique spectral fingerprint for the molecule. The relationship between energy and frequency is expressed as the equation below:

$$E=h\cdot\nu \tag{3.4}$$

where E is energy, h is Planck's constant, and ν is frequency.

Unlike traditional dispersive IR spectroscopy, which uses monochromatic light, FTIR employs a Michelson interferometer to expose the sample to multiple IR frequencies simultaneously. The interferometer splits a beam of IR light into two paths: one reflects off a stationary mirror, and the other off a movable mirror. When the beams recombine, interference occurs due to differences in their path lengths, creating a time-domain interferogram. This interferogram is then transformed into a frequency-domain spectrum using Fourier Transform, revealing the sample's IR absorption characteristics.

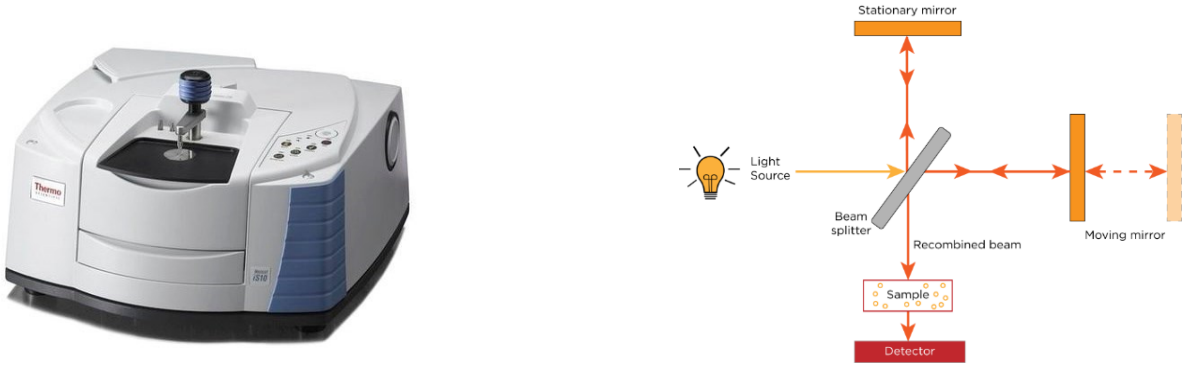

Figure 3.3. *Scheme of a Nicolet IS50 spectrophotometer and the configuration of placed sample*

The spectrophotometer used in this study is the Nicolet IS50 Thermo Scientific (Figure 3.3). In which, the FTIR analysis can be performed in following two modes:

Transmittance analysis: IR light passes through the sample, and the transmitted light is measured. This method requires sample preparation, such as forming pellets or films, but is versatile for solid, liquid, or gaseous samples.

Reflectance analysis: This method measures the light reflected from the sample, eliminating the need for extensive preparation. Attenuated total reflectance (ATR) is a common reflectance

technique, where IR light passes through an internal reflection element (IRE) crystal in contact with the sample.

In this project, this instrument has been used to be sure if the imidization process took place and the PAA cyclodehydrated to PI or not by checking the peaks on the FTIR diagram of each of them which correspond to their bonds [40].

IV. Environmental Scanning Electron Microscope (ESEM)

The Environmental Scanning Electron Microscope (ESEM) is a powerful tool for analyzing the morphology of membranes. Unlike optical microscopes, which use light, the ESEM employs an electron beam to achieve significantly higher resolution and a greater depth of field. This allows for detailed, high-magnification, three-dimensional imaging of samples.

Figure 3.3. *Scheme of an Environmental Scanning Electron Microscope (ESEM)*

In the ESEM, an electron beam is generated and accelerated by magnetic lenses, then scanned across the sample. Interactions between the electrons and the sample's atoms produce various signals, including secondary electrons, which are emitted from the sample's surface (typically within ~10 nm depth). These signals are used to create detailed images of the sample's external structure.The instrument operates under different vacuum levels: a high vacuum is maintained near the electron source and magnetic lenses, while a lower vacuum is used in the sample and detector region. Samples are mounted on a holder using conductive adhesive. Non-conductive materials,

such as polyamic acid or polyimide, are coated with a thin layer of conductive material using techniques like sputter coating or vacuum evaporation.

ESEM imaging allows for the measurement of fiber diameters and the assessment of membrane morphology, which are critical for evaluating their performance. In figure 3.5, the ESEM images of membranes before and after the heat treatment have been shown which can provide some information about the fibers morphology change during the heat treatment as we can see after the heat treatment [41].

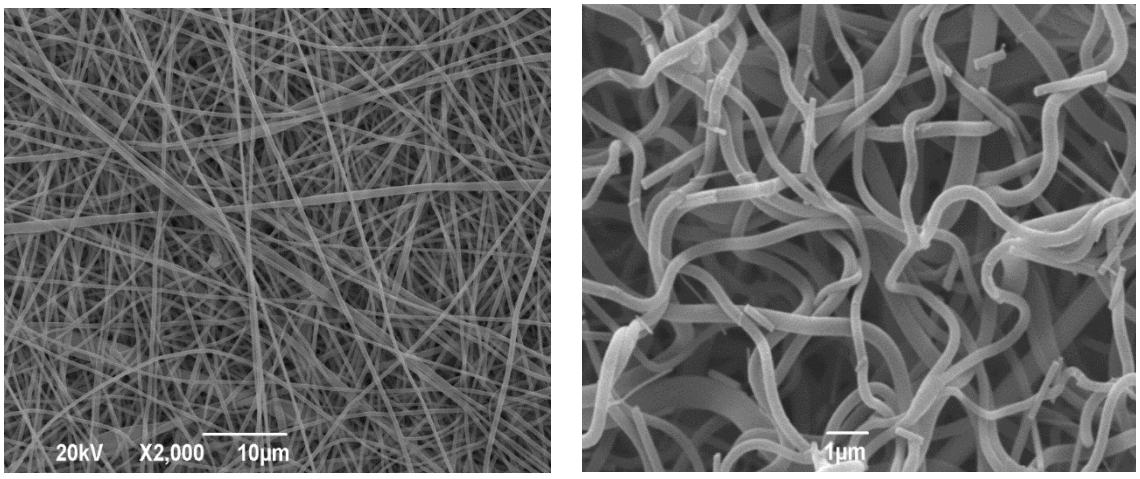

a b

Figure 3.5. *The ESEM image of a specific membrane before(a) and after(b) the heat treatment*

V. Thermogravimetric analysis (TGA)

Thermogravimetric analysis (TGA) is a thermal analysis technique used to measure changes in a sample's mass as it is heated or cooled over time. The instrument consists of a precision balance and a sample pan housed inside a furnace with programmable temperature control, the one that I used for this study is the TGA SDT-600 model, as shown in figure 3.6.

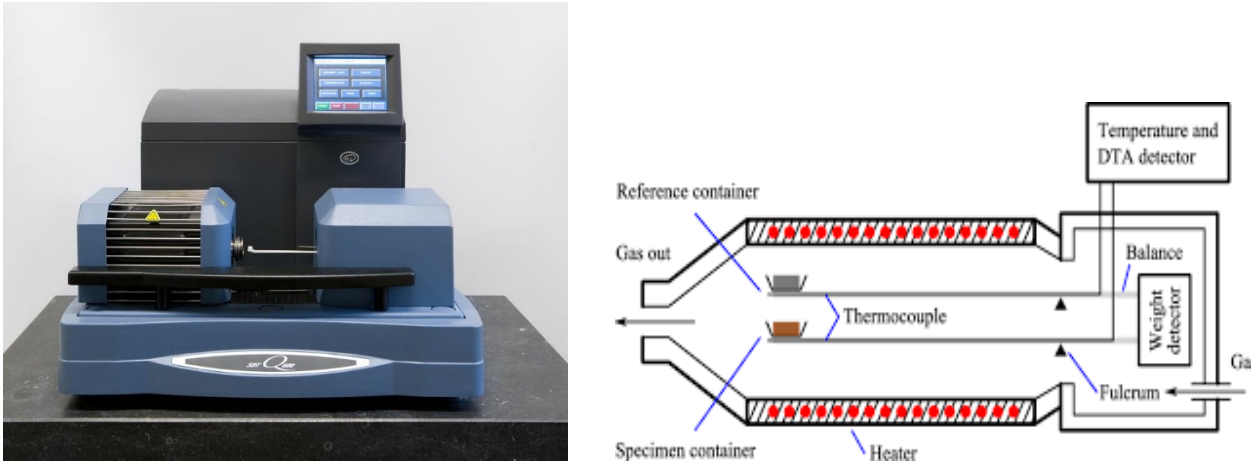

Figure 3.6. *Scheme of a TGA SDT-600 produced by TA instruments*

During TGA, the temperature is typically increased at a constant rate, and the analysis can be performed under various atmospheric conditions, such as ambient air, vacuum, or inert gases like nitrogen, as well as at different pressure levels. The sample and an empty reference capsule are placed on the balance and heated according to a set program. While the sample's weight changes during the process, the reference remains constant. The data collected is plotted as mass (or percentage of initial mass) on the y-axis against temperature or time on the x-axis, producing a TGA curve. In this study, it has been used to measure the amount of catalyst in our membranes.

VI. Photoreactor setup

The photoreactor is the main part of the experimental setup, consisting of a stainless-steel container designed to hold the membrane with three holes around its perimeter to allow continuous water flow. Water is circulated through the system using a centrifugal pump, entering the reactor and flowing either over the membrane (retentate) or through it (permeate) which both of them are returned directly to the container, however, there would be a flow in permeate without using any pump here.

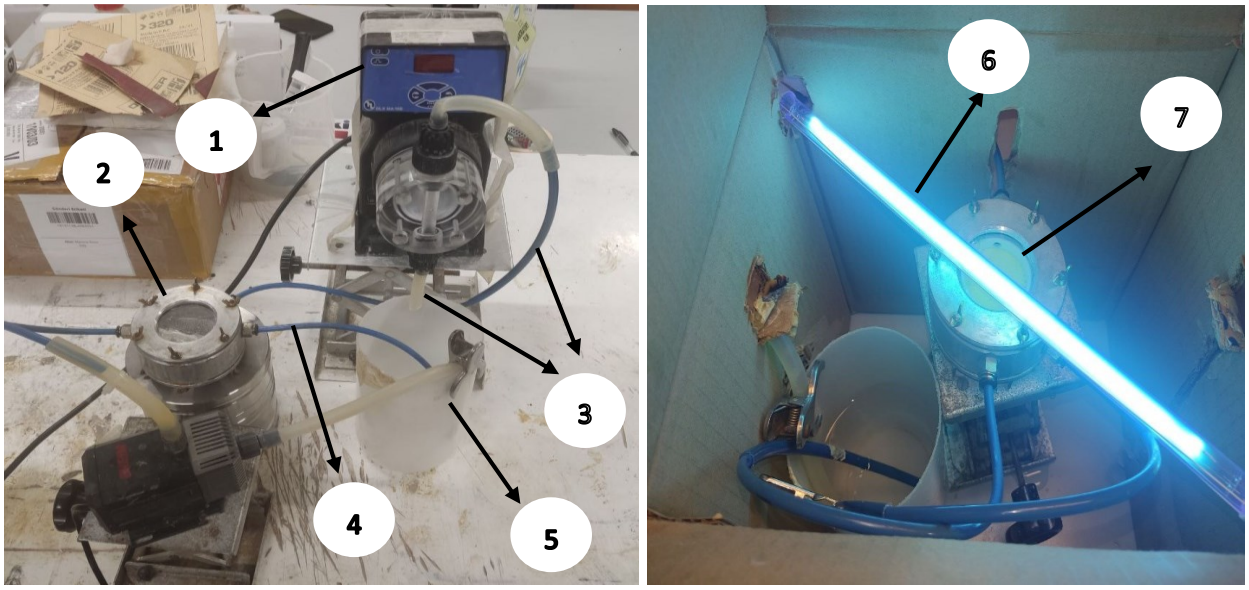

Figure 3.7. *The experiments setups for degrading PFOA*

A UV-C lamp is positioned above the photoreactor using a support to ensure uniform irradiation and minimize light dispersion for all the experiments. The experiments setup is illustrated in Figures 3.7, including the centrifugal pump (1), photoreactor (2), retentate (3), permeate (4), container (5), UV-c lamp (6), and positioned membrane.

In this study, the target contaminant (PFOA) and reagents required for experiment were added to the MilliQ water and sonicated for 45 minutes to ensure complete dissolution. The system operated 7 hours, one hour without using UV lamp and 6 hours under the lamp that the samples were collected each hour and take for analyzing by HPLC-MS.

VII. High-Performance Liquid Chromatography (HPLC)

High-performance liquid chromatography (HPLC) is an analytical technique used to separate, identify and quantify each of the compounds in a mixture. The process is based on pumping a liquid solvent, called the mobile phase (typically water, acetonitrile, methanol or a combination) under pressure through a column filled with a solid stationary phase. The components of the sample will interact differently with the stationary phase as they move through the column, explaining why they will elute at different retention times. The separation is vital for isolating target analyses to further analysis. Upon elution, each component generates a signal proportional to its

concentration, depending on the detector employed (e.g., UV/Vis or mass spectrometry (MS) detectors). The signals are recorded versus time as a chromatogram, which is used for quantitative analysis. Figure 3.8 represents the chromatogram of a certain contaminated sample from the combined-AOPs experiment, measuring the peaks area which is related to different PFAS (e.g, PFOA, PFHpA, PFHxA, PFBA,…) will give us the ability to calculate the concentration of them in ppm using the equation below:

$$C=\left(\frac{\frac{A_{PFAS}}{A_{IS}}-INT}{S}\right)*MW*D*1000 \tag{3.5}$$

In which C is the concentration of each PFAS in [ppm], A_{PFAS} related to the peaks area of the PFOA and the other byproducts and A_{IS} is also peaks area of the standard considered for the PFAS. INT and S are the intercept and slop of the calibration lines according to each PFAS and D is the dilution percentage used for each samples.

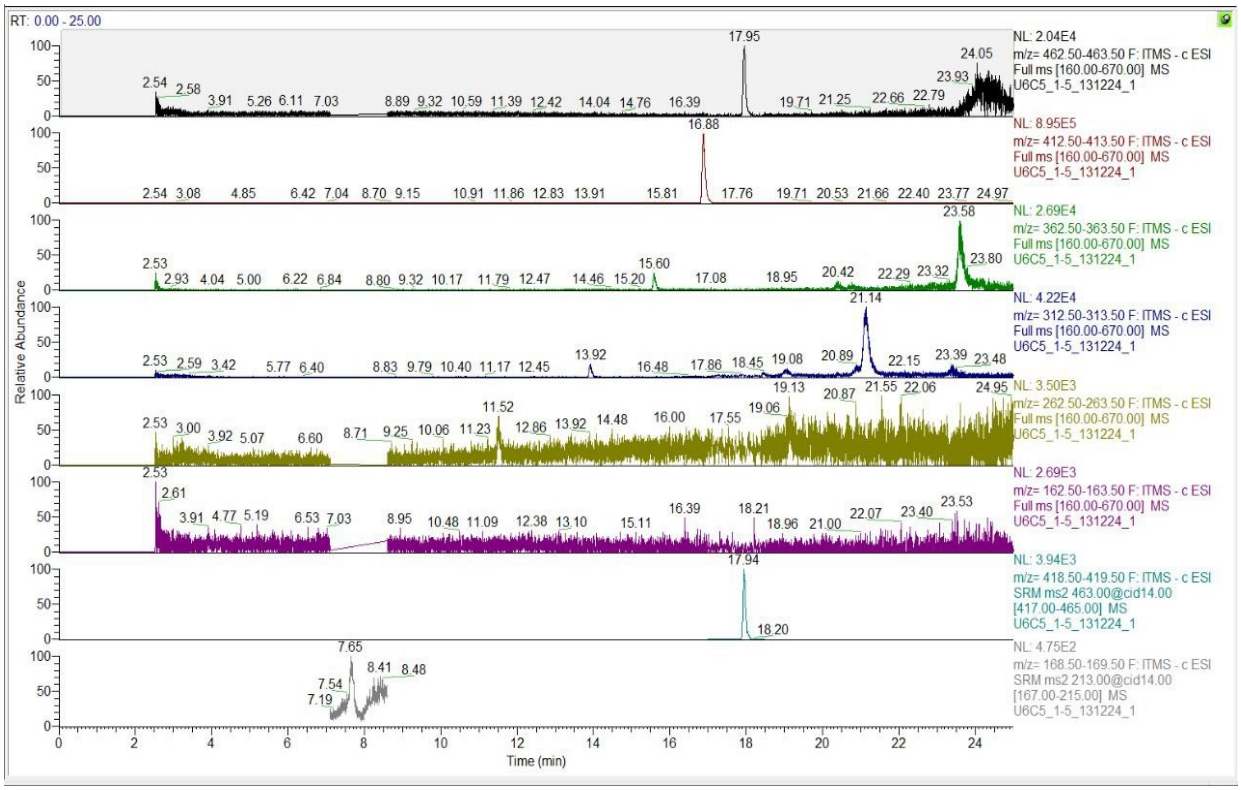

Figure 3.8. *chromatogram of a certain contaminated sample for the combined-AOPs experiment*

The analysis of perfluoroalkyl compounds (PFCs) such as perfluorooctanoic acid (PFOA) was adopted according to the EPA Method 537.1. The technique utilizes ultra-high-performance liquid chromatography (UHPLC) for high-resolution separation along with triple-quadrupole mass spectrometry (MS/MS) for sensitive and selective detection. The analytical system comprises of a Thermo Scientific™ Ultimate 3000 UHPLC system coupled to a MS Thermo Scientific™ LTQ XL as shown in Figure 3.9.

Figure 3.9. *Ultimate 3000 UHPLC system coupled with MS Thermo scientific LTQ XL*

Chromatographic separation is performed on a Thermo Scientific™ Accucore™ Vanquish C18+ column (2.1 × 100 mm, 1.5 µm) at 40°C with 5 mM ammonium acetate in Milli-Q water (A) and methanol (B) as mobile phase at a flow rate of 0.4 mL/min, gradient elution. The injection volume will be 5 µL to obtain a high sensitivity and reduce matrix effects.

All mass spectrometry was performed using a mass spectrometer operating in negative electrospray ionization (ESI-) mode (as described in the data section above) with optimized parameters (spray voltage = 2800 V; vaporizer temperature = 300°C; ion transfer tube temperature = 350°C). Perfluorononanoic acid (PFNA) was used as an internal standard for quantification and

calibration curves were created using analyte-to-PFNA response ratios. Thus, all samples are stored in clean polypropylene vials at 4°C to minimize degradation until analysis.

Detection is increased using the TSQ triple quadrupole system with selective reaction monitoring (SRM), were selected precursor ions are filtered out in the Q1 region, collided and fragmented in Q2 (collision cell), then product ions are filtered in Q3. Such multi-stage mass filtering allows for the highest species specificity and lowest detection limits, which are essential to trace PFOA and its transformation products in the environment.

Here, UHPLC-MS/MS allows for careful tracking of PFOA levels and degradation byproducts over time, vital for determining the efficiency of advanced treatment methods like photocatalytic degradation [42].

Chapter 4

Electrospinning

In this chapter we're going to investigate the highly versatile technique used to produce ultrafine fibers with diameters ranging from nanometers to micrometers called, Electrospinning. These fibers possess unique characteristics, such as high surface area-to-volume ratios, tunable porosity, and remarkable mechanical flexibility, making them invaluable across a wide array of applications including filtration, tissue engineering, drug delivery, and energy storage. This section explores the historical evolution, theoretical underpinnings, and critical process parameters of electrospinning, providing an overview of its importance in modern materials science.

4.1 Historical development of Electrospinning

It can be traced to the earliest works of investigation in electrohydrodynamic phenomena of the late 19th and early 20th centuries when initially observed were the phenomena by which liquids that had been exposed to electric fields could emit jets and spread out in thin droplets. It laid the bases in accordance with which electrospinning functions at the moment. Practical applications began to emerge in the early 20th century with the first patented methods for producing continuous fibers using electrostatic forces. During the mid-20th century, further developments led to the production of electrostatic equipment that could produce lightweight, nonwoven materials, and industrial interest in the process was opened up [43].

Another revolutionary theoretical achievement in the 1960s was mathematically explaining droplet deformation and jet generation under an electric field, important insight into why a conical structure is formed prior to the formation of the fibers. In later decades, research into electrospinning spread widely and proved most successful in the 1990s, by which time it was discovered that numerous forms of polymers can be electrospun into nanofibers of many sizes within the micrometer to nanometer ranges. This opened the doors to investigating the general applicability of electrospinning and cementing its position as a better technique for producing ultrafine fibers.

Recently, the move is being made towards non-conventional single-needle designs to elaborate structures such as multi-jet, coaxial, triaxial, and centrifugal electrospinning devices which allow intricate fiber architecture generation and functionally polyvariant nanomaterial generation. Near-field electrospinning and electrospinning integrated additive manufacturing have grown the application horizons too. Electrospun nanofibers are being used in more and more high-tech applications in tissue engineering, drug delivery, wearable electronics, filtration membranes, energy harvesters, and environmental remediation [44]. Here, electrospinning has been a critical process in the manufacture of high-tech membranes for water purification, air filtration, and battery separators and in meeting significant technological and environmental demands. Improvement of process scalability, fiber surface modification to add functionality, and green electrospinning from biopolymers and harmless solvents to pursue the path of sustainability have remained the primary research objectives so far.

4.2 Theoretical foundations of Electrospinning

Electrospinning works by releasing a polymer solution or melt through a needle or spinneret and applying a high-voltage electric field. The process starts with the electric field inducing charge accumulation at the surface of the polymer solution, which generates electrostatic forces that counteract the surface tension of the solution. Due to the high electric field strength, a conical shape solution is formed at the needle tip referred to as Taylor cone (As it's exhibited in figure 4.1). At this stage, electrostatic forces overcome the surface tension, allowing a charged polymer jet to be expelled from the cone tip [44].

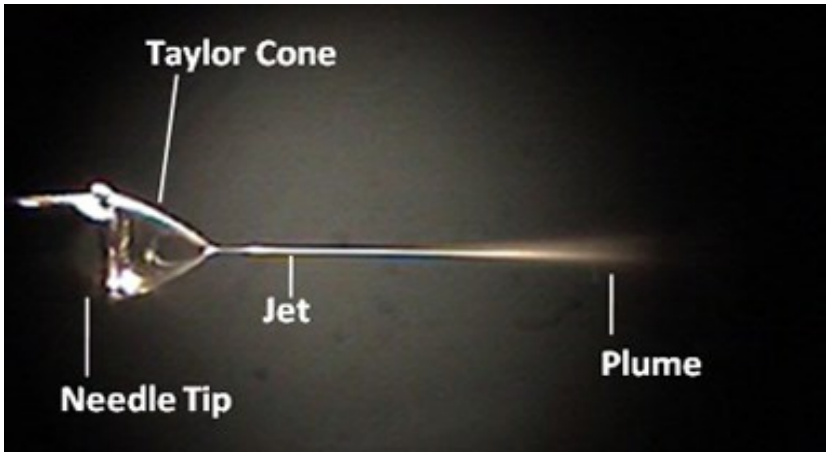

Figure 4.1. *The configuration of Taylor cone when the polymer jet pumps out of the needle tip*

Between the needle tip and grounded collector, the polymer jet experiences stretching and whipping instabilities, caused by electrostatic repulsion and the evaporation of solvent. Such instabilities lead to a strong thinning of the jet and the formation of ultrafine fibers with diameters in the nanometer range. The fibers are randomly deposited on the collector resulting in a non-woven mat with a high porosity and high surface area. Fiber morphology and properties can be tuned by varying polymer solution properties, processing conditions, and environmental factors.

4.3 Mechanism of fiber formation

The key formation mechanism in electrospinning is the complex interplaying force as shown in figure 4.2, which includes electrostatic forces, surface tension, viscoelasticity, and environmental interactions among others. In order to grasp this process, it is important to assess the steps during which the polymer solution turns into solid filaments. The jet formation, segment elongation, instability zone, and solvent evaporation filaments with solidification. Successful spinning requires correctly executing each stage of the process, as this directly influences the morphology and properties of the final fibers.

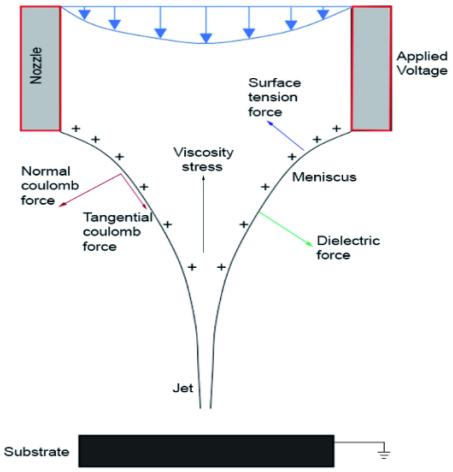

Figure 4.2. *The contributed forces at Taylor cone during the electrospinning*

I. Jet Formation

The electrospinning process begins with the formation of a polymer solution droplet at the tip of the needle. At this stage, gravity and surface tension are the dominant forces acting on the droplet.

When a high voltage is applied between the needle (positive electrode) and the collector (grounded or negatively charged), an electric field is established. This electric field induces charge separation within the droplet, with negative charges accumulating in the inner region and positive charges migrating to the surface. The droplet remains stable as long as the inward force of surface tension, which holds the negative charges together, exceeds the repulsive force generated by the accumulation of positive charges on the surface [45].

As the voltage increases, the droplet undergoes deformation, and its diameter decreases. When the applied voltage surpasses a critical threshold, the repulsive forces overcome the surface tension, and the droplet assumes a conical shape known as the Taylor cone. The angle of this cone is approximately 49.2°, a result of the balance between surface tension and electrostatic forces. Once the critical charge threshold, as defined by the Rayleigh condition, is exceeded, a charged jet of polymer solution is ejected from the tip of the Taylor cone. This marks the initiation of the fiber formation process [45].

II. Segment Elongation

After the jet is ejected, it is driven along the electric field lines to the collector. In this phase, the jet is elongated a lot, which causes its diameter to decrease. Stretching happens due to the electrostatic forces acting upon the charged jet and evaporation of the solvent. The space between fibers (distance between Taylor and jet) creates the space required to pull the fiber to get thinner as the jet draws away from the Taylor cone, and the velocity of the jet increases. During this process, the entanglements form a network that keeps the jet from breaking up immediately [46].

III. Instability Zone

At the beginning of stable elongation phase, the jet undergoes a phase of instability, which is oscillations and whipping motion. This is referred to as whipping instability, which is driven by the fact that the charges on the jet surface will repel each other. Whipping increases the jet's surface area, which decreases the surface charge density, further thinning the fiber. Experiments indicate that the jet oscillates in a conical region with fiber orientations randomly distributed around the linear casting axis. In this process, different forces such as gravitational forces, surface

tension, viscoelasticity, electrostatic forces, and Coulomb forces overlap with other forces so as to determine the trajectory and diameter of the jet. In figure 4.3, all these regions that the polymer passes towards the collector, have been exhibited.

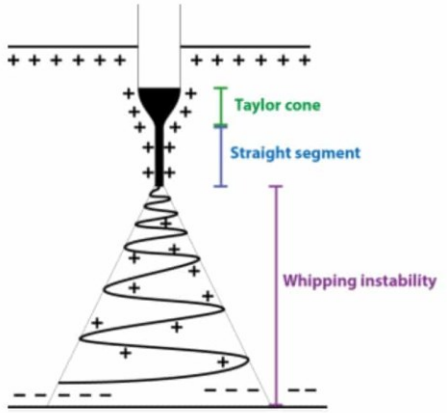

Figure 4.3. *The regions the polymer passes toward the collector*

IV. Solvent Evaporation and Filament Solidification

The solvent evaporates as the jet moves toward the collector and leaves solid polymer fibers. These include distance between the needle and the collector, solvent vapor pressure and ambient parameters like temperature and relative humidity affecting the rate of solvent evaporation. The best process parameters guarantee a total evaporation of the solvent leading to dry fibers on the collector. Incomplete evaporation can produce residual solvent which can swell and dissolve the fibers with poor fiber morphology. Hence, optimized modulation of process parameters during the fiber formation process is critical to obtain advanced fibers.

The electrospinning fiber jet mechanism, a dynamic process from the polymer solution to solid fibers, introducing those forces and mechanisms that led to the electrospinning. In order to control this process and get the fiber properties to fit one purpose or the other, one need to understand the mechanism behind this process. Previous researches emphasized controlling jet behavior to create nanofibrous membranes for water treatment, also highlighted the influence of process parameters on fiber diameter and morphology. With proper intrigue of these parameters, fibers with precise features are obtainable for vision in crossing fields, beginning from filtration to tissue engineering [46].

4.4 Key Parameters Influencing Electrospinning

During the electrospinning we need to carefully control various parameters which can be categorized into three groups: **process conditions**, **environmental conditions**, and **solution conditions**. Each group plays a critical role in determining the morphology, diameter, and quality of the resulting fibers. Below is a detailed discussion of these key parameters:

4.4.1 Process Conditions

Process conditions are directly related to the setup and operation of the electrospinning equipment. These include the potential difference (voltage), flow rate, needle diameter, collector type, and needle-collector distance.

I. Potential difference(Voltage)

The applied voltage is a critical factor in electrospinning. It generates an electric field that induces charge separation in the polymer solution, leading to the formation of the Taylor cone and the ejection of a charged jet. Higher voltages create stronger electric fields, which increase the stretching force on the jet, resulting in finer fibers. However, excessively high voltages can cause the jet to accelerate too quickly, reducing the time for solvent evaporation and leading to thicker fibers or defects. Optimizing the voltage is essential for achieving uniform fiber diameters and avoiding multi-jet formations [47].

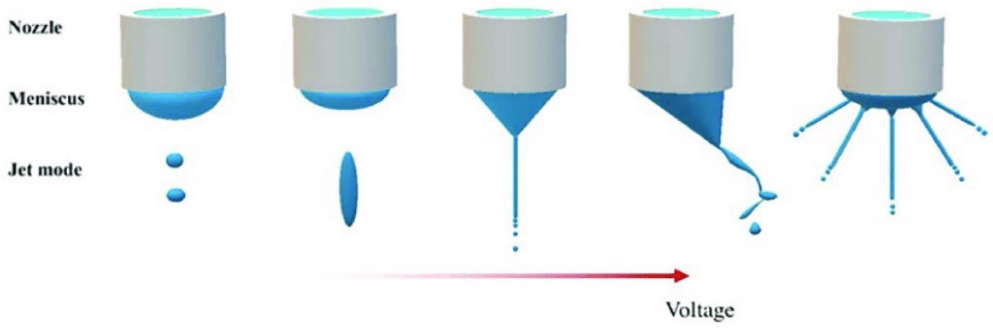

Figure 4.4. *The Effect of increasing voltage on jet stability*

II. Flow rate

The flow rate determines the volume of polymer solution delivered to the needle tip. A balanced flow rate is crucial; if it is too high, the solution may not have enough time to evaporate before reaching the collector, leading to wet fibers and poor morphology. Conversely, a low flow rate can result in insufficient material for continuous fiber formation. As noted, the flow rate must be synchronized with the voltage to maintain a stable Taylor cone and ensure consistent fiber production [47].

III. Needle diameter

The diameter of the needle influences the size of the fibers produced. Smaller needle diameters increase the surface tension at the needle tip, requiring higher voltages to overcome it. This can lead to finer fibers but may also cause clogging, especially with highly viscous solutions. Coaxial electrospinning, which uses needles of different diameters, can be employed to create core-shell fibers for advanced applications [46].

IV. Collector Type

The collector plays a significant role in determining fiber alignment and mat structure. Static collectors, such as flat plates, produce randomly oriented fibers, while dynamic collectors, like rotating drums, can align fibers in specific directions. The choice of collector depends on the desired application; for instance, aligned fibers are often preferred for tissue engineering scaffolds.

V. Needle-Collector Distance

The distance between the needle and the collector affects the electric field strength and the time available for solvent evaporation. A shorter distance increases the electric field but may not allow sufficient time for drying, leading to wet fibers. A longer distance provides more time for stretching and solvent evaporation, resulting in thinner fibers. However, if the distance is too large, the electric field may become too weak to deposit fibers effectively [46].

4.4.2 Environmental Conditions

The surrounding environment, including temperature, pressure, and relative humidity, can significantly influence the electrospinning process and fiber morphology:

I. Temperature

Higher temperatures promote solvent evaporation and reduce solution viscosity, leading to thinner fibers. However, excessively high temperatures can cause premature drying of the solution at the needle tip, leading to clogging. Maintaining an optimal temperature is crucial for consistent fiber production.

II. Pressure

Electrospinning is typically performed at atmospheric pressure. Operating under reduced pressure can destabilize the jet and alter the flow rate, while excessive pressure reduction can cause the solution to boil, disrupting the process. Stable pressure conditions are essential for achieving uniform fibers.

III. Relative Humidity

Humidity affects the rate of solvent evaporation and the formation of pores on the fiber surface. Lower humidity speeds up evaporation, which can lead to smoother fibers. However, if the evaporation rate is too high, it can cause needle blockage. Conversely, higher humidity can result in porous fibers due to water condensation on the jet surface [46].

4.4.3 Solution Conditions

The properties of the polymer solution, including molecular weight, viscosity, surface tension, conductivity, and solvent type, are critical for successful electrospinning.

I. Polymer Molecular Weight and Viscosity

The molecular weight of the polymer directly affects the solution viscosity. Higher molecular weights result in more entangled polymer chains, which are necessary for forming continuous

fibers. However, excessively high viscosity can lead to bead formation, while low viscosity may result in spray-like droplets instead of fibers [46].

II. Surface Tension

Surface tension must be overcome by the electric field to initiate jet formation. Solutions with low surface tension are easier to electrospin, resulting in smoother fibers. Additives can be used to modify surface tension and improve fiber quality [47].

III. Conductivity

The conductivity of the solution determines the charge density on the jet surface. Higher conductivity increases the stretching force, leading to finer fibers. However, excessively high conductivity can cause jet instability. Adding salts or ionic compounds can enhance conductivity, but care must be taken to avoid exceeding the critical threshold [48].

IV. Solvent Nature

The choice of solvent affects the solubility of the polymer and the rate of solvent evaporation. Solvents with high dielectric constants expand the instability zone, resulting in thinner and smoother fibers. The solvent must also have appropriate volatility to ensure complete evaporation during fiber formation [46].

Chapter 5

Membrane preparation and characterization

According to the advanced oxidation process that we are going to analyze, two different kinds of membranes need to be prepared which all of them must have the features below:

- Maintaining water insolubility for use in aqueous environments.
- Retaining adequate mechanical properties.
- Resisting UV radiation.
- Supporting catalysts for advanced oxidation reactions.
- Containing a high catalyst load to enhance photo-oxidative degradation of PFOA.

The proposed membrane is a composite material consisting of a structural polymer and a catalytic element. These components are simultaneously deposited onto a rotating cylindrical collector using electrospinning, resulting in a randomly aggregated fibrous structure, however, the membranes used for the persulfate oxidation and Photo-Fenton experiments consisting only the structural polymer so no need for simultaneous electrospinning. This chapter details the preparation of the polyamic acid (PAA) solution, the electrospinning process, and the characterization of the membranes following heat treatment, with a particular focus on their morphological properties as influenced by the viscosity of the initial PAA solution.

5.1 Polyamic Acid (PAA)

Membrane production requires the crucial step, PAA (polyamic acid) synthesis as an intermediate step before polyimide (PI) production. This is a very detail-oriented process since even minor deviations can hugely affect the properties of the final product. Polycondensation of pyromellitic dianhydride (PMDA) and 4,4'-oxydianiline (ODA) in dimethylformamide (DMF) was used as a

solvent in the preparation process. The mechanism of reaction is based on a type of nucleophilic substitution where the amino group of ODA attacks the carbonyl group of PMDA, resulting in a polymeric material known as polyamic acid. This reaction is very sensitive to environmental variables, especially humidity and temperature, which can affect the molecular weight and the viscosity of the PAA obtained.

The polycondensation reaction occurs in two steps. In the first step, amino group of ODA attacks carbonyl group of PMDA, opening anhydride ring and forming a reactive nitrogen (N^+) and carboxylate group (COO^-) intermediate. In the next step, The intermediate continues to undergo nucleophilic substitution reactions by the aprotic polar solvent (DMF) to give long-chain polyamic acid molecules. Figure 5.1 depicts all these steps.

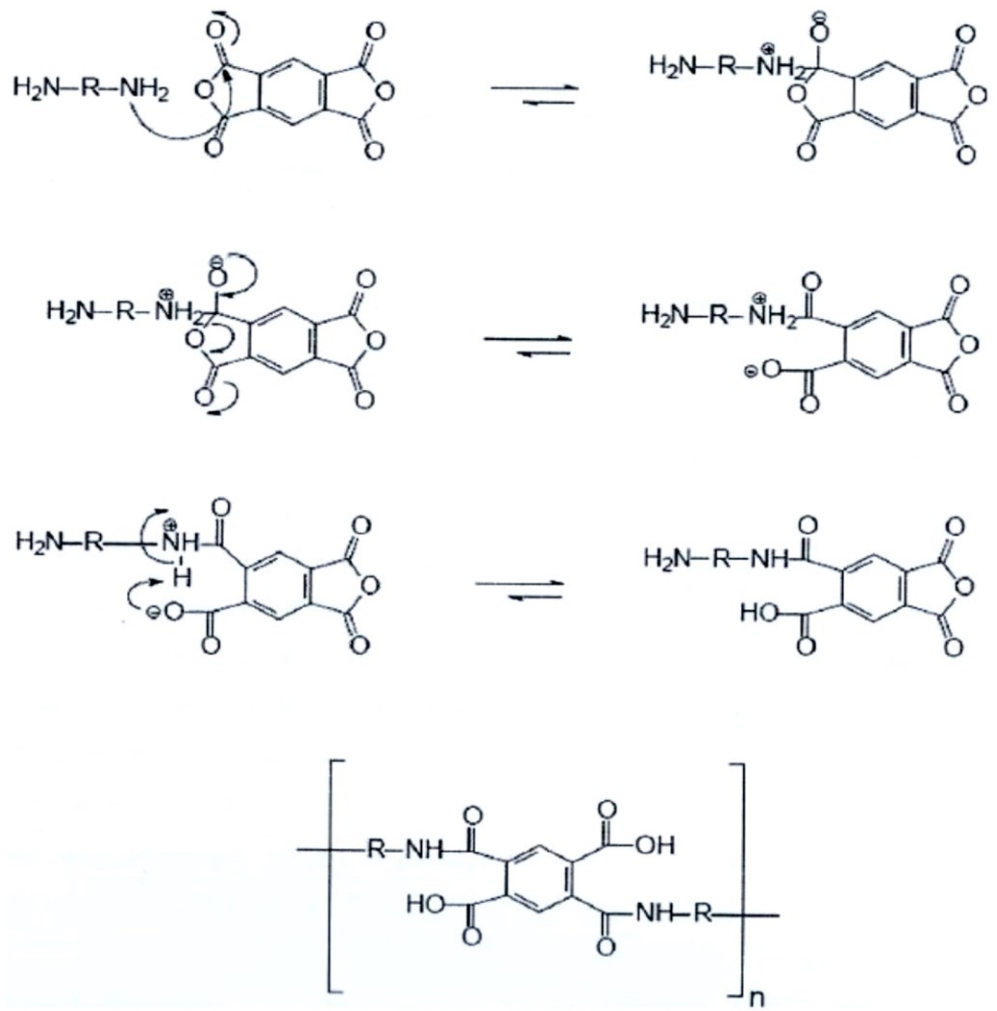

Figure 5.1. *The polycondensation reactions occur in PAA synthesis*

The reaction is reversible, and secondary reactions, such as hydrolysis of the anhydride or degradation of PAA, can occur if moisture is present. These side reactions reduce the availability of PMDA for polycondensation and lead to lower molecular weight PAA. Therefore, maintaining an inert and dry environment is crucial for achieving high-quality PAA [49].

The preparation of 21.6% PAA solution begins with the preparation of the solvent. Approximately 16.4 grams of DMF are weighed and transferred to a glass flask equipped with a magnetic stirrer. The flask is placed on a magnetic stirrer, and mixing is initiated at a moderate speed. To prevent moisture interference, the flask is continuously purged with nitrogen gas for at least 30 minutes before adding the reagents. This step is critical, as even trace amounts of water can hydrolyze PMDA and reduce the reaction yield.

After purging, 2.144 grams of ODA are added to the DMF while maintaining the nitrogen flow. The mixture is stirred until the ODA is completely dissolved, which typically takes about 15 minutes. Once the ODA is fully dissolved, 2.372 grams of PMDA are slowly added to the solution. The addition of PMDA must be done carefully to ensure complete solvation. Rapid addition can lead to the formation of solid residues, which will not participate in the reaction. To enhance uniform mixing, the stirring speed is increased to at least 800 rpm.

The reaction is allowed to proceed under nitrogen flow for approximately 15 minutes. During this time, the solution gradually turns yellowish, indicating the formation of PAA. Once the reaction is complete, the nitrogen flow is turned off, and the flask is sealed to prevent moisture ingress. The solution is then left to mix continuously for 24 hours at room temperature to ensure homogeneity and complete polymerization.

Several factors must be carefully controlled to achieve high-quality PAA with the desired molecular weight and viscosity. The order of reagent addition is essential; adding ODA before PMDA ensures the formation of high-molecular-weight PAA. Reversing the order leads to premature hydrolysis of PMDA, resulting in lower viscosity and molecular weight. Moisture control is also critical, as water in the reaction environment can hydrolyze PMDA. According to the figure 5.2, H_2O molecules attack carbonyl group of PMDA, which leads to the opening of the ether ring and creating two carboxyl groups this reduces its availability for polycondensation. Working under a nitrogen atmosphere and using dried reagents are necessary to minimize this effect.

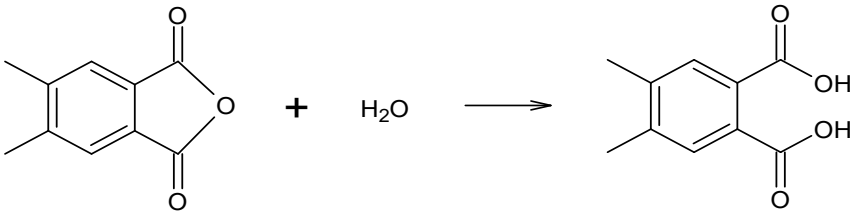

Figure 5.2. *Hydrolysis of PMDA and producing acid*

Temperature control is another important factor. The reaction should be conducted at a temperature between 15°C and 35°C. For small-scale reactions (less than 1 liter), a temperature control system is recommended to maintain consistent conditions. Additionally, PAA solutions are highly sensitive to temperature and moisture. For long-term storage, the solution should be kept below 0°C to prevent degradation [49].

The viscosity of the PAA solution is a key indicator of its quality and suitability for electrospinning. It must not that much high to create beads on membrane and it shouldn't be very low because in that case, membranes with lower fiber diameter are created. In this study, I used membranes with larger diameter (420-450 nm) for the experiments, However, the smaller ones have larger surface area which interact more with our contaminant but it also induces more pressure drop on membrane here the primary objective is not to move the contaminant from the aqueous phase to the solid phase but to bring it to complete decomposition. To monitor viscosity, the solution's viscosity is measured 24 hours after preparation using a viscometer exactly before injection to the syringe for electrospinning. Previous researches in storing portions of the solution at different temperatures (e.g., room temperature and 5°C), and monitoring viscosity changes over 10 days, reveal that solutions prepared under an inert atmosphere and stored at 5°C maintain high viscosity for several days, making them suitable for electrospinning [50]. In contrast, solutions exposed to ambient air or stored at room temperature exhibit rapid viscosity decline, making them unsuitable for fiber formation. So before running the electrospinning the solution viscosity must be checked to be in 60-90 poise range to prepared membrane with the corresponding diameter.

5.2 Catalyst Solution

The catalytic solution is a critical component of the membrane, as it provides the precursor for the active catalyst, titanium dioxide (TiO_2), which is essential for promoting photo-oxidative reactions. The solution consists of two main parts: the catalyst precursor, titanium butoxide (TBT), and a supporting polymer, polyvinylpyrrolidone (PVP). The preparation of the catalytic solution involves the careful dissolution and mixing of these components in appropriate solvents to ensure homogeneity and stability.

The process begins with the preparation of the support phase, which is composed of PVP dissolved in ethanol. Approximately 1.65 grams of PVP are weighed and added to 11.15 grams of ethanol in a clean, dry container. The mixture is stirred continuously for at least two hours to ensure complete dissolution of the PVP. The resulting solution is clear and viscous, indicating that the polymer has fully dissolved in the solvent.

Simultaneously, the catalyst precursor, TBT, is prepared by dissolving 4.5 grams of TBT in 8.65 grams of acetic acid. The mixture is stirred for two hours to achieve a homogeneous solution. Acetic acid is chosen as the solvent for TBT due to its ability to stabilize the precursor and prevent premature hydrolysis, which could lead to the formation of undesirable by-products.

Once both solutions are fully prepared and homogeneous, they are combined by slowly adding the TBT solution to the PVP solution under continuous stirring. The mixing process is carried out carefully to ensure uniform distribution of the catalyst precursor within the polymer matrix. The resulting mixture is a yellowish liquid with a distinct acetic acid odor, indicating the successful integration of the components.

After mixing, the catalytic solution is left to be for 24 hours at room temperature to allow for further homogenization and stabilization. During this period, the solution is stirred intermittently to prevent sedimentation or phase separation. Once the aging process is complete, the solution is stored in a refrigerator at approximately 5°C to maintain its stability and prevent degradation.

It is important to note that the catalytic solution has a limited shelf life. Over time, phase separation occurs, and a white powder settles at the bottom of the container. This powder consists of hydrolyzed TBT and other by-products, rendering the solution unusable for further applications. Therefore, the catalytic solution should be used within a few days of preparation to ensure optimal performance.

The role of PVP in the catalytic solution is to act as a stabilizing agent, preventing the aggregation of TBT and ensuring uniform distribution of the catalyst precursor within the membrane. PVP also contributes to the mechanical properties of the membrane, providing structural support during the electrospinning process. The combination of TBT and PVP in the catalytic solution ensures that the resulting membrane will have a high catalyst content and excellent mechanical integrity, both of which are essential for effective photocatalytic activity.

5.3 Electrospinning Process

In this study, electrospinning is employed to produce two types of membranes: one containing both structural and catalytic components for photocatalytic applications, and another containing only the structural component for Photo-Fenton and persulfate oxidation experiments. The process involves the simultaneous deposition of two solutions—polyamic acid (PAA) for the structural component and a catalytic solution containing titanium butoxide (TBT) and polyvinylpyrrolidone (PVP)—onto a rotating cylindrical collector.

Before beginning the electrospinning process, the PAA solution and the catalytic solution are prepared as described in previous sections. The PAA solution, with a concentration of 21.6%, is carefully prepared to ensure high viscosity and stability, while the catalytic solution is a homogeneous mixture of TBT and PVP in ethanol and acetic acid. Two separate syringes are filled with these solutions and mounted onto the electrospinning apparatus.

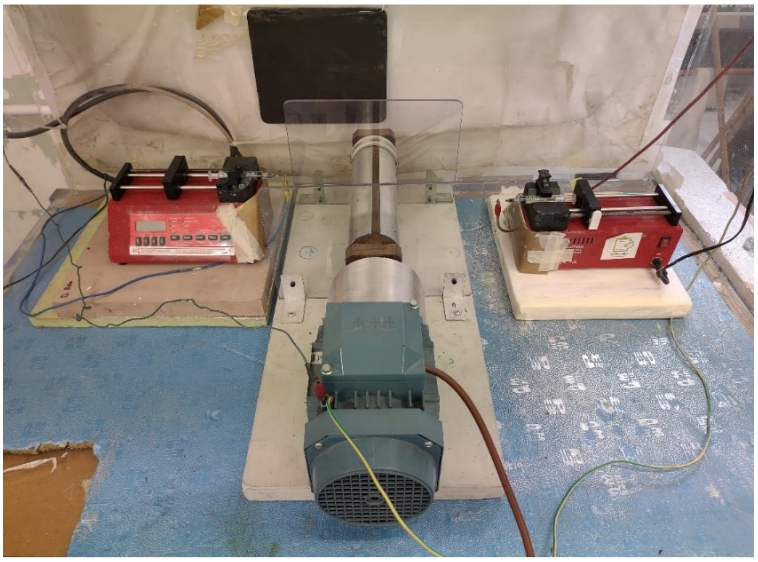

Figure 5.3. *The setup for simultaneous electrospinning*

The electrospinning setup consists of two volumetric pumps, a high-voltage power supply, and a rotating cylindrical collector, as shown in figure 5.3. The PAA solution is loaded into one syringe, and the catalytic solution is loaded into the other. The process parameters for each solution are optimized based on their properties and the desired fiber morphology. For the PAA solution, the flow rate is set to 0.8 mL/hour, and a voltage of 18 kV is applied. The needle used for the PAA solution is a 21-gauge (21G) needle, and the distance between the needle tip and the collector is maintained at 15 cm. The collector rotates at a speed of 900 rpm to ensure uniform fiber deposition. For the catalytic solution, the flow rate would not be constant and it will be changed from 3 to 9 mL/hour to ensure the high percentage of catalyst in the final membrane, and a constant voltage of 11 kV is applied. A 22-gauge (22G) needle is used, and the needle-to-collector distance is set to 10 cm. The relative humidity in the electrospinning chamber is maintained at 55% to prevent rapid solvent evaporation, which could lead to fiber defects. The amount of catalytic solution used during the electrospinning was almost 33 ml for only 4 ml of PAA solution, in that case, we could only produce membranes with high concentration of TBT.

Once the parameters are set, the electrospinning process begins. The PAA and catalytic solutions are simultaneously ejected from their respective syringes under the influence of the applied electric field. The high voltage causes the solutions to form charged jets, which are drawn toward the rotating collector. As the jets travel through the air, the solvents evaporate, leaving behind solid fibers that are deposited onto the collector. The deposition process continues for 5 hours, depending on the desired membrane thickness. During this time, the fibers accumulate on the collector, forming a yellowish-white membrane. The resulting membrane is composed of randomly oriented fibers with a uniform morphology. Scanning electron microscopy (SEM) images reveal that the fibers are straight and homogeneous, with no visible differences between the PAA and PVP/TBT fibers. In the figures below we can see the membranes with catalyst and without catalyst, but it’s obvious that the fibers with higher diameter correspond to PAA because of the higher molecular weight and viscosity and the finer one related to the catalyst solution probably.

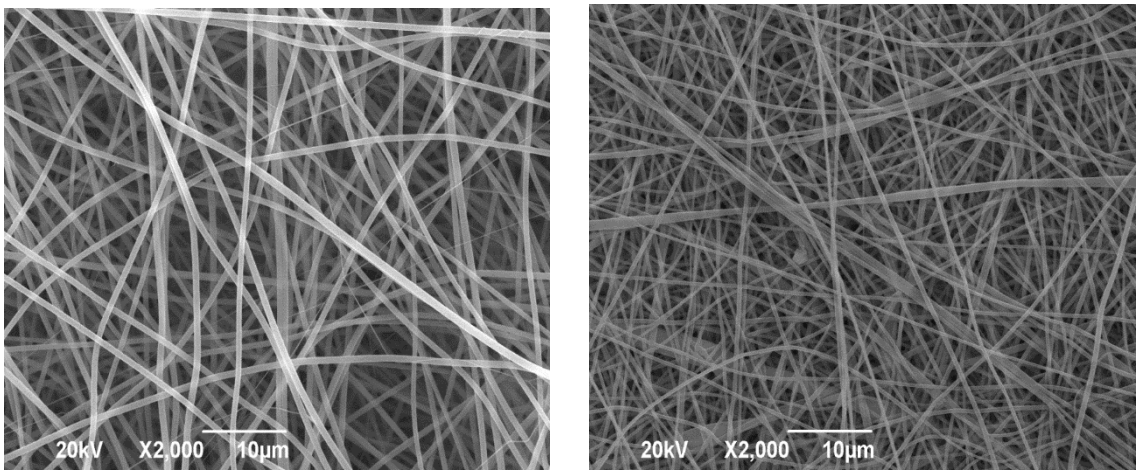

Figure 5.4. *The ESEM images of membranes with(a) and without(b) catalyst*

After the deposition process is complete, the membrane is carefully removed from the aluminum foil covering the collector. The membrane exhibits excellent mechanical properties, which are attributed to the presence of PVP in the catalytic solution. PVP provides structural support to the fibers, ensuring that the membrane can be handled with ease. However, it is important to note that the mechanical properties of the membrane are temperature-dependent. At elevated temperatures, PVP begins to degrade, which can compromise the membrane's integrity.

In addition to the catalytic membrane, a second type of membrane is fabricated for use in Photo-Fenton and persulfate oxidation experiments. This membrane contains only the structural component (PAA) and does not include the catalytic solution. The electrospinning process for this membrane is identical to that described above, except that only the PAA solution is used. The resulting membrane is composed solely of PAA fibers and is used as a control or support structure in experiments where catalytic activity is not required.

5.4 Polyimide (PI) synthesis

The PAA membrane undergoes a controlled heat treatment to convert it into polyimide (PI) and activate the catalyst. The thermal process involves a 12.5hr gradual temperature ramp from 80°C up to 400°C with a rate of 2 °C/min, as expressed in figure 5.5, promoting cyclodehydration of PAA(imidization) and transformation of TBT into titanium dioxide (TiO_2). In fact, the heat treatment involves the removal of water and the formation of imide rings, resulting in the final PI structure. The grafting of imide support ensures the membrane maintains its integrity even after

exposure to high temperatures. Polyimide is chosen for its ability to withstand temperatures exceeding 200 °C while retaining excellent mechanical properties.

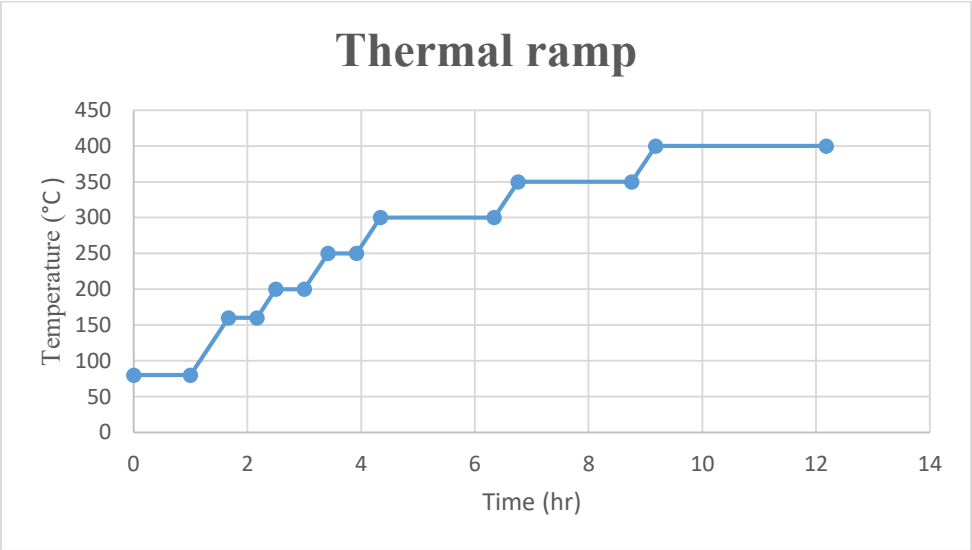

Figure 5.5. *The thermal ramp for heat treatment of membranes*

In addition to thermal imidization, other methods for imidization include chemical imidization and catalytic imidization. Chemical imidization involves the use of acetic anhydride, pyridine, or triethylamine as catalysts to facilitate the cyclodehydration of PAA at lower temperatures. Catalytic imidization, on the other hand, uses high-temperature polycondensation in phenol or m-cresol solvents, followed by catalytic imidization using isoquinoline or benzoic acid. However, the thermal imidization method is preferred in this study because it produces an insoluble polyimide, making it suitable for supporting catalysts in aqueous environments without requiring additional substances to achieve the desired polyimide state according to the reaction below.

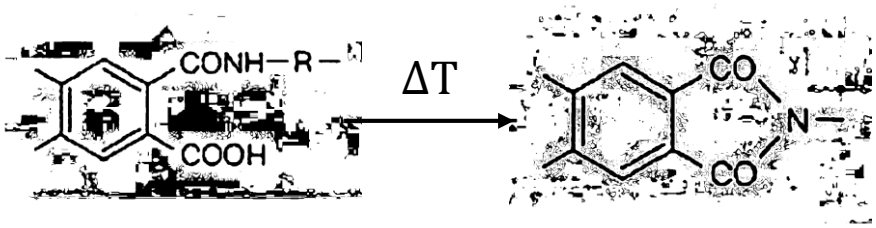

Figure 5.6. *The cyclodehydration of PAA to PI through heat*

The resulting PI membrane exhibits a yellowish color, reduced flexibility, and improved mechanical stability. Figure 5.7 expresses the both membranes with and without catalyst after the heat treatment in which the membrane without catalyst is uniformly yellow, however, the one with 30% w/w TBT consists some parts with different color which may because of existence of PVP and TiO_2.

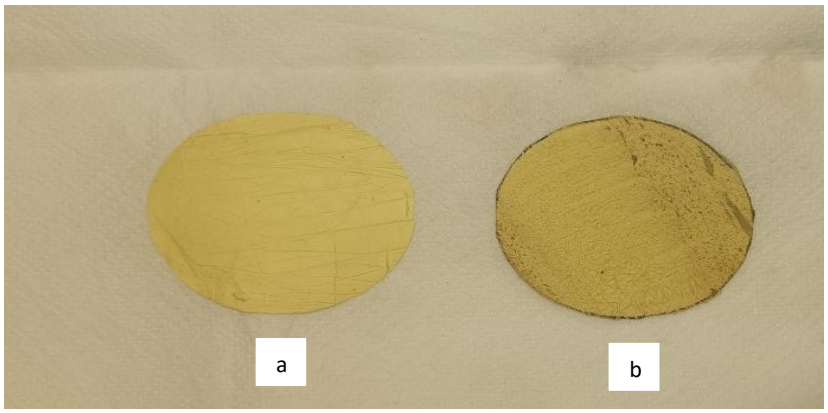

Figure 5.7. *Configuration of membranes without(a) and with(b) catalyst after the heat treatment*

5.5 Polyimide (PI) characterization

The characterization of synthetic polyimide (PI) involves evaluating its fundamental properties, such as thermal stability, transition temperatures, mechanical behavior, and density. In this context, the focus is primarily on analyzing the FT-IR spectra and thermal stability of polyimide, as these provide critical insights into the material's structural and thermal properties. FT-IR spectroscopy is a widely used technique for monitoring structural changes during the transformation of polyamic acid (PAA) into polyimide. It allows for well-founded conclusions about the material's structure by comparing absorption peaks corresponding to specific functional groups. Notably, not all functional groups exhibit the same absorption characteristics. For example, the typical bonds of PAA, which absorb near 1600 cm^{-1}, are less pronounced compared to the carbonyl groups associated with the imide ring. As the imidization reaction progresses, the peaks related to PAA diminish and eventually overlap with the absorption range of imide groups, disappearing entirely.

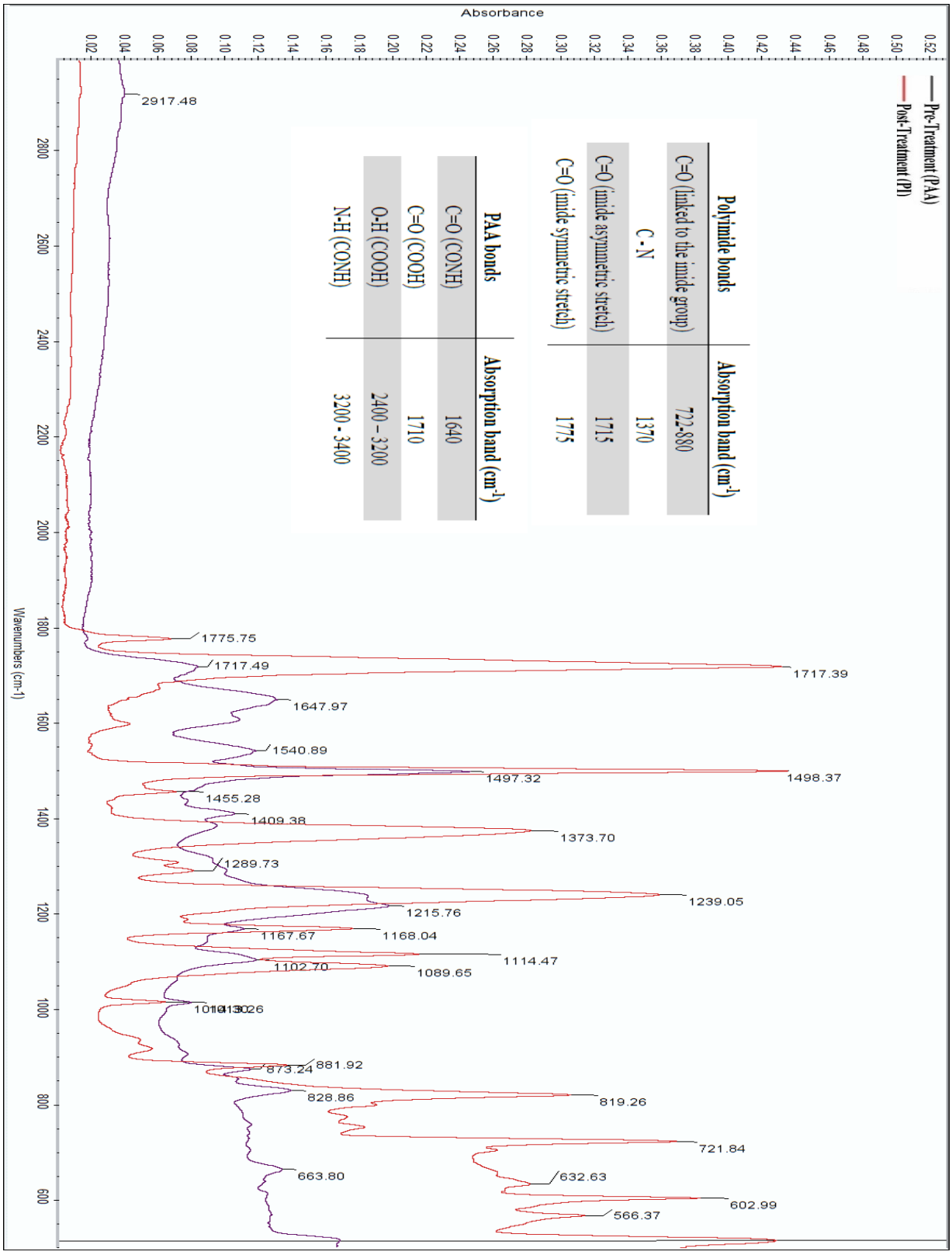

Figure 5.8. *The FT-IR spectra of PAA and PI*

The FT-IR spectra of PAA and PI reveal distinct absorption bands that are characteristic of each material. For PAA, the absorption bands include C=O (CONH) at 1640 cm^{-1}, C=O (COOH) at 1710 cm^{-1}, O-H (COOH) in the range of 2400–3200 cm^{-1}, and N-H (CONH) between 3200–3400 cm^{-1}. In contrast, the FT-IR spectra of PI show absorption bands at 722–880 cm^{-1} for C=O linked to the imide group, 1370 cm^{-1} for C-N stretching, 1715 cm^{-1} for asymmetric stretching of C=O in the imide group, and 1775 cm^{-1} for symmetric stretching of C=O in the imide group. These peaks are critical for confirming the successful conversion of PAA to PI. The peak at 722 cm^{-1} corresponds to the bending of the C=O bond in the imide ring, while the peak at 1370 cm^{-1} indicates the stretching of the C-N bond within the imide ring. The peaks at 1715 cm^{-1} and 1775 cm^{-1} represent the asymmetric and symmetric stretching of the C=O bond, respectively. Additionally, the peak at 1495 cm^{-1}, attributed to the aromatic ring, serves as an internal standard since it remains unchanged throughout the reaction.

Thermal stability is another crucial aspect of polyimide characterization, often assessed using thermogravimetric analysis (TGA). TGA involves heating a polyimide sample at a controlled rate, typically 20 °C/min, to evaluate its weight loss and degradation behavior. Polyimide exhibits exceptional thermal stability, with no significant weight loss observed until temperatures reach approximately 500 °C. Beyond this threshold, degradation begins, highlighting the material's ability to withstand extreme temperatures that would cause most other polymers to fail. In contrast, a TGA analysis of PAA reveals distinct changes in the initial part of the curve. The first weight reduction occurs due to the evaporation of residual solvent, such as DMF, which has a boiling point of around 153 °C. Subsequently, the imidization process induces structural transformations in the sample at approximately 180 °C, leading to further weight loss as the material transitions to the final polyimide structure.

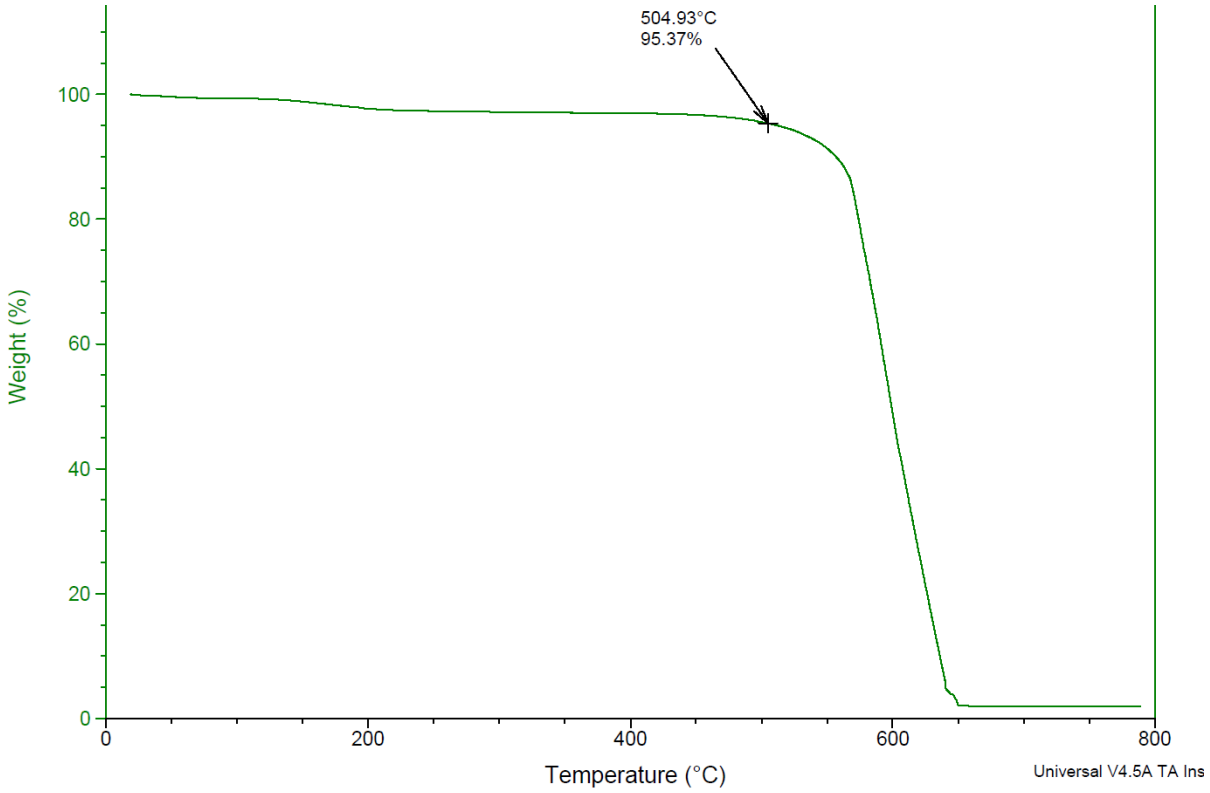

Figure 5.9. *The thermogravimetric analysis (TGA) of PI-only membrane*

The combination of FT-IR and TGA analyses provides a comprehensive understanding of the imidization process and the resulting polyimide's properties. FT-IR spectra confirm the structural changes from PAA to PI, while TGA demonstrates the material's remarkable thermal stability. These characterization techniques are essential for ensuring the quality and performance of polyimide membranes, particularly in high-temperature applications where thermal and mechanical stability are critical. The ability of polyimide to maintain its integrity at temperatures exceeding 500 °C, coupled with its well-defined imide structure, makes it a highly desirable material for advanced industrial and technological applications.

5.6 Titanium dioxide (TiO_2) characterization

The characterization of titanium dioxide (TiO_2) in polyimide (PI) membranes involves several analytical techniques to confirm its presence, structure, and distribution. Following the heat treatment process, which causes the evaporation of polyvinylpyrrolidone (PVP) and the conversion

of titanium butoxide (TBT) into TiO_2, the membranes exhibit an intense yellow color. In some areas, a white layer is observed, indicating the presence of TiO_2 after calcination. This white layer is more pronounced in regions with uneven TiO_2 dispersion, as shown in Figure 5.8. The SEM images of the whiter area indicates the accumulation of Nano-rods corresponding to the higher concentration of TiO_2.

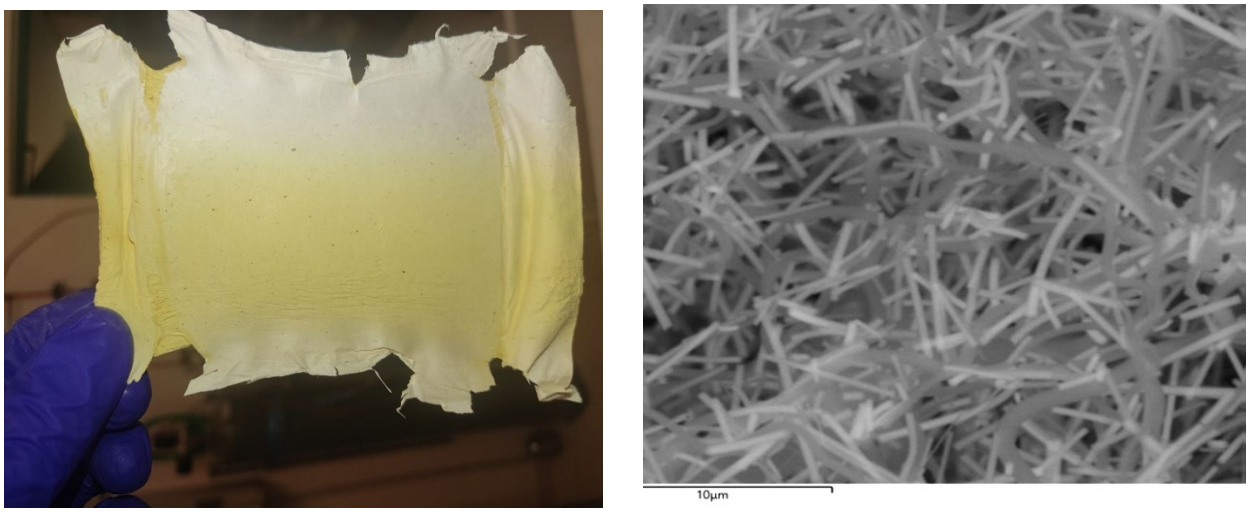

Figure 5.10. *The thermogravimetric analysis (TGA) of PI-only membrane*

To further confirm the presence and structure of TiO_2, scanning electron microscopy (SEM) and energy-dispersive X-ray spectroscopy (EDS) are employed. Figure 5.10 reveals that TiO_2, after calcination, appears as cracked fibers or Nano-rods with different lengths but similar diameters. The EDS spectra confirm that these structures are composed of titanium and oxygen, with traces of carbon likely originating from the polyimide matrix.

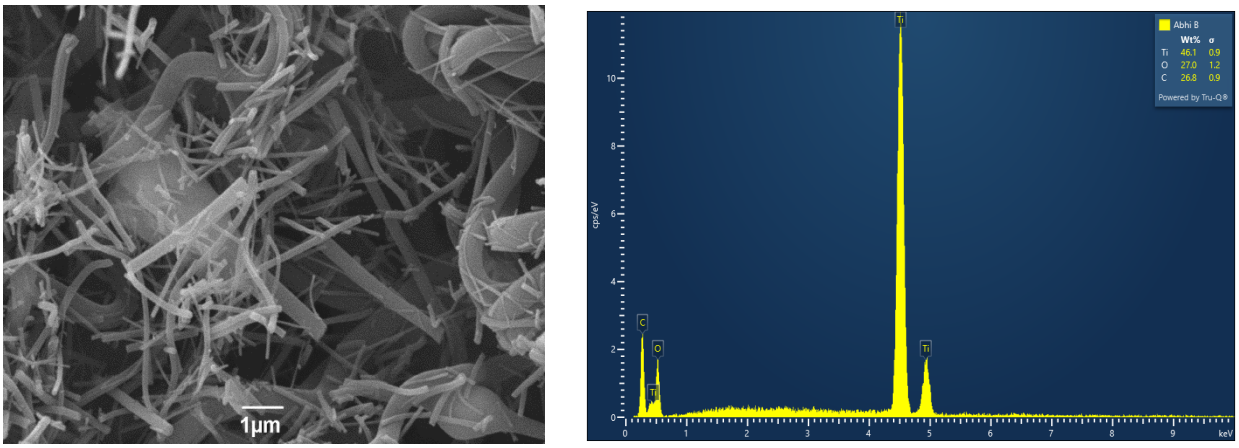

Figure 5.11. *The SEM image and EDS analysis of membrane with 36% w/w TiO_2*

The TiO_2 content in the membranes is also analyzed using thermogravimetric analysis (TGA). The TGA curve provided in the Figure 5.12 shows the weight loss of the membrane as a function of temperature. The curve indicates a significant weight loss of approximately 36.79% at higher temperatures, which can be attributed to the decomposition of the polyimide matrix and the residual organic components. The remaining weight corresponds to the inorganic content, primarily TiO_2. This analysis helps determine the catalyst content in the membrane, which is crucial for balancing the membrane's mechanical properties and catalytic activity. Ideally, the TiO_2 content should be around 30% by weight to ensure sufficient catalytic activity without compromising the membrane's mechanical integrity.

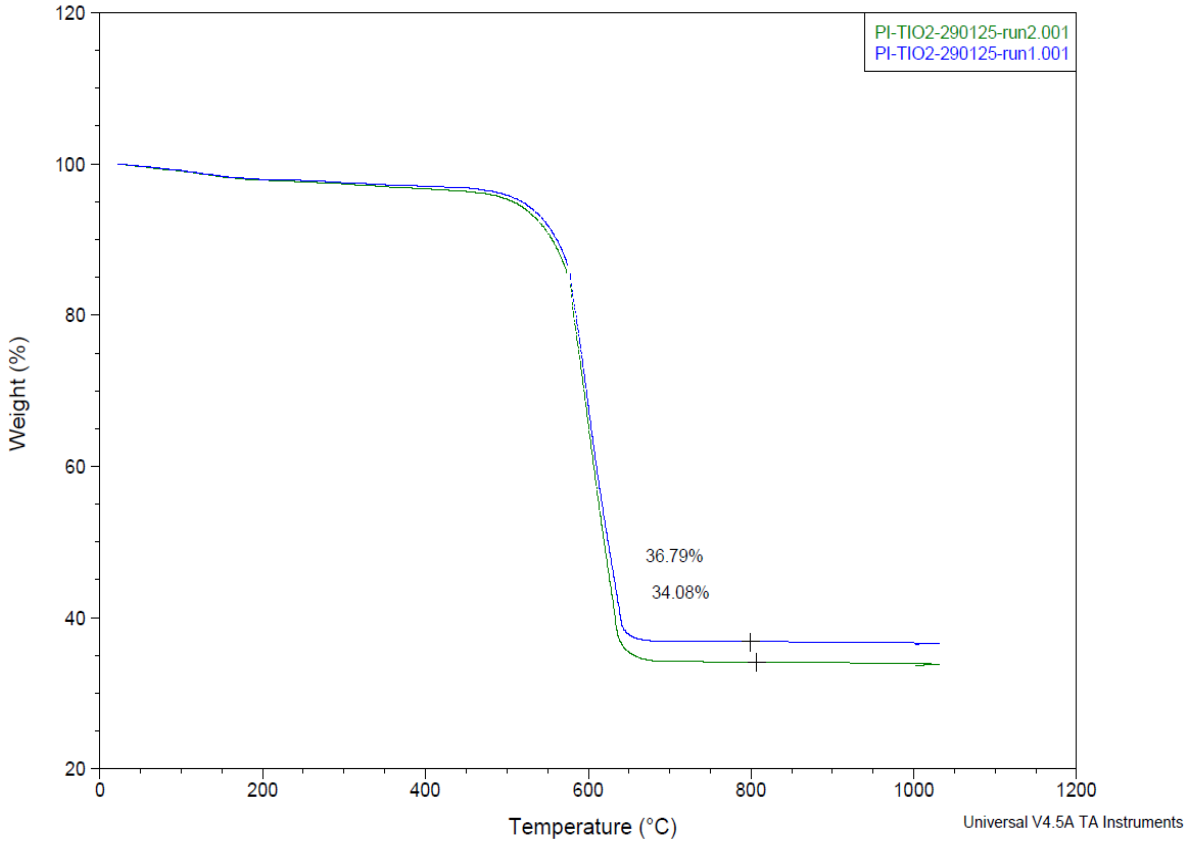

Figure 5.12. *The thermogravimetric analysis (TGA) of PImembrane with 36% w/w TiO_2*

The TGA results align with the objective of achieving a TiO_2 content of 30% by weight in the membranes. The deposition of TiO_2 is influenced by factors such as the TBT content in the catalytic solution and the flow rate during the electrospinning process. These parameters are carefully controlled to optimize the TiO_2 distribution and content in the final membrane. The TGA

curve also provides insights into the thermal stability of the membrane, showing no significant weight loss until temperatures exceed 500 °C, which is consistent with the high thermal stability of polyimide

Chapter 6

Experimental tests and results

In this final chapter, the data from all experiments related to different advanced oxidation processes (AOPs) are presented. Each experimental run lasted 7 hours—1 hour without UV light and 6 hours under UV irradiation. However, experiments involving MOFs (metal-organic frameworks) were an exception, running for only 6 hours under UV light since no membrane was used. Throughout each run, samples were collected hourly for HPLC analysis. This analysis not only determined the concentration of PFOA but also helped to identify other PFAS byproducts, such as PFHpA, PFHxA, and PFBA.

6.1 Theoretical foundation of the experiments

After weighting the specific components corresponding to each AOPs by balance they must be added to 1L MilliQ water. First sample must be taken at this time before system operation to know the initial concentration of PFOA in the system. Following this preliminary measurement, the membrane is carefully positioned within the photo-reactor chamber and the UV illumination system is activated when required by the specific experimental conditions. Previous researches showed that the membrane thickness couldn't play a significant role in degradation and PFOA removal but it should be between 20-40mm. During the reaction period, aqueous samples are systematically collected each for seven consecutive hours to monitor the temporal evolution of PFOA concentrations. These samples must be preserve at 0°C to not losing their chemical integrity until analysis can be performed using high-performance liquid chromatography-mass spectrometry (HPLC-MS), which provides sensitive detection of both the PFOA compound and its various degradation byproducts.

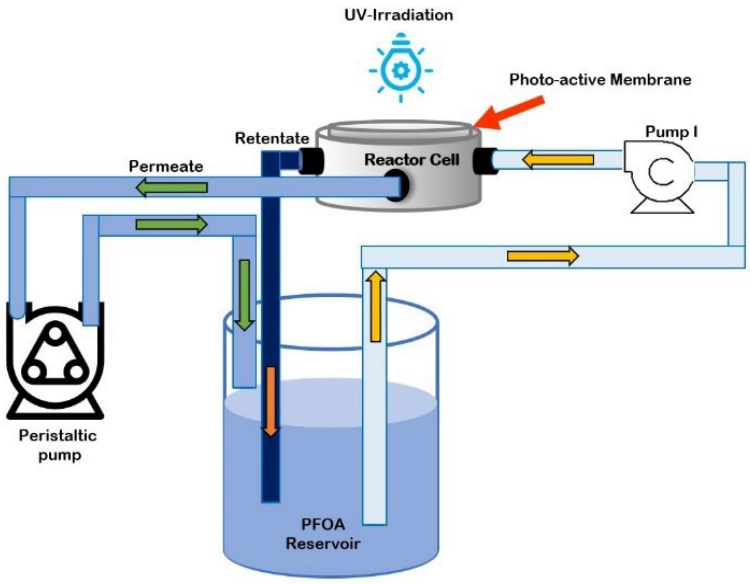

Figure 6.1. *The configuration of experimental setup*

The reactor system operates as a closed batch configuration as shown in figure 6.1, allowing for precise mass balance calculations. The fundamental mass balance equation (Eq. 6.1) accounts for all potential material flows within the system. However, given the completely contained nature of the experimental setup with no inputs or outputs during operation, the equation can be simplified to (Eq. 6.2), focuses only on the production and consumption terms for all chemical species present in the system, including the original PFOA contaminant and its various transformation products such as PFHpA, PFHxA, PFPA, and PFBA that emerge during the degradation process.

$$ACC = IN - OUT + PRODUCT\text{-}\ CONSUMPTION \quad (6.1)$$

$$ACC = PRODUCT\text{-}\ CONSUMPTION \quad (6.2)$$

This investigation primarily examines three key processes governing PFOA elimination from the system. Adsorption describes the physical transfer and retention of PFOA molecules within the membrane matrix, effectively removing them from the aqueous phase. Defluorination represents the more complete destruction pathway involving cleavage of carbon-fluorine bonds, ultimately yielding inorganic fluoride compounds and carbon dioxide as end products. The overall removal efficiency encompasses all elimination mechanisms, including both partial degradation into shorter-chain perfluoroalkyl compounds and complete mineralization through defluorination.

These processes are carefully quantified through a combination of chemical analysis techniques and mass balance calculations to provide a comprehensive understanding of the system's performance in PFAS remediation.

6.2 Experimental tests

The results corresponding to each experiments have been dedicated in the following sections also the calculation related to defluorination and PFOA removal during the experiment have been done to compare the efficiency of each oxidation process.

6.2.1 Membrane without $TiO_2 + K_2S_2O_8$ reservoir

$K_2S_2O_8$ (potassium persulfate) is a storage compound of the persulfate group ($S_2O_8^{2-}$) and indirectly related to sulfate groups as well. 10 gr of $K_2S_2O_8$ and 5 mg PFOA have been weighted and add into the 1L MilliQ-water container, to make sure about the solubilization the container is placed in an ultrasonic bath for 45 minutes. After getting the first sample and position the membrane containing only PI in the photo-reactor chamber, we can run the system for 7 hours (6 hours under UV lamp 16W). The concentration of PFOA during the experiments has been monitored which is represented in figure 6.2.

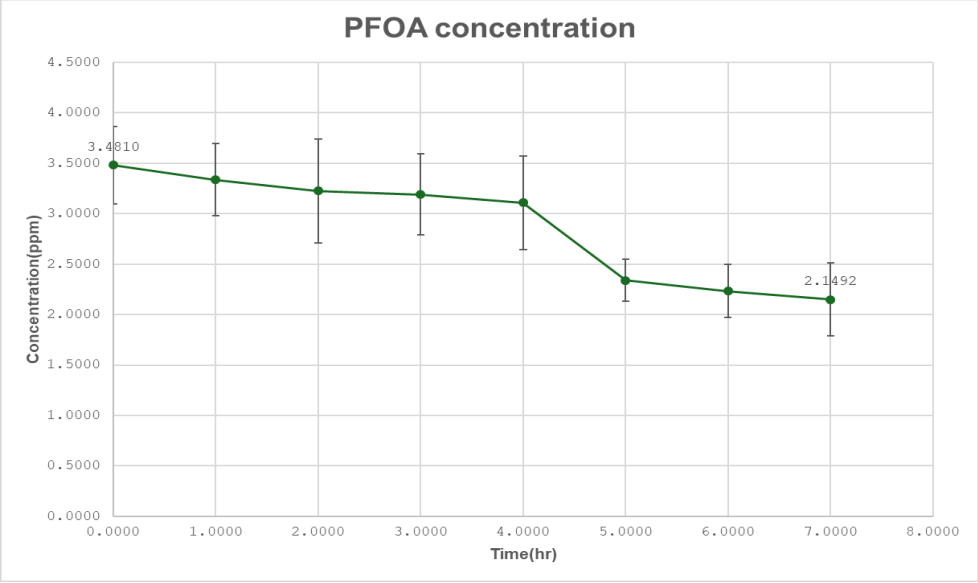

Figure 6.2. *The concentration of PFOA in persulfate-based experiments under 16W UV-Lamp*

As we can see, the concentration of PFOA has decreased mostly at the last 3 hours of experiments which is reasonable somehow, because of the intensity of the UV-lamp which can be more effective over time. In table 6.1, we can explore the concentrations of PFOA component during the7hours oxidation by persulfate activated radicals, the other PFAS components may not generated or the amounts of them are that much low which is not possible to detected by the calibration methods used in HPLC analysis.

Table 6.1 *The concentration of PFOA during the persulfate-based experiments under 16W UV-lamp*

Time(hr)	PFOA(ppm)
0	3.4810 ± 0.3805
1	3.3359 ± 0.3569
2	3.2251 ± 0.5173
3	3.1901 ± 0.4031
4	3.1089 ± 0.4659
5	2.3396 ± 0.2072
6	2.2335 ± 0.2634
7	2.1492 ± 0.3601

Obviously, by increasing the Lamp power the process must be more effective on degrading the PFOA, this has been investigated in an experiment using 48W UV-lamp instead of 16W. The data showed the effect of intensity on degradation even only one experiment has been done because of the lab-limitations but we will see next by using the 48W lamp the PFOA removal and defluorination increased also the existence of some byproducts has been detected during the process expressed in figure 6.3. Although, the amount of them are really low but couldn't be detected in all the experiments done with 16W UV-Lamp. According to the data, it seems that the PFOA in our system mostly degrade to PFBA which these PFBA will be degraded next under UV-lamp that's why the amount of that is not stable during the process. Also PFHpA is another PFAS that could be detected only in the last 3 hours of experiment.

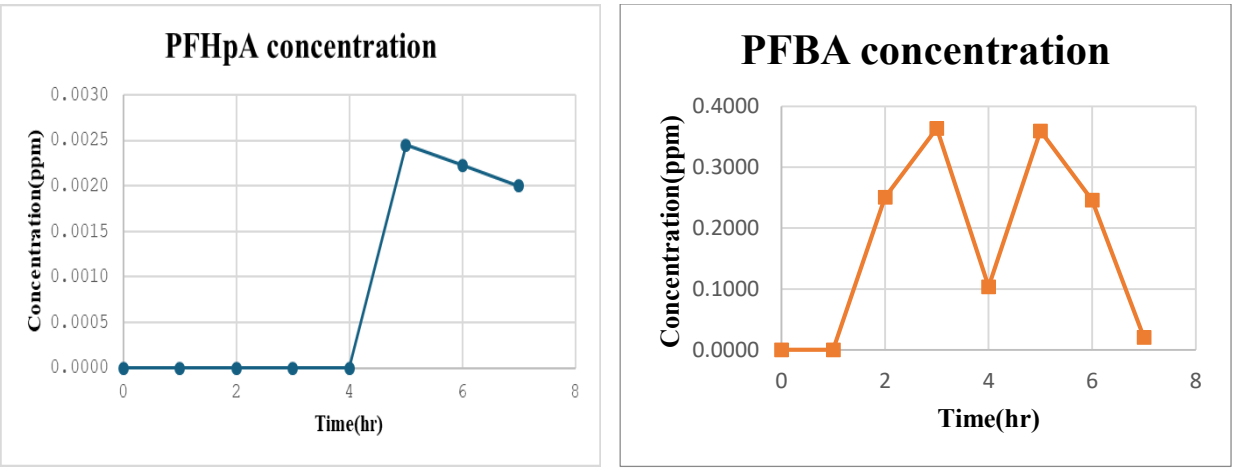

Figure 6.3. *The concentration of PFHpA and PFBA in persulfate-based experiments under 48W UV-Lamp*

Table 6.2 shows the data related to the experiment has been done with 48W UV-Lamp, here all the PFAS concentration has been collected during these 7 hours which help us in following calculation.

Table 6.2 *The concentrations of PFAS during the persulfate-based experiment under 48W UV-lamp*

Time(hr)	PFOA(ppm)	PFHpA(ppm)	PFBA(ppm)
0	4.5648	0.0000	0.0000
0	4.2997	0.0000	0.0000
0	4.1887	0.0000	0.2504
3	3.9013	0.0000	0.3639
4	3.9837	0.0000	0.1035
5	3.4830	0.0025	0.3597
6	3.0577	0.0022	0.2462
7	2.4518	0.0020	0.0205

The PFOA removal can be express as the difference between the initial concentration and the final concentration of PFOA divided by the initial concentration, as written in equation 6.3:

$$PFOA_{removal} = \frac{PFOA_0 - PFOA}{PFOA_0} \tag{6.3}$$

Which the $PFOA_0$ is the initial concentration and PFOA is the final concentration in ppm. The PFOA removal derived for this advanced oxidation process (AOP) is around **38.26%** for the experiments using the 16W UV-Lamp which this number increased to **46.29%** under 48W UV-Lamp , but this removal can be related to the absorption by the membrane matrix or the fluorine atoms could be defluorination that leads to the mineralization of PFOA in HF and CO2, this can be calculated easily by writing The mass balance for the fluorine atoms in the system by tracking fluorinated species from the initial time point (t = 0) to the end of the experiment. Initially, the system contains only PFOA, which breaks down into shorter-chain perfluoroalkyl compounds over time. To quantify the removal of fluorine (in moles or millimoles), the following equation can be applied:

$$F_{removal} = \left(\frac{PFOA_0 - PFOA_{7h}}{MW_{PFOA}}\right). n_F^{PFOA} - \sum_i \frac{PFAS_{i,7h}}{MW_i} . n_F^{PFAS_i} \quad (6.4)$$

In which $n_F^{PFAS_i}$ and MW_i are the number of fluorine atoms and molecular weight of each PFAS produced during the experiment respectively that could be derived from the table 6.3, also $PFAS_{i,7h}$ corresponding to the final concentration of each PFAS in ppm except PFOA.

Table 6.3 *The PFAS molecular weight and number of fluorine atoms*

Perfluorinated species	MW[g/mol]	n_F
PFOA	414.07	15
PFHpA	364.06	16
PFHxA	314.05	11
PFPA	264.05	9
PFBA	214.04	7

The defluorination can be simply expressed as the ratio between the F moles eliminated through mineralization and the initial F moles. (equation 6.5)

$$DEF = \frac{F_{removal} - F_{asd}}{F_0} \quad (6.5)$$

$F_{removal}$ can be derived using equation 6.4, in the oxidation process under 16W UV-Lamp, 0.0482 mmoles fluorine has been removed. F_{asd} is the mole of fluorine captured inside the membrane matrix, due to the absence of further experimental data regarding the pure adsorption of PFOA

inside the membrane and lack of information about the membrane absorption capacity in equilibrium, some assumptions have been considered in this part, however, previous researches showed that Adsorption, after 5 hours, is responsible for the removal of **29.95%** of fluorine in the system. Although, this value can be assumed to remain constant during the experiments with UV lamp because the light does not change the adsorption capacity of a membrane. In this study, the value of F_{asd} has been considered **30%** of F_0 which is the initial number of fluorine in the system can be calculated using the equation below.

$$F_0 = \left(\frac{PFOA_0}{MW_{PFOA}}\right). n_F^{PFOA} \tag{6.6}$$

According to the explanation above, about 0.0378 mmoles of fluorine absorbed inside the membrane matrix in 7 hours which is contribute to **8.26%** defluorination. If we do the same calculation for the data related to 48W UV-Lamp, we can reach **16.29%** defluorination which is doubled, this contribute to the intensity effect of lamp on the number of active radicals attacking C-F bonds.

6.2.2 Membrane without TiO_2 + ($FeSO_4$+H_2O_2) reservoir

In this study, a Photo-Fenton reaction was also operated in a laboratory-scale batch reactor. The initial solution same as the previous experiment contained 5 mg of PFOA dissolved in 1 liter of MilliQ water, however, here 25 mg of $FeSO_4$ with100 mg of H_2O_2 are added to the solution instead of $K_2S_2O_8$, the acidic environment would develop the activation process that's why 1ml H_2SO_4 also added to the container. The reactor was equipped with a UV lamp to initiate the Fenton reaction. A catalyst-free electrospun membrane was used, which served solely as a physical support and control for observing chemical transformation without added catalytic influence. This design allowed for isolated evaluation of the degradation performance of the Photo-Fenton process under controlled irradiation.

The experiment lasted 7 hours. During the first hour, the system was left in the dark to allow for equilibration and potential adsorption effects. Subsequently, the 16W UV lamp was activated and kept on for the remaining 6 hours. Getting samples has been done hourly for analysis using high-performance liquid chromatography (HPLC), enabling quantification of the remaining PFOA and its degradation products.

As shown in figure 6.4, PFOA concentrations exhibited a gradual decline over the course of the experiment. The most notable decrease occurred after the fourth hour—coinciding with extended exposure to UV light, which activates the iron-mediated Fenton reaction to produce hydroxyl radicals capable of attacking the PFOA molecule.

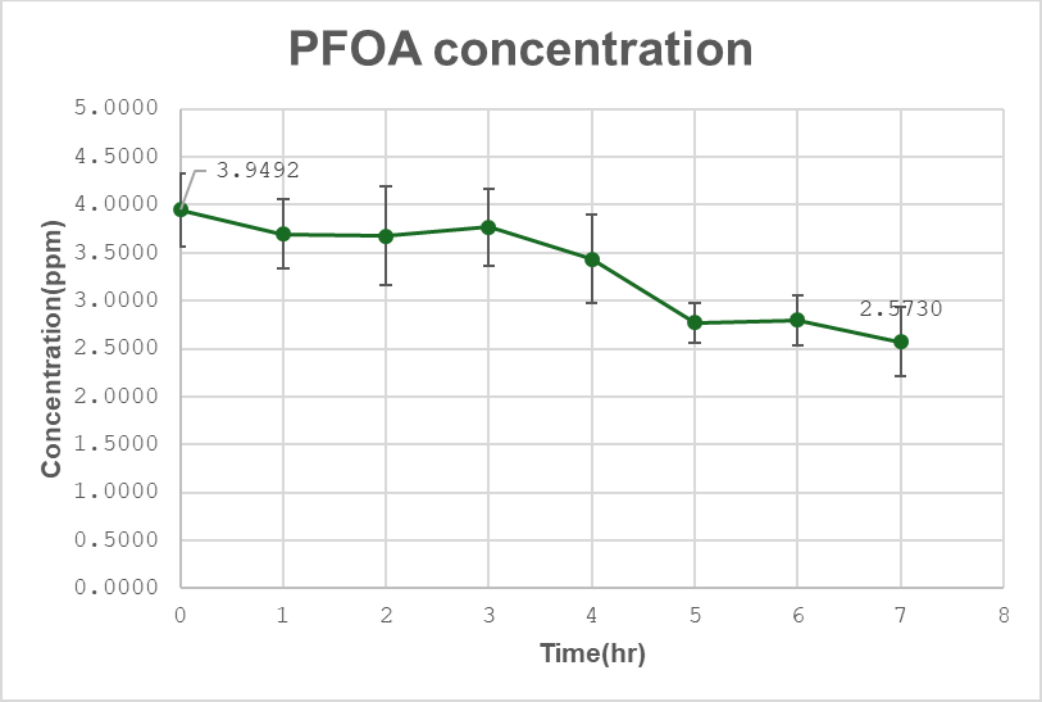

Figure 6.4. *The concentration of PFOA in Photo-Fenton experiments under 16W irradiation*

The initial PFOA concentration at time zero was approximately **3.95 ppm**, which dropped to **2.57 ppm** by the seventh hour, corresponding to a removal efficiency of **34.74%**. This is notably lower than what was achieved using the persulfate-based oxidation process, suggesting that the Photo-Fenton system, while effective, may require optimization for PFAS degradation—such as longer exposure, higher oxidant doses, or catalyst-functionalized supports.

Degradation of PFOA is typically associated with the stepwise shortening of the fluorinated carbon chain, leading to the generation of short-chain PFAS byproducts but same as Persulfate-based AOP, the amount of them are not that much to be detected by the calibration method used in HPLC analysis, however, by increasing the intensity of the lamp to 48W two key byproducts were observed—perfluoroheptanoic acid (PFHpA) and perfluorobutanoic acid (PFBA), as illustrated in figure 6.5.

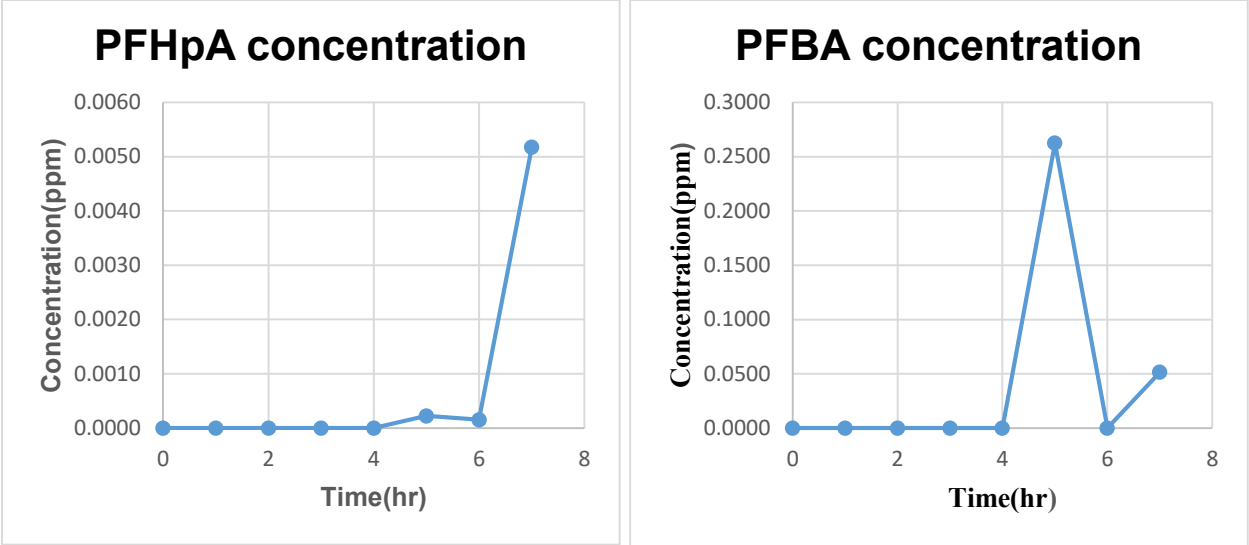

Figure 6.5. *The concentration of PFHpA and PFBA in Photo-Fenton experiments under 48W UV-Lamp*

PFBA exhibited a sharp increase after 4 hours, reaching a peak concentration of around 0.26 ppm which seems all of them degraded in two hours under UV-Lamp. This trend suggests a transient accumulation of PFBA followed by its partial degradation, either via further chain scission or transformation into non-fluorinated species.

PFHpA was undetectable during the first five hours but appeared at low concentrations after the fifth hour, reaching a maximum of 0.0052 ppm at hour 7. Interestingly, no detectable concentrations of other intermediate PFASs (e.g., PFHxA, PFPeA, PFPrA) were observed, implying either rapid conversion to shorter species or their concentrations remained below the detection limits.

Table 6.4 *The concentration of PFOA during the Photo-Fenton experiment under 16W UV-LAmp*

Time(hr)	PFOA(ppm)
0	3.9492 ± 0.1026
1	3.6959 ± 0.0985
2	3.6771 ± 0.0932
3	3.7659 ± 0.0061
4	3.4365 ± 0.1311
5	2.7693 ± 0.2230
6	2.7948 ± 0.1293
7	2.573 ± 0.070

Table 6.5 *The concentrations of PFAS during the Photo-Fenton experiment under 48W UV-LAmp*

Time(hr)	PFOA(ppm)	PFHpA(ppm)	PFBA(ppm)
0	3.4663	0.0000	0.0000
1	2.9847	0.0000	0.0000
2	2.9847	0.0000	0.0000
3	2.4372	0.0000	0.0000
4	2.6644	0.0000	0.0000
5	2.0505	0.0002	0.2624
6	1.7950	0.0002	0.0000
7	2.0529	0.0052	0.0515

In addition to tracking byproduct PFAS compounds, we assessed the extent of defluorination by analyzing the release of inorganic fluorine. This provides insight into the degree of mineralization, which is the ultimate goal of PFAS treatment.

The initial fluorine content from PFOA was calculated based on its molecular structure—15 fluorine atoms per molecule and a molecular weight of 414.07 g/mol. The total initial fluorine concentration (F_0) using equation 6.6 was determined to be 0.1431 mmol. After 7 hours of reaction, the fluorine atoms removed (F_removal) was calculated as 0.0499 mmol using equation 6.4 that the amounts accounted for in residual PFAS (F_asd) was 0.0429 mmol using the previous researches in which the membrane collaborate in 30% absorption of initial fluorine. Therefore, net fluorine defluorinated to inorganic forms (likely F^- or HF) derived as 0.0048 mmol.

The defluorination efficiency (DEF) was computed using the formula:

$$DEF = \frac{F_{removal} - F_{asd}}{F_0} = \frac{0.0499 - 0.0429}{0.1431} = \mathbf{4.847\%} \quad (6.7)$$

This relatively low DEF indicates that while partial transformation of PFOA occurred, complete breakdown of the carbon-fluorine backbone into fluoride ions was minimal. This aligns with the broader literature, where full mineralization of PFOA is often challenging and requires prolonged treatment durations or enhanced oxidative conditions. Future improvements may include the use of iron-functionalized membranes, higher H_2O_2 concentrations, or synergistic processes (e.g.,

combining with electrochemical oxidation) to enhance radical production and improve both degradation rates and defluorination efficiency.

Table 6.6 *The comparison of efficiency of the two lamps with different power on degradation*

	16W UV-Lamp	**48W UV-Lamp**
PFOA removal(%)	34.84	40.77
DEF(%)	4.85	8.93

As we can see in the table above, higher lamp power leads to better PFOA removal and degradation efficiency. The 48W lamp can generate a higher concentration of radicals and faster catalyst activation, leading to better contaminant degradation compared to the 16W lamp that's why even the DEF has been doubled same as persulfated AOP. In short, higher UV power boosts both direct photochemical reactions and photocatalytic efficiency, leading to stronger PFOA removal and defluorination.

6.2.3 Membrane with TiO_2(Photocatalyst)

In this sort of experiment, the degradation of perfluorooctanoic acid (PFOA) through a photocatalytic process was investigated using a TiO_2-functionalized polyimide membrane under UV irradiation. We want to explore the role of UV light and the TiO_2 catalyst in promoting the degradation of PFOA in aqueous media. The experimental setup was carried out in a laboratory-scale batch reactor same as the other experiments, designed to assess the effects of varying UV lamp power (16 W and 48 W) on PFOA removal efficiency and defluorination performance.

The initial solution contained only 5 mg of PFOA dissolved in 1 liter of Milli-Q water, with the membrane containing catalyst positioned in the photo-reactor. No additional oxidizing agents were added to the solution, emphasizing the role of photoinduced oxidation facilitated by the TiO_2 photocatalyst under UV light. The experimental procedure began with a one-hour cycling the components without using UV-Lamp, providing sufficient time for the adsorption of PFOA molecules onto the membrane surface, ensuring a baseline measurement of any initial removal through adsorption alone. After equilibration, the reactor was exposed to UV light. Hourly samples were collected throughout the experiment and analyzed using High-Performance Liquid

Chromatography (HPLC) to monitor changes in PFOA and the other PFAS concentrations produce during the process, as well as assess the degree of defluorination.

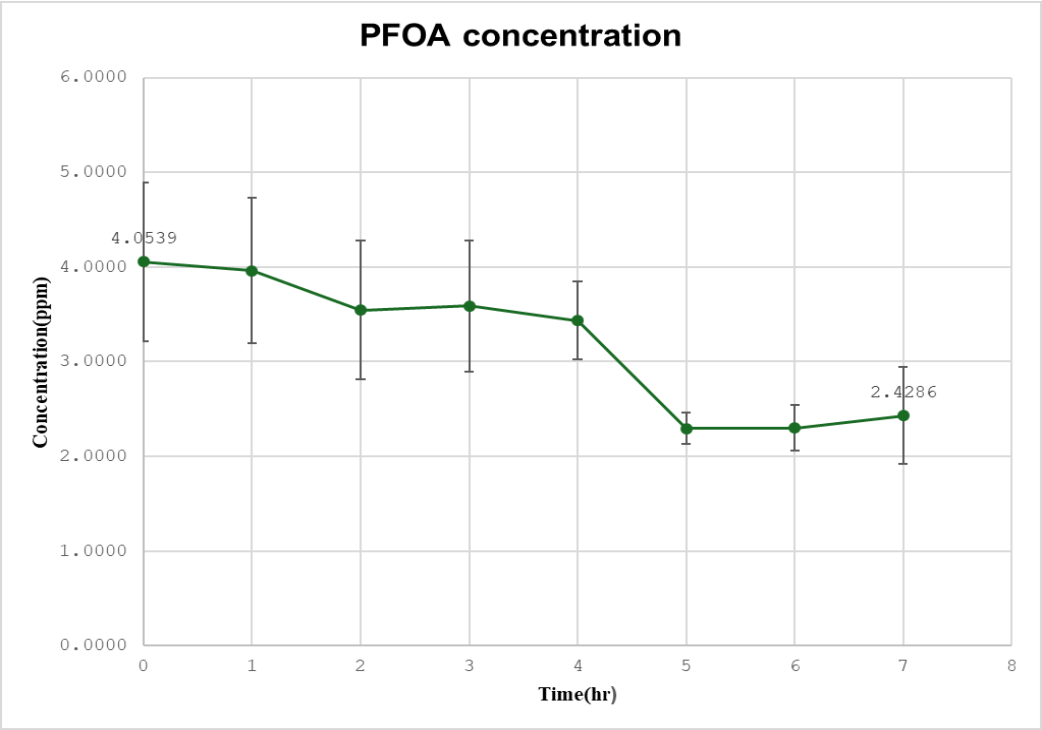

Figure 6.6. *The concentration of PFOA in Photocatalyst experiments under 16W irradiation*

The experimental results clearly demonstrate the effect of UV power intensity on the degradation efficiency of PFOA. Under 16 W UV irradiation, the degradation of PFOA was observed to be moderate. In figure 6.5, we can see that the concentration of PFOA drops from 4.05 ppm to 2.43 ppm in 7 hours which contribute to a removal efficiency of approximately **40.09%** using equation 6.3. The formation of PFBA (perfluorobutanoic acid) as a key intermediate was evident, with its concentration peaking at approximately 0.144 ppm after 4 hours of UV exposure, before it was subsequently mineralized into non-fluorinated species.

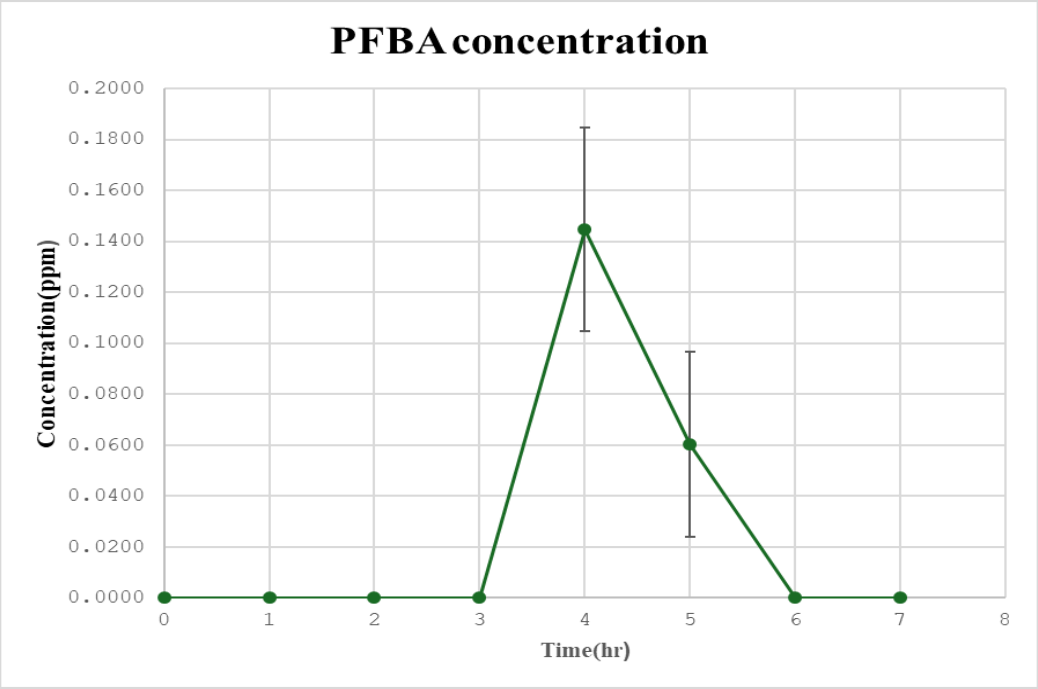

Figure 6.7. *The concentration of PFBA in Photocatalyst experiments under 16W irradiation*

To continue with the calculation, we need to know exactly the amount of components during the process which have been reported in the table 6.6. According to the data, from 0.1469 mmol fluorine at time zero, 0.059 mmol have been removed (F_removal) using the equation 6.4 and 0.047 mmol have been absorbed (F_ads) inside the membrane matrix.

Table 6.7 *The concentrations of PFAS during the Photocatalyst experiments under 16W UV-Lamp*

Time(hr)	PFOA(ppm)	PFBA(ppm)
0	4.0538 ± 0.4854	0.0000
1	3.9616 ± 0.4430	0.0000
2	3.5452 ± 0.4232	0.0000
3	3.5871 ± 0.4016	0.0000
4	3.4356 ± 0.2380	0.1445 ± 0.04
5	2.2949 ± 0.0956	0.0603 ± 0.0364
6	2.3004 ± 0.1382	0.0000
7	2.4286 ± 0.2956	0.0000

the defluorination efficiency (DEF) in this case was calculated to be **8.09%**, which signifies the partial breakdown of the fluorinated carbon backbone into smaller fluorine-containing byproducts

$$DEF = \frac{F_{removal} - F_{asd}}{F_0} = \frac{0.059 - 0.047}{0.1469} = \mathbf{8.09\%} \quad (6.8)$$

In contrast, when the UV lamp power was increased to 48 W, a significant enhancement in both PFOA removal and defluorination efficiency was observed. According to table 6.8, the PFOA removal efficiency under the 48 W UV-Lamp reached **51.99%,** As in the 16 W trials, PFBA was also observed as an intermediate byproduct; however, the concentrations of PFBA were higher under the 48 W UV conditions, reaching a peak of 0.5301 ppm at the 3-hour mark before degrading within the subsequent 2 hours.

Table 6.8 *The concentrations of PFAS during the Photocatalyst experiments under 48W UV-Lamp*

Time(hr)	PFOA(ppm)	PFHpA(ppm)	PFBA(ppm)
0	4.8222	0.0000	0.0000
1	4.7346	0.0000	0.0000
2	3.2909	0.0000	0.0000
3	3.3425	0.0000	0.5301
4	2.9689	0.0000	0.0000
5	2.4343	0.0000	0.0000
6	2.3053	0.0000	0.0000
7	2.3152	0.0052	0.0000

The increased UV intensity under the 48 W lamp appears to have played a significant role in activating more TiO_2 surface sites, which resulted in a higher rate of hydroxyl radical generation and faster degradation kinetics. This trend aligns with the expected behavior in photocatalytic degradation, where higher UV intensity typically leads to higher catalyst activation and enhanced reaction rates.

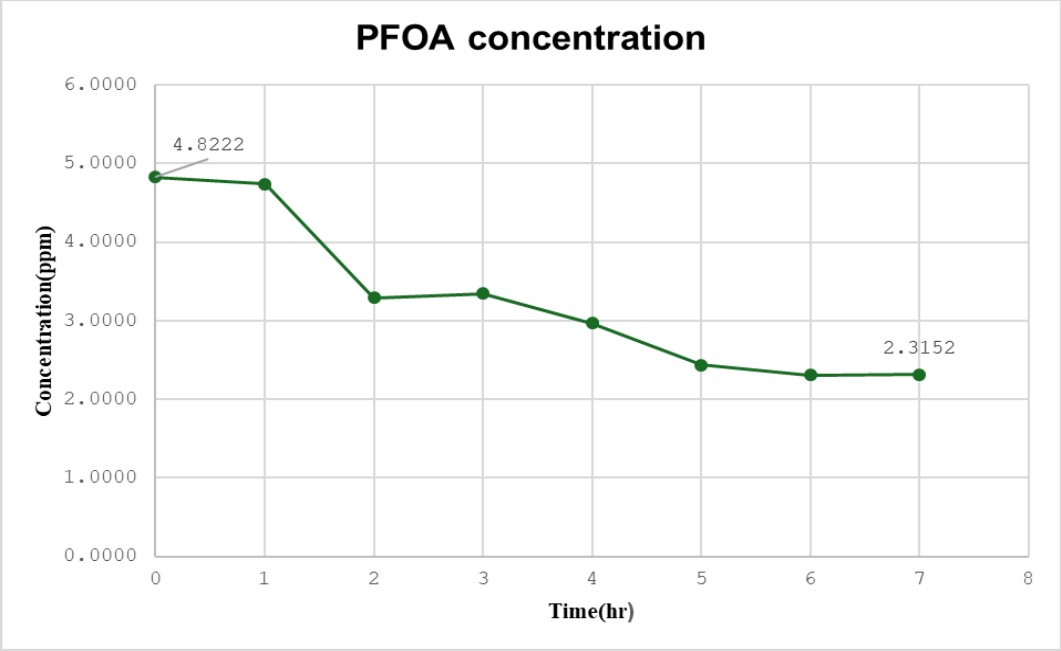

Figure 6.8. *The concentration of PFOA in Photocatalyst experiments under 48W irradiation*

In this study, defluorination was quantified by measuring the inorganic fluorine released during the degradation process. The initial fluorine content (F_0) for PFOA was determined to be 0.1747 mmol based on its molecular structure, and the fluorine removed (F_removal) after 7 hours of exposure to 48 W UV light was 0.0906 mmol. After accounting for the adsorbed fluorine (F_ads) on the membrane (which was approximately 0.0559 mmol), the net defluorination (F_def) was calculated as 0.0048 mmol.

The defluorination efficiency (DEF), calculated using the formula:

$$DEF = \frac{F_{removal} - F_{asd}}{F_0} = \frac{0.0906 - 0.0559}{0.1747} = \mathbf{19.88\%} \tag{6.9}$$

This result indicates that although substantial defluorination occurred, the mineralization of PFOA (complete breakdown into fluoride ions) was not achieved to the same extent as other degradation products. This observation is consistent with the challenges faced in the full mineralization of PFOA as reported in the literature, which often requires longer treatment times or enhanced oxidative conditions. However, the improvement in DEF at the higher UV power demonstrates the potential of this photocatalytic system in promoting partial mineralization of PFOA. This increase in degradation efficiency can be attributed to the greater production of hydroxyl radicals at higher

UV power, which accelerates the oxidative degradation of PFOA and its transformation into shorter PFAS byproducts. Also to evaluate catalyst efficiency, PFOA removal was normalized to the TiO_2 content within the membrane. Based on TGA analysis, the TiO_2 fraction was about 36.79%, corresponding to 0.077 g of catalyst in the 0.21 g membrane used. The net PFOA removal of 1.63 mg in 1L water yielded a normalized abatement of **21.17** mg of PFOA per gram of TiO_2 under 16W UV irradiation. This provides a comparative metric for evaluating catalyst performance across different experimental conditions. This number increased to **32.55** mg of PFOA per gram of catalyst under 48W UV irradiation.

6.2.4 Membrane with TiO_2 + reagents reservoir (Combined experiment)

In this section, a comprehensive combined process involving persulfate-based advanced oxidation, Photo-Fenton reaction, and photocatalysis was studied for the degradation of perfluorooctanoic acid (PFOA). The goal was to leverage the advantages of all three oxidation pathways to enhance PFOA degradation and defluorination efficiency under controlled laboratory conditions. The same experimental setup was used as before, involving a 1 L batch reactor containing an initial amount of 5 mg PFOA dissolved in MilliQ water. The system was supplemented with 25 mg $FeSO_4$, 100 mg H_2O_2, and potassium persulfate ($K_2S_2O_8$) to initiate the oxidation reactions. Additionally, a TiO_2-functionalized electrospun membrane was installed as a photocatalytic support. A 16W UV lamp was used to drive the photo-activation steps necessary for both the Photo-Fenton and photocatalytic reactions.

The experiment run for 7 hours (1 hour without UV irradiation and 6 hours under UV-Lamp). Same as the previous experiments, the samples were taken each hour for analyzing with high-performance liquid chromatography (HPLC) for PFOA and its degradation products, alongside fluoride ion quantification to assess mineralization.

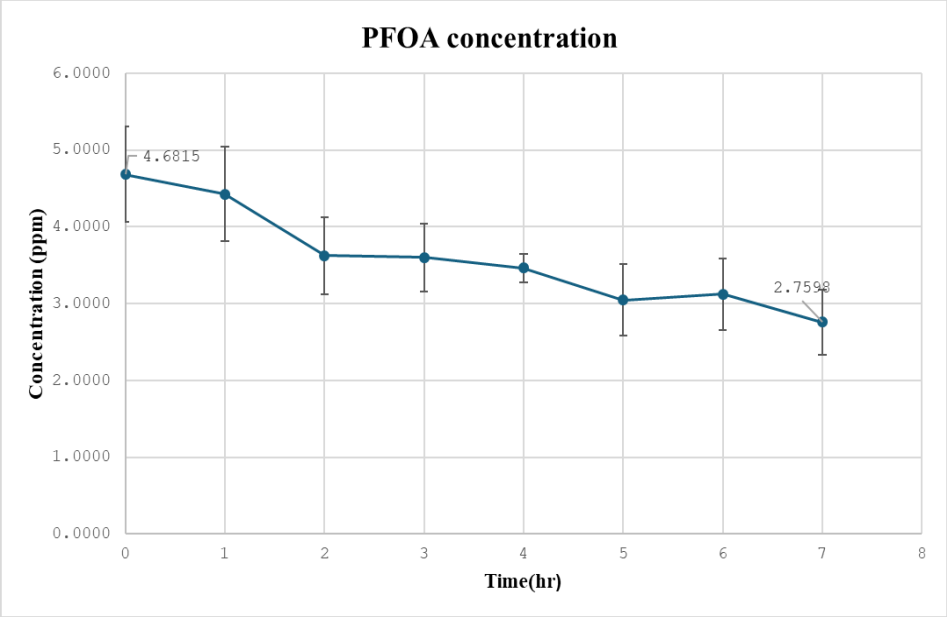

Figure 6.9. *The concentration of PFOA in combined experiments under 16W irradiation*

As shown in Figure 6.9, PFOA concentration exhibited a substantial decline over time. The initial PFOA concentration measured at time zero was 4.68 ppm, which gradually dropped to approximately 2.76 ppm after 7 hours of reaction, corresponding to a PFOA removal efficiency of **41.05%** using equation 6.3. Compared to the individual treatments (Persulfate AOP, Photo-Fenton, or Photocatalysis alone), the combined process demonstrated a higher removal efficiency, indicating the synergistic effect of multiple oxidation pathways operating simultaneously.

Degradation products were monitored throughout the experiment. PFBA (perfluorobutanoic acid) was detected early during the reaction, but at low concentrations (~0.002–0.007 ppm range). Additionally, short-chain intermediates such as PFHpA (perfluoroheptanoic acid), PFHxA (perfluorohexanoic acid), and PFPeA (perfluoropentanoic acid) were also observed at low but increasing concentrations as the reaction progressed. As we can see in figure 6.10, PFPeA reached the highest concentration among the short-chain byproducts (~0.15 ppm at hour 3–4), suggesting active stepwise shortening of the PFOA carbon-fluorine backbone. The concentration of these byproducts peaked around the third or fourth hour and then slightly decreased and stabilized, indicating their subsequent degradation, possibly leading to the release of fluoride ions or conversion into smaller organic acids.

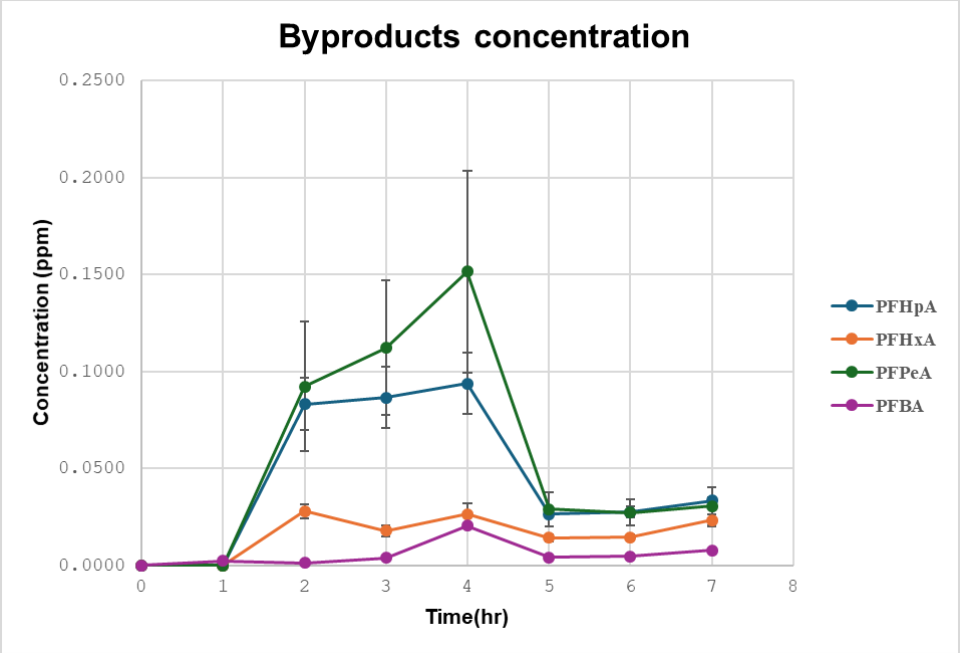

Figure 6.10. *The concentrations of PFAS in combined experiments under 16W irradiation*

Table 6.9 shows the PFOA and the byproducts concentrations which are monitoring during the process. The initial total fluorine content (F_0) based on PFOA molecular structure was determined as 0.1696 mmol using equation 6.6. After 7 hours of reaction, the amount of fluorine removed (F_removal) was measured as 0.0667 mmol. Based on the literature-reported, the membrane adsorbs 30% of the initial fluorine, so the fluorine adsorbed onto the membrane (F_ads) was calculated as 0.0492 mmol. Thus, the defluorination efficiency (DEF) achieved during the combined treatment was approximately **10.33**% if we put the corresponding data in equation 6.5. This is significantly higher than what was achieved with the individual processes under the 16W lamp, indicating an enhanced mineralization capability when combining persulfate, Photo-Fenton, and photocatalytic oxidation pathways.

Table 6.9 *The concentrations of PFAS during the combined experiments under 16W UV-Lamp*

Time(hr)	PFOA(ppm)	PFBA(ppm)	PFHpA(ppm)	PFHxA(ppm)	PFHeA(ppm)
0	4.6815 ± 0.6217	0	0	0	0
1	4.4266 ± 0.6187	0.0022 ± 0.0014	0	0	0
2	3.6250 ± 0.4982	0.0013 ± 0.0007	0.0831 ± 0.0135	0.0279 ± 0.0036	0.0922 ± 0.0333
3	3.5996 ± 0.4451	0.0037 ± 0.0023	0.0866 ± 0.0156	0.0177 ± 0.0030	0.1122 ± 0.0346
4	3.4632 ± 0.1819	0.0204 ± 0.0179	0.0939 ± 0.0159	0.0264 ± 0.0055	0.1516 ± 0.0519
5	3.0488 ± 0.4699	0.0040 ± 0.0021	0.0265 ± 0.0012	0.0141 ± 0.0019	0.0289 ± 0.0089
6	3.1219 ± 0.4675	0.0047 ± 0.0028	0.0274 ± 0.0028	0.0146 ± 0.0010	0.0271 ± 0.0066
7	2.7597 ± 0.4260	0.0077 ± 0.0042	0.0335 ± 0.0017	0.0232 ± 0.0030	0.0305 ± 0.0098

The results clearly demonstrate that combining multiple oxidation pathways can synergistically enhance the overall PFOA degradation rate and defluorination. In this setup, sulfate radicals ($SO_4^{\cdot-}$) from persulfate decomposition, hydroxyl radicals ($OH^{\cdot}$) from the Photo-Fenton reaction, and photogenerated electron-hole pairs from TiO_2 photocatalysis collectively contributed to a more aggressive oxidative environment.

The observed stepwise degradation to short-chain PFAS (PFHpA, PFHxA, PFPeA) follows the known degradation pathways for perfluorinated compounds, where sequential cleavage of the C-C bond occurs. However, full mineralization, as evidenced by DEF values, remains a challenge, reflecting the inherent stability of the C-F bond and suggesting that further optimization (e.g., higher oxidant dosage, longer irradiation time, stronger UV light) could be necessary for complete degradation.

Overall, the combined system displayed a promising approach for PFAS treatment, offering higher degradation and mineralization efficiencies compared to single treatment processes.

In Figure 6.11 which the PFOA concentration during the 7 hours are provided for 48W UV-Lamp. Here the concentration decreased significantly over the course of the experiment. Starting from an initial concentration of approximately 4.11 ppm, the PFOA levels dropped to around 1.93 ppm after 7 hours, corresponding to a removal efficiency of **52.99%**. This removal rate is substantially higher than that observed in the 16W combined experiment, highlighting the positive influence of increased UV intensity on PFAS degradation processes.

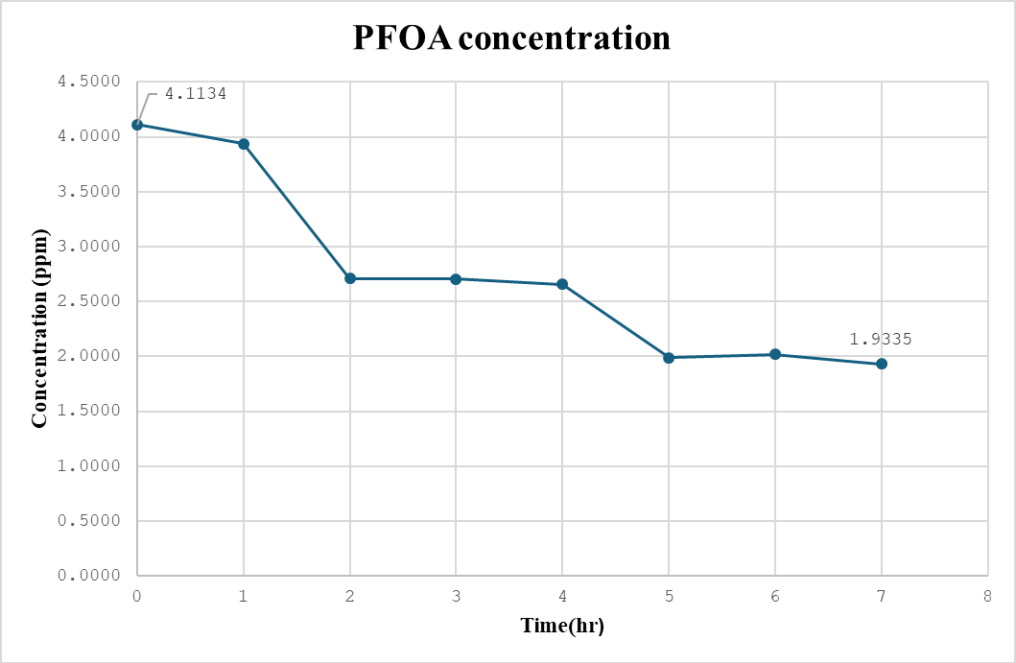

Figure 6.11. *The concentration of PFOA in combined experiments under 48W irradiation*

In addition to monitoring PFOA decay, intermediate perfluorinated products were analyzed. PFHpA (perfluoroheptanoic acid) formation remained minimal, with concentrations barely above detection limits (~0.0004 to 0.0025 ppm). However, PFBA (perfluorobutanoic acid) showed significant transient formation. Initially, PFBA concentration was already detectable at 0.18 ppm, and it increased to a maximum of approximately 0.88 ppm at the third hour, corresponding to the peak degradation stage of PFOA. Afterward, PFBA levels slightly declined, indicating that even short-chain PFAS were undergoing further transformation under the aggressive oxidative conditions provided by the 48W system.

This observation confirms that PFBA is a major intermediate in PFOA degradation pathways in combined experiment using 48W UV-Lamp, often formed by stepwise removal of CF_2 units. However, under high-energy UV irradiation combined with strong radical production, PFBA itself becomes susceptible to degradation into fluoride ions and possibly ultra-short-chain PFAS or non-fluorinated species.

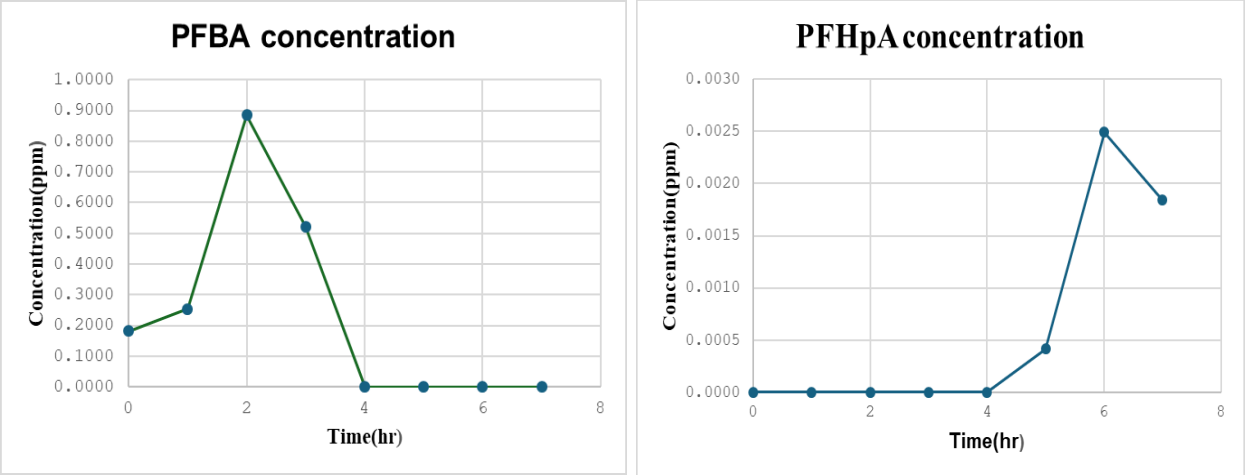

Figure 6.12. *The concentration of PFHpA and PFBA in Combined experiments under 48W UV-Lamp*

The mineralization level of the system was evaluated by calculating the defluorination efficiency (DEF). First, the initial fluorine content (F_0) must be determined by using the equation 6.6 which results in 0.1490 mmol. After 7 hours of reaction, the amount of fluoride removed (F_removal) was calculated as 0.0789 mmol if we put the corresponding data in equation 6.4, also here we assumed that F_ads is 30 % of the initial fluorine as was derived in previous researches, the defluorination was determined by applying the DEF formula:

$$DEF = \frac{F_{removal} - F_{asd}}{F_0} = \frac{0.0789 - 0.0432}{0.1490} = \mathbf{23.95\%} \quad (6.10)$$

Thus, the defluorination efficiency achieved was approximately **23.95%**, more than double of the 16W combined experiment.

6.2.5 MOF (metal-organic framework)

In this section, the degradation of PFOA using a MOF (metal-organic framework) system was investigated. Samples were collected at three time points (0, 3, and 6 hours) because as shown in figure 6.13 the experimental scale is not that much to take sample each hour same as before, the samples then brought to HPLC analysis Laboratory to evaluate the changes in PFOA concentration, the formation of intermediate short-chain PFASs (specifically PFBA and PFHpA).

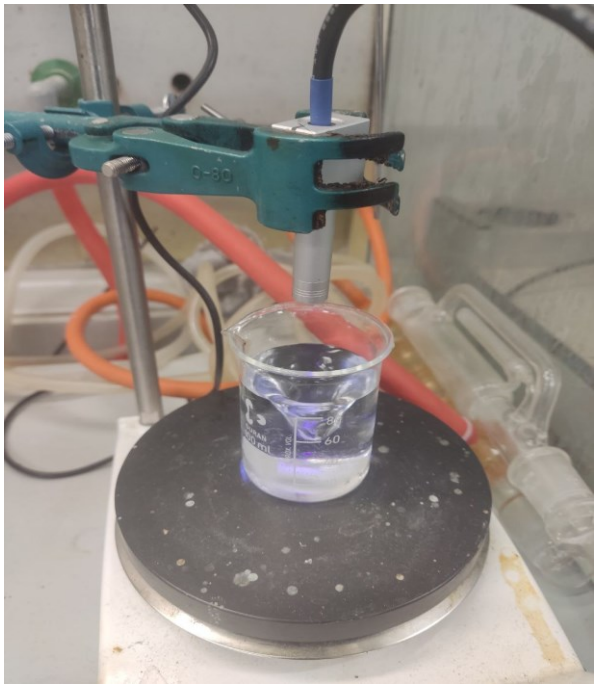

Figure 6.13. *The experimental setup related to MOF AOP*

The results showed a gradual decrease in PFOA concentration over time (Figure 6.14). The initial concentration of PFOA was measured at 5.06 ppm. After 3 hours of treatment, the concentration decreased to 4.34 ppm, and by 6 hours it further decreased to 3.30 ppm. This corresponds to a PFOA removal efficiency of approximately **34.80%** regarding to equation 6.3**.** The consistent downward trend in PFOA concentration suggests that the MOF was able to adsorb or partially degrade PFOA over time. However, compared to the previous experiments combining persulfate-based advanced oxidation, Photo-Fenton, and photocatalysis, the efficiency achieved here was relatively lower.

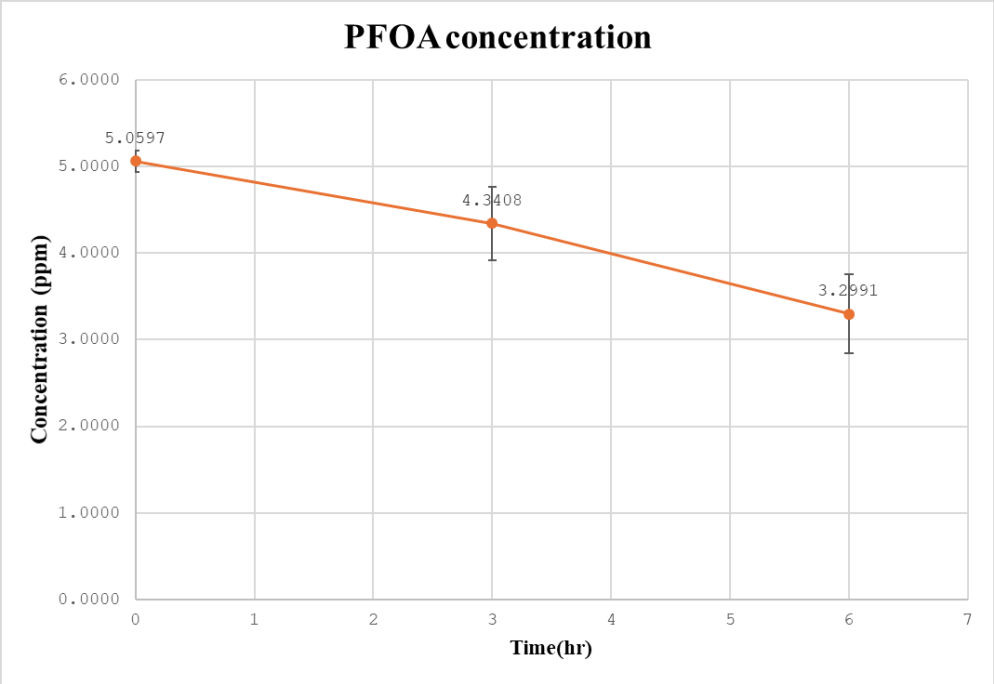

Figure 6.14. *The concentration of PFOA in MOF AOP under 48W irradiation*

Intermediate products, mainly PFBA (perfluorobutanoic acid), were detected during the degradation process. As shown in Figure 6.15, the PFBA concentration initially increased, peaking at 0.424 ppm at 3 hours, before decreasing sharply to 0.0131 ppm at 6 hours. The sharp rise followed by a decline indicates a transient formation of PFBA, which might have resulted either from PFOA chain-shortening reactions or possible adsorption of PFBA back onto the MOF surface. Also very little PFHpA (perfluoroheptanoic acid) was detected throughout the experiment. Only trace amounts (approximately 0.00033 ppm) were found at the 6-hour sampling point, suggesting that the degradation pathway favored the production of shorter-chain PFASs, with negligible accumulation of intermediate seven-carbon species.

Table 6.10 *The concentrations of PFAS during the MOF AOP under 16W UV-Lamp*

Time(hr)	PFOA(ppm)	PFBA(ppm)	PFHpA(ppm)
0	5.0597 ± 0.1258	0.0349 ± 0.0349	0
3	4.3408 ± 0.4224	0.4240 ± 0.2222	0
6	3.2991 ± 0.4519	0.0131 ± 0.013	0.0003 ± 0.0001

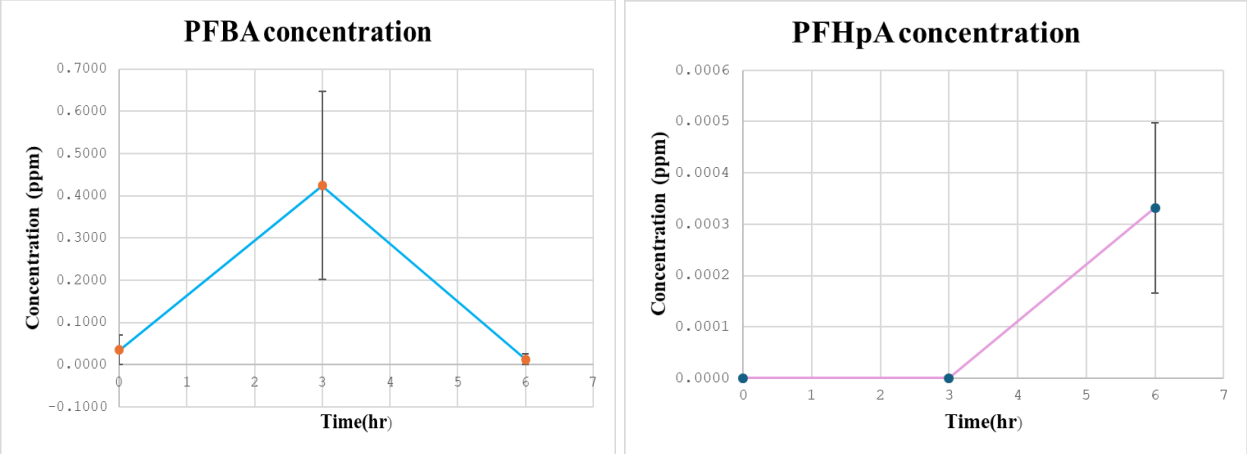

Figure 6.15. *The concentration of PFHpA and PFBA in MOF AOP under 48W UV-Lamp*

According to the table 6.10, we can continue with the corresponding calculations. Fluoride ion (F^-) measurements were used to assess the extent of defluorination during the MOF treatment. The initial fluoride concentration (F_0) was calculated 0.1833 mmol using the equation 6.6. After treatment, only 0.0632 units of fluoride were released, with an adsorption loss (Fads) of approximately 0.0638 units. This could be reasonable because the MOF doesn't participate in mineralization of fluorine that's why the calculated defluorination efficiency (DEF) was -0.30%, indicating that no significant mineralization of PFOA into fluoride ions occurred under the tested conditions. This negative DEF% suggests that slight re-adsorption or analytical variability may have influenced the final fluoride measurements. The negative value of that related to the calculation assumption which are not precise and the actual value for DEF here must be zero.

When comparing this result with those obtained in the combined photocatalytic or Photo-Fenton systems (where defluorination was notably higher), it becomes clear that the MOF primarily acts as an adsorptive material rather than an efficient catalyst for PFOA mineralization. While MOFs offer large surface areas for capturing pollutants, their intrinsic catalytic activity toward C–F bond cleavage remains limited unless further functionalized.

6.3 Comparison of the results

The processes studied were persulfate activation, Photo-Fenton process, photocatalysis, MOF-assisted oxidation, and a hybrid treatment system. The performance of each system was compared based on PFOA removal efficiency, defluorination percentage (DEF), and the temporal concentration decay (C/C_0) of PFOA over time.

Table 6.11 *The initial mean concentrations of PFOA for each AOPs under 16W UV-Lamp*

	Persulfate	Photo-Fenton	Photocatalyst	Combined	MOF
Initial mean PFOA concentration (ppm)	3.48 ±0.38	3.94 ± 0.10	4.05 ± 0.48	4.68 ± 0.62	5.05 ± 0.15

As can be seen in Figure 6.16, the PFOA removal efficiency varied among the tested processes. The combined system achieved the highest removal rate at 41.05%, slightly outperforming the photocatalyst system, which demonstrated 40.09% removal. Persulfate oxidation alone achieved a moderate removal efficiency of 38.26%. In contrast, the Photo-Fenton and MOF-based systems exhibited the lowest removal efficiencies at 34.85% and 34.79%, respectively. This ranking highlights the benefit of mixing different treatment mechanisms, as the hybrid system obviously benefits from the merits of both oxidative degradation and adsorption processes to provide superior performance.

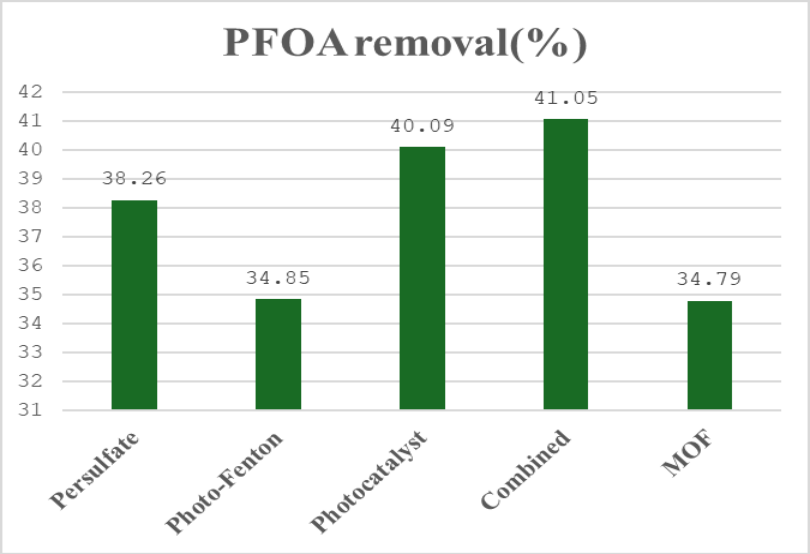

Figure 6.16. *The comparison of PFOA removal for different AOPs under 16W UV-Lamp*

The C/C$_0$ profiles depicted in Figure 6.17 also indicate the kinetics of degradation within the 7-hour reaction time under 16W UV-Lamp irradiation. For all systems, a common trend of reduced PFOA concentration was observed, but the extent and rate of reduction were different for the systems. At the initial stage, up to two hours, all the processes demonstrated relatively slow degradation, and there were insignificant differences between them. Approximately three hours later, however, the combined system started to demonstrate a more rapid decline in C/C$_0$ values compared to the others. By the sixth hour, the combined system had recorded significant reduction, which is equal to its greatest final percentage of removal.

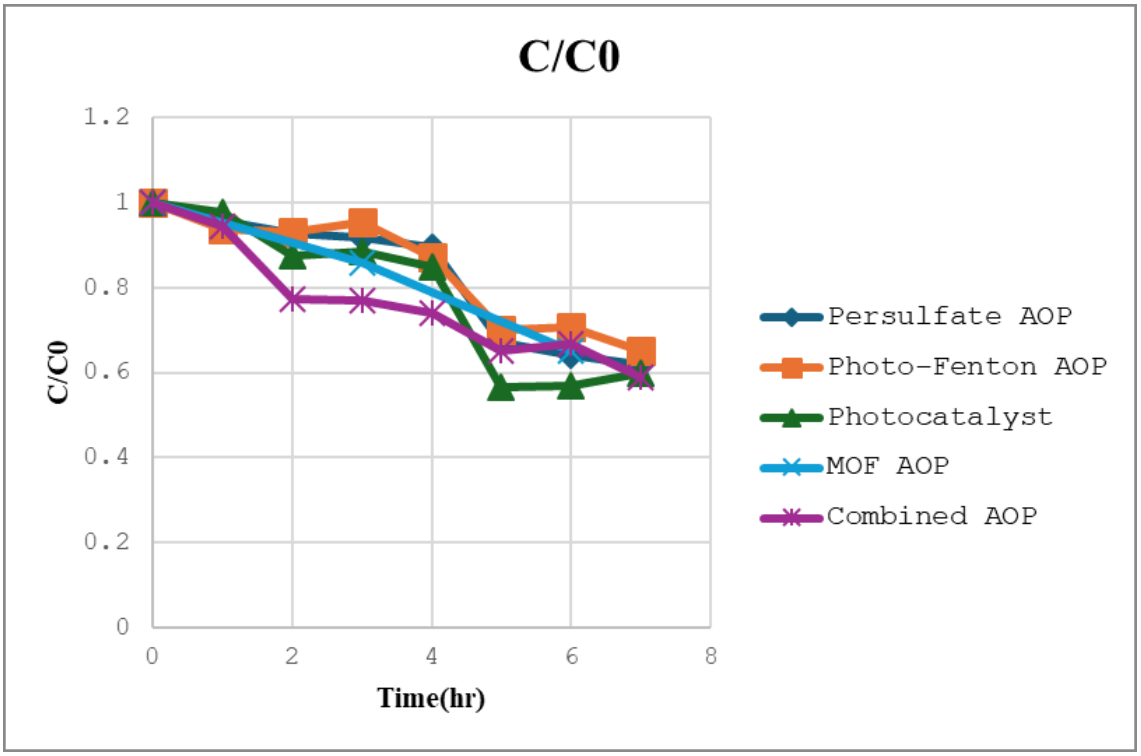

Figure 6.16. *The comparison of temporal concentration decay (C/C$_0$) of PFOA over time for different AOPs*

The photocatalyst system also demonstrated a successful degradation pattern, showing a relatively steep decline from the fourth to sixth hours. This suggests that with light irradiation, photocatalytic activation yielded a sufficient amount of reactive species, such as hydroxyl and sulfate radicals, which could effectively degrade the stable C-F bonds of PFOA. The persulfate-alone system showed a gradual and modest decrease in the concentration of PFOA throughout the experiment.

Persulfate by itself, without any external stimulus like UV or catalysts, can activate and generate sulfate radicals at a lower rate, and thus less effective than the photocatalyst and combined systems. Surprisingly, the Photo-Fenton process, though the efficiency of the Fenton reaction is well established in most organic pollutant degradations, performed worse in this case. The Photo-Fenton system degraded only 34.85% PFOA. There are several possible reasons that this might be the case. The Fenton reaction is extremely sensitive to pH and works best under acidic pH (around pH 3). However, PFOA is a highly stable chemical, and even under ideal Fenton conditions, the production of hydroxyl radicals may not be vigorous enough to break down its stable carbon-fluorine bonds. Furthermore, in persulfate case or under UV irradiation, iron species can be engaged in side processes that are radical-scavenging and consequently reduce the total oxidative capacity available for the degradation of PFOA.

The MOF system performed the worst in removing PFOA. Whereas MOFs are excellent adsorption materials with their large surface areas and tunable pore sizes, they have negligible oxidative degradation capacity if no external activation (such as UV or oxidants) is present. Under such conditions, MOF was functioning as a better adsorbent rather than an active oxidative catalyst. Therefore, the observed removal was mostly because of physical adsorption rather than chemical conversion, which is consistent with the lower final percentage removal observed.

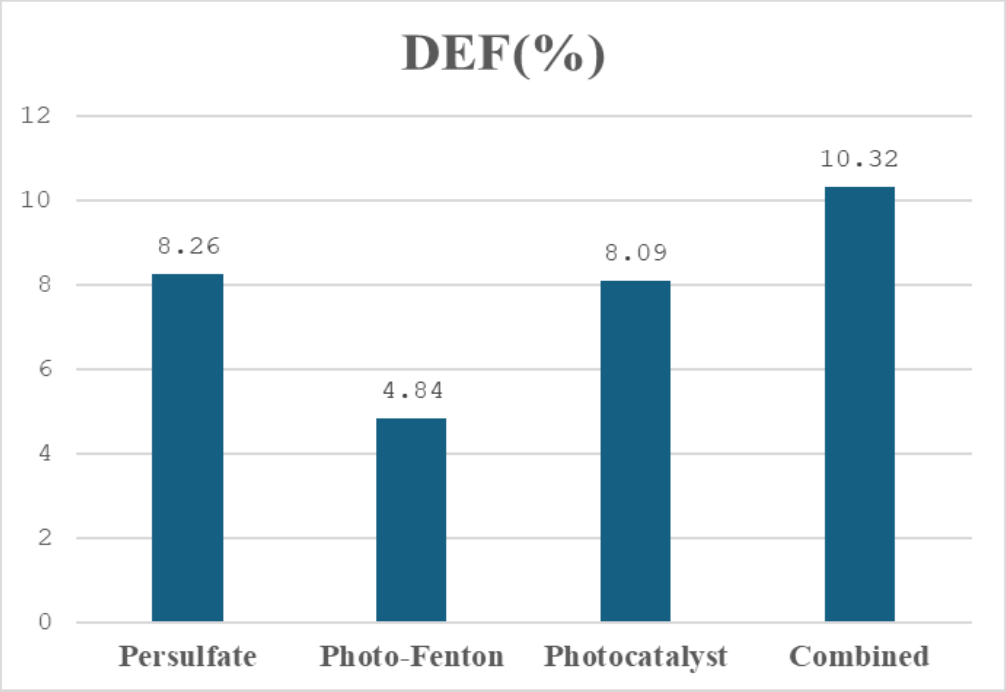

Figure 6.16. *The comparison of defluorination efficiency (DEF) for different AOPs under 16W UV-Lamp*

Based on the defluorination efficiency (DEF%), the values were mostly lower than the percentages of PFOA removal, consistent that partial degradation or conversion to intermediate products was suffered rather than complete mineralization. The composite system again exhibited the highest DEF (10.32%), which indicates relatively improved ability for cleaving the strong C-F bonds compared to individual systems. Persulfate and photocatalyst systems gave DEF values of 8.26% and 8.09%, respectively, while Photo-Fenton and MOF systems yielded the lowest DEFs of 4.84% and 4.79%. These results highlight that though some elimination was realized, destruction of the fluorine atoms on the backbone of PFOA was significantly harder.

Another fascinating aspect of the C/C_0 curves is that the combined system degraded faster initially compared to the other systems. This suggests that the initial adsorption of PFOA on the MOF surface followed by oxidative degradation through the assistance of reactive radicals provided a synergistic route, which sped up the overall removal. The other systems relying on a single mechanism, e.g., pure photocatalysis or persulfate activation, showed a slow degradation tren

Conclusion

The overall results reveal the complexity of PFOA degradation. Cleaving the C–F bond, one of the strongest organic bonds, under normal conditions requires highly oxidative conditions or sophisticated catalysts. The discovery of PFBA as an intermediate in several experiments confirms the hypothesis that degradation of PFOA is associated with sequential shortening of the fluorocarbon chain through the putative decarboxylation and radical-mediated cleavage routes.

The variation of intermediate profiles and fluoride release during the different methods indicates that degradation mechanism depends on the species of the oxidizing agent. Persulfate-based systems, which form both sulfate and hydroxyl radicals, are anticipated to favor greater defluorination than photocatalytic or Photo-Fenton treatment protocols.

Another key scientific finding was the effect of operating conditions like reaction time. Higher removal and mineralization were favored for extended irradiation or reaction time, though there were diminishing returns beyond specific points, suggesting the stabilization of the recalcitrant intermediate species.

The combined advanced oxidation system, which containing persulfate activation, photocatalysis, and Photo-Fenton processes, was the most effective in degrading PFOA. In this system, several radical species are produced during the process simultaneously, most notably sulfate radicals ($SO_4^{\cdot-}$) produced through persulfate activation and hydroxyl radicals ($OH^{\cdot}$) produced through photo-Fenton reaction and photocatalysis under UV irradiation. The synergy of the two processes manifested in the large drop in the concentration of PFOA with respect to time, accompanied by the significant production of fluoride ions, showing that the defluorination and partial mineralization of PFOA were realized. The degradation pathway seemed to entail both the direct radical attack on the PFOA molecule as well as successive shortening of the perfluorinated carbon chain, evidenced by transient short-chain byproducts, such as perfluorobutanoic acid (PFBA) and perfluoroheptanoic acid (PFHpA).

Photocatalysis alone, would be less effective compare to the combined system but not that much, also played an important contribution to the transformation of PFOA. Under irradiation and the presence of a photocatalyst, notable PFOA concentration reductions were realized, though the magnitude of mineralization, as indicated by fluoride ion release, was relatively low. The

production of PFBA during photocatalysis experiments indicated incomplete degradation and the persistent stability of short-chain perfluorinated acids under photocatalytic conditions individually. The photocatalytic system, however, proved to be an encouraging route to the degradation of PFOA, especially when supplemented by the use of external oxidation such as persulfate and Photo-Fenton process.

The adsorption experiments with MOFs yielded a different set of insights into the removal of PFOA. The MOFs were found to possess reasonable adsorption capacity for PFOA, and the aqueous concentrations of PFOA were measurable to decrease. The adsorption procedure, however, did not induce defluorination or mineralization, as indicated by the complete absence of fluoride ion release. The nearly zero value for the calculated defluorination efficiency further proved that the MOFs served as adsorbents and did not cause chemical conversion of the PFOA molecule. This result highlights the function of MOFs mainly as concentrators and less as destruction agents of perfluorinated compounds. While adsorption can be a useful preliminary step in the treatment of waters to decrease pollutant loads, its sole use cannot guarantee the removal of environmental and health risks posed by PFAS persistence.

Comparing the various treatment procedures, it is clear that radical-mediated, system-based techniques — specifically the one combining various mechanisms including photocatalysis, persulfate activation, and Photo-Fenton reaction — are better able to effect complete degradation and partial mineralization of PFOA. The lowest defluorination efficiency (DEF) belong to Photo-Fenton which is half of the value compare to the other AOPS which is reasonable because The main oxidizing species in the Photo-Fenton process is the hydroxyl radical ($OH^{\cdot}$), which itself is a very potent oxidant. However, hydroxyl radicals tend to attack most efficiently to the organic materials with easily oxidizable functional groups such as aromatic rings, C-H bonds, or unsaturated bonds (C=C). therefore, the hydroxyl radicals prefer to attack the carboxylic group at the terminal end of the PFOA molecule instead of being able to break the C–F bonds along the chain effectively. Consequently, during the Photo-Fenton process, although degradation of the structure of PFOA— through substitutions around the functional group—is seen to a certain extent, the efficient deep mineralization giving rise to free fluoride ion release is not attained. This results in lower DEF values than obtained through other advanced oxidation processes (AOPs) involving different radicals. Even though the overall PFOA removal rate can appear high (due to partial

conversions to shorter-chain PFAS or intermediates), the actual breakage of the carbon-fluorine backbone, which will lead to the release of fluoride ions, is nevertheless relatively limited.

In comparison, in persulfate-based AOPs and particularly in the combined system where photocatalyst, persulfate activation, and Photo-Fenton reactions work together, the chemistry is different. In such systems, sulfate radicals ($SO_4^{\cdot-}$) are generated due to persulfate activation, and the radicals have a unique oxidation mechanism different from that of hydroxyl radicals. Sulfate radicals are more efficient at attacking the carbon-fluorine bonds, leading to greater degradation of the PFAS molecules and increased release of fluoride ions. In addition, use of a photocatalyst also supplies photogenerated electrons and holes (e^-/h^+) that also help further in the process of breakdown in generating some reactive species. Not only does UV light allow the generation of hydroxyl radicals through the conventional Fenton reaction but also excites the photocatalyst and possesses the ability of directly exciting persulfate. This mix provides a more militant oxidative environment in which the several radicals fill up each other to optimize cleavage of the hard C–F bonds.

One of the important observation in all the experiments was how the short-chain by-products behaved. PFBA, one of the short-chain products, appeared quickly during the degradation process but then its concentration also dropped afterward. This shows that the PFOA molecules were breaking down into smaller parts during treatment. However, these short-chain compounds, especially under conditions like simple adsorption and photocatalysis, were still quite stable. This raises concerns about whether the water is fully detoxified after treatment. Because short-chain PFAS are very mobile and hard to break down, future treatment methods should aim not only to remove the original compounds like PFOA but also to fully destroy any by-products that form during the process.

The results of the present work have significant consequences regarding future PFAS remediation technology design. It is apparent that the combination of various oxidative processes can overcome the restrictions associated with sole-method treatments. Multistep systems integrating photocatalysis, persulfate activation, and Photo-Fenton reaction generate an oxidative environment full of different reactive species, and as such, the likelihood of complete degradation is improved. However, proper management of operation conditions, including pH, concentration of oxidants, irradiation duration, and catalyst dosage, is still quite important to maximize performance and avoid the production of persistent intermediate species.

Modifications and recommendations for future research

From the results of this research, some directions for future research can be offered. One of the most important directions would be catalyst optimization. Future studies must strive to create more efficient photocatalysts or redox-active site-functionalized metal-organic frameworks (MOFs). Methods such as doping with transition metals or heterojunction structure may increase the charge separation efficiency and enhance the generation of reactive species, thereby increasing the degradation rates of PFAS compounds. An alternative could be integration of treatments. A combination of adsorption techniques, for instance, using MOFs with oxidative degradation techniques such as persulfate activation or photocatalysis has the possibility of yielding synergistic outcomes. In such integrated processes, PFASs can first be preconcentrated from diluted aqueous solutions through adsorption and then be successfully degraded through advanced oxidation processes, thus yielding greater overall efficiency of treatment.

In addition, more detailed kinetic and mechanistic studies need to be carried out to identify the degradation pathways of PFOA and associated compounds in more detail. Kinetic model-based research combined with radical scavenging experiments would elucidate the dominating mechanisms as well as intermediate steps in the conversion. This knowledge could help in rational design of second-generation remediation technologies that are more efficient and site-specific.

Follow-up research should also involve experiments with actual water matrices, such as wastewater or groundwater, rather than simple laboratory experiments with pure water. Experiments in more complicated environments, where natural organic matter and other inorganic ions are present, would more effectively evaluate the applicability and robustness of the proposed treatment processes under actual and competitive conditions.

Finally, there needs to be incorporated a study on sustainability in follow-up work. Costing and life cycle assessment (LCA) would be essential to determine the environmental impact and cost-effectiveness of the upscaling of the most promising technologies. Such analyses would not only give an estimate of the technical efficiency but also of the long-term feasibility and sustainability of PFAS treatment technologies.

Nomenclature

AOPs	Advanced Oxidation Processes
PFAS	Perfluoroalkyl Substances
PFOA	Perfluorooctanoic Acid
PFOS	Perfluorooctanesulfonic Acid
TBT	Tetrabutyl Titanate
FT-IR	Fourier-Transformed Infrared Spectroscopy
ESEM	Environmentalscanning Electron Microscope
EPA	Environmental Protection Agency
ECHA	European Chemicals Agency
WHO	World Health Organization
BDE	Bond Dissociation Energies
POP	Persistent Organic Pollutant
PBT	Persistent, Bioaccumulative, And Toxic
MCLs	Maximum Contaminant Levels
PCO	Conventional Photocatalytic Oxidation
UIO-67	Universitetet I Oslo-67
PVP	Polyvinylpyrrolidone
PAA	Polyamic Acid
PI	Polyimide
PPE	Personal Protective Equipment
PMDA	Pyromellitic Dianhydride
DMF	Dimethylformamide

PVP	*Polyvinylpyrrolidone*
TBT	Tetrabutyl Titanate
PFOA	Perfluorooctanoic Acid
TGA	Thermogravimetric Analysis
HPLC	High-Performance Liquid Chromatography
MS	Mass Spectrometry
SRM	Selective Reaction Monitoring
UV	Ultraviolet

Bibliography

1. U.S. Environmental Protection Agency (EPA). (2024). *Final PFAS National Primary Drinking Water Regulation.*
2. OECD. *Reconciling Terminology of the Universe of Per- and Polyfluoroalkyl Substances: Recommendations and Practical Guidance*. OECD Series on Risk Management No. 61, 2021.
3. United States Environmental Protection Agency (EPA). *PFAS Strategic Roadmap: EPA's Commitments to Action 2024–2027*. 2024.
4. United States Environmental Protection Agency (EPA). *CompTox Chemicals Dashboard – PFAS Master List of Substances*. Updated 2025
5. Buck, R. C., et al. (2011). "Perfluoroalkyl and polyfluoroalkyl substances in the environment: a review of their sources, fate, and effects." *Environmental Toxicology and Chemistry*, 30(7), 1492-1495.
6. Lindstrom, A. B., et al. (2011). "Polyfluorinated compounds: past, present, and future." *Environmental Science & Technology*, 45(19), 8038-8048.
7. Hogue, C., Reiner, E. J., & Scheringer, M. (2017). Chemical and thermal stability of perfluoroalkyl and polyfluoroalkyl substances: Implications for remediation efforts. *Environmental Science & Technology*, 51(9), 4973-4984.
8. Wang, Z., Wang, Y., & Zhang, X. (2017). Resistance of perfluoroalkyl substances (PFAS) to conventional degradation methods. *Environmental Science & Technology*, 51(13), 7844-7853.
9. Fenton, T. M., & Glaze, W. H. (2021). Thermal stability of perfluorinated chemicals and their degradation pathways: An overview. *Environmental Pollution*, 276, 116748.
10. Liu, Y., & Zeng, X. (2020). Surface properties of perfluoroalkyl substances: Effect on surface tension and their behavior in aqueous and non-aqueous systems. *Journal of Colloid and Interface Science*, 567, 58-65.

11. Seow, H. F., & Achen, C. M. (2015). Perfluorinated compounds in textile engineering and product manufacturing: Challenges and advancements. *Journal of Industrial Textiles*, 45(5), 635-650.
12. Mackay, D., & Pfaender, F. (2013). The use of PFAS in flame retardant and waterproofing technology in aviation and defense industries. *Journal of Hazardous Materials*, 250, 400-407.
13. Lin, Y., & Schaefer, L. (2018). PFAS in construction materials: Impact on environmental durability and resilience of building technologies. *Construction and Building Materials*, 163, 358-366.
14. Sullivan, M., & Roberts, D. (2021). PFAS in renewable energy: Contributions to solar panel and energy storage technology. *Renewable and Sustainable Energy Reviews*, 135, 110292.
15. Grandjean, P., & Clapp, R. (2015). Perfluorinated alkyl substances: Emerging health threats to children. *Environmental Health Perspectives*, 123(3), 270-275
16. Liu, J., & Twardowska, I. (2020). Ecological impacts of PFAS: Bioaccumulation and transfer in freshwater ecosystems. *Environmental Toxicology and Chemistry*, 39(1), 78-87.
17. Xu, P., & Ding, Y. (2020). PFAS in human health and environmental contamination: A global review of the health impacts and regulatory frameworks. *Environmental International*, 135, 105332.
18. European Commission. (2020). *Directive (EU) 2020/2184 of the European Parliament and of the Council on the quality of water intended for human consumption*. Official Journal of the European Union.
19. U.S. Environmental Protection Agency (EPA). (2024). *National Primary Drinking Water Regulation (NPDWR) for Per- and Polyfluoroalkyl Substances (PFAS)*.
20. Stockholm Convention on Persistent Organic Pollutants (POPs). (2009). *Amendments to Annexes A, B, and C of the Stockholm Convention to list PFOS, its salts and PFOSF*. United Nations Environment Programme (UNEP).
21. Health Canada. (2023). *Guidelines for Canadian Drinking Water Quality – Per- and Polyfluoroalkyl Substances (PFAS)*.

22. World Health Organization (WHO). (2022). *Background document for the development of WHO Guidelines for Drinking-water Quality: Perfluorooctanoic acid (PFOA) and perfluorooctane sulfonate (PFOS)*.
23. Liu, J., Mejia Avendaño, S., (2017). Microbial degradation of polyfluoroalkyl chemicals in the environment: A review. *Environment International*, 61, 98–114.
24. Rao, D., Lei, Y., Qin, Q., Zhang, Y., Huang, W., (2020). Defluorination of Perfluoroalkyl Substances (PFASs) in a UV/electrochemical system: Structure dependence and reaction mechanism. *Chemical Engineering Journal*, 389, 124409.
25. Singh, R. K., Fernando, S., Baygi, S. F., Multari, N., Thagard, S. M., Holsen, T. M., (2021). Breakdown products from perfluorinated alkyl substances (PFAS) degradation in electrochemical systems: A review. *Environmental Science: Water Research & Technology*, 7(2), 225–249.
26. Huang, J., Deng, S., Wang, B., Yu, G., (2020). Development of a novel magnetic fluorinated carbon nanotube-based adsorbent for efficient removal of PFAS from aqueous solution. *Water Research*, 173, 115521.
27. Hou, J., Jin, Q., Li, Y., Zhang, S., (2021). Solar-driven peroxymonosulfate activation by lignin-based MOF nanofibers for efficient degradation of PFAS. *Applied Catalysis B: Environmental*, 288, 120047.
28. Hoffmann, M. R., Martin, S. T., Choi, W., & Bahnemann, D. W. (1995). Environmental applications of semiconductor photocatalysis. *Chemical Reviews*, 95(1), 69–96.
29. Deng, W., Liu, W., Zhan, J., Zhao, D., & Xu, Z. (2021). Photocatalytic degradation of perfluorooctanoic acid (PFOA) and perfluorooctane sulfonate (PFOS) in water: A critical review. *Chemosphere*, 263, 127890.
30. hang, J., Wang, Y., Jin, J., & Zhang, S. (2022). Advances in photocatalytic degradation of per- and polyfluoroalkyl substances (PFAS) in water. *Journal of Hazardous Materials*, 424, 127419.
31. Yadav, A. K., Kumar, S., Sharma, A. K., & Chakraborty, S. (2021). Photo-Fenton oxidation for the degradation of perfluorooctanoic acid (PFOA) and perfluorooctane sulfonate (PFOS) in water: A review. *Chemosphere*, 263, 128101.

32. Wang, S., & Wang, J. (2018). Degradation of perfluorooctanoic acid by a photo-Fenton process: Optimization, mineralization mechanism, and synergistic effect. *Water Research*, 144, 482–491.
33. Fang, G., Gao, J., Dionysiou, D. D., Liu, C., & Zhou, D. (2013). Activation of persulfate by naturally occurring iron minerals: Implications for the degradation of organic contaminants. *Environmental Science & Technology*, 47(21), 12415–12423.
34. Chu, W., Lam, W., & Li, X. (2019). Effective degradation of macrolide antibiotics by gamma irradiation enhanced persulfate activation. *Chemical Engineering Journal*, 361, 1396–1404.
35. Lutze, H. V., Kerlin, N., Schmidt, T. C. (2015). Sulfate radical-based oxidation of micropollutants in water: A critical review. *Chemosphere*, 145, 288–292.
36. Abdi, J., Vossoughi, M., & Alemzadeh, I. (2017). Synthesis and characterization of UiO-67 metal-organic framework decorated with TiO_2 nanoparticles for photocatalytic degradation of organic pollutants. *Journal of Photochemistry and Photobiology A: Chemistry*, 336, 42–53.
37. Shang, Y., He, X., Li, Q., & Liu, J. (2020). Efficient photodegradation of perfluorooctanoic acid over TiO_2/metal-organic frameworks hybrid under UV and visible light irradiation. *Applied Catalysis B: Environmental*, 260, 118195
38. Macosko, C.W., "Rheology: Principles, Measurements, and Applications," Wiley-VCH, 1994.
39. Electrospinning of Nanofibers: Reinventing the Wheel?," Advanced Materials, 2004.
40. Griffiths, P.R., de Haseth, J.A., "Fourier Transform Infrared Spectrometry," Wiley, 2007.
41. Foundations of Environmental Scanning Electron Microscopy," Advances in Electronics and Electron Physics, 1988.
42. Determination of Selected Per- and Polyfluorinated Alkyl Substances (PFAS) in Drinking Water by SPE and LC-MS/MS, U.S. EPA, 2020.
43. Doshi, J., & Reneker, D. H. (1995). *Electrospinning process and applications of electrospun fibers*. Journal of Electrostatics, 35(2-3), 151-160.
44. Taylor, G. (1969). *Electrically driven jets*. Proceedings of the Royal Society of London. Series A, Mathematical and Physical Sciences, 313(1515), 453-475.

45. Huang, Z. M., Zhang, Y. Z., Kotaki, M., & Ramakrishna, S. (2003). *A review on polymer nanofibers by electrospinning and their applications in nanocomposites*. Composites Science and Technology, 63(15), 2223-2253.
46. Liao, Y., Zheng, Y., & Chen, L. (2018). *Recent advances in electrospun nanofibers for energy applications*. Energy Science & Engineering, 6(5), 553-575.
47. Sun, B., Yuan, X., Wang, Z., & Zhang, P. (2014). *Electrospinning: A versatile technique for the fabrication of nanofibers in biomedical applications*. Journal of Biomedical Nanotechnology, 10(5), 886-900.
48. Xue, J., Wu, T., Dai, Y., & Xia, Y. (2019). *Electrospinning and electrospun nanofibers: Methods, materials, and applications*. Chemical Reviews, 119(8), 5298-5415.
49. Dine-Hart, R. A. & Wright, W. W. Preparation and fabrication of aromatic polyimides. *J. Appl. Polym. Sci.* 11, 609–627 (1967).
50. Yang, G., Su, J., Guo, Y., Xu, H. & Ke, Q. Fabrication of TiO2/PI composite nanofibrous membrane with enhanced photocatalytic activity and mechanical property via simultaneous electrospinning. *J. Mater. Sci.* 52, 5404–5416 (2017).

Acknowledgments

I would like to express my deepest gratitude to Professor Martina Roso for her superb supervision, support, and encouragement during the course of this project. Her experience and guidance were fundamental in the successful completion of this project. I am also sincerely thankful to Ing. Abhishek Anand, the project correlator, whose explanations, patience, and continuous assistance helped me better understand and navigate the technical aspects of the study.

I would also like to extend my heartfelt thanks to my family for their ongoing encouragement, motivation, and unwavering support during this journey. Finally, a special thanks to my friends Mahsa Vian and Milad Alinejad, whose friendship and encouragement were a source of strength throughout this process.